VOLUME 15 (2021)

CUSJ

COLUMBIA UNDERGRADUATE SCIENCE JOURNAL

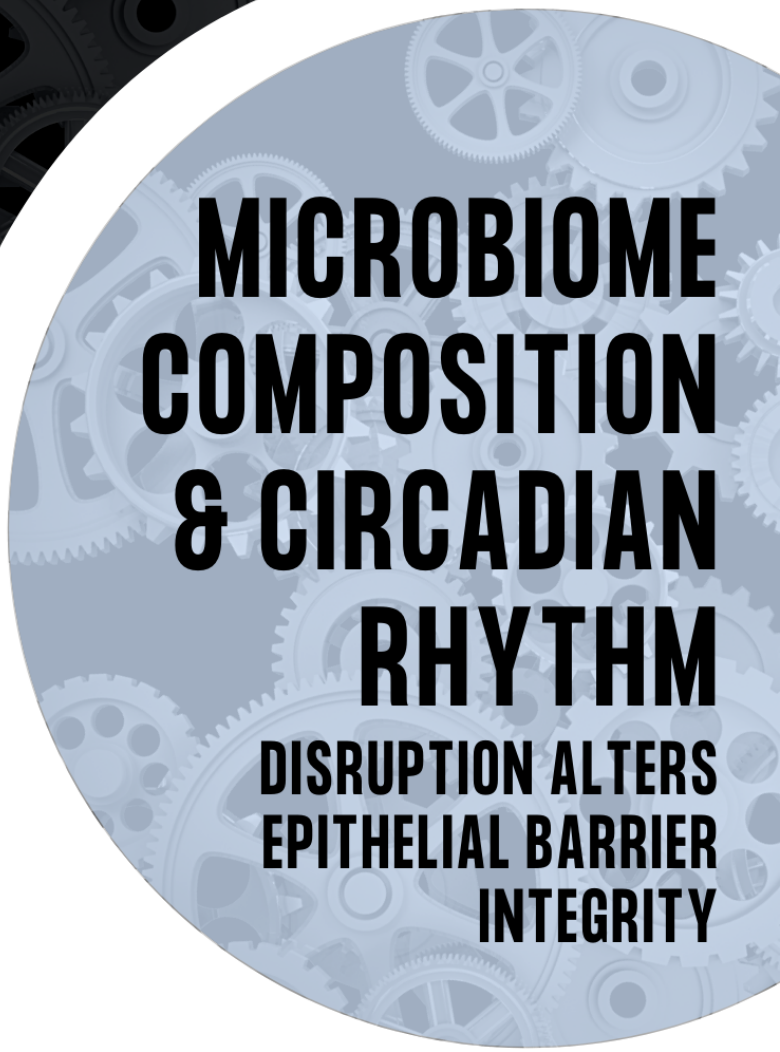

MICROBIOME COMPOSITION & CIRCADIAN RHYTHM

DISRUPTION ALTERS EPITHELIAL BARRIER INTEGRITY

ALSO IN THIS ISSUE

CUSJ
COLUMBIA UNDERGRADUATE SCIENCE JOURNAL

About the Journal

Aims and Scope

The Columbia Undergraduate Science Journal (CUSJ) was founded in 2006 by students who were passionate about showcasing undergraduate excellence in scientific research. Since then, CUSJ has remained Columbia's premier publication for original scientific research and scholarly reviews, and is managed by an editorial board of undergraduates with a vast scope of interests across all disciplines. We are a peer-reviewed, open-access academic journal published annually in the spring semester, with life sciences, physical sciences, and social sciences featured; any currently enrolled undergraduate is welcome to submit their work. The editorial board also manages the Columbia Junior Science Journal (CJSJ), a publication designed to introduce high school students to research. In addition to our publications, the CUSJ team is dedicated to fostering the scientific community, both within Columbia and in the surrounding Morningside Heights and Harlem communities. To this end, the board frequently plans outreach and networking events relevant to young and early career scientists, including an annual Research Symposium poster session each spring.

Copyrights and Permissions

Contact

Email cusj@columbia.edu with any inquiries. Visit cusj.columbia.edu for more information about the journal.

CUSJ
COLUMBIA UNDERGRADUATE SCIENCE JOURNAL

Table of Contents

Administrative

Research Papers

Review Papers

Columbia Spring Research Symposium

Letter from the Editor-in-Chief

Dear Readers,

It is with great pleasure that the editorial board of the Columbia Undergraduate Science Journal presents the 15th edition of our publication. Since 2006, CUSJ has aimed to create a space to highlight the accomplishments of undergraduate scientists and to foster the academic growth of students across all universities. To this end, this cycle saw a record number of submissions, and I am proud to witness the rapidly growing number of undergraduates gaining experience and accessing research opportunities.

This edition of CUSJ features research and review articles that traverse disciplines in their scope. Starting with our featured cover story on epithelial barrier integrity, this issue also explores topics from the microwave imaging of pipes to neural oscillations in second language proficiency. I am ecstatic to see the wide variety among these papers, and hope that you will find them as insightful as our editorial board did. Coming from undergraduates working at universities located around the world, we hope that you appreciate the importance of their diverse voices.

In a year where our organization had to move to a virtual format, producing an issue filled with outstanding research was more difficult than ever, and I would like to show my appreciation to everyone who was involved in the process. This includes but is not limited to the CUSJ editorial board, the CUSJ editorial committee, our Faculty Advisory Board, our advisors at Columbia Libraries, our peer reviewers, research mentors, and all students who submitted their work. In particular, thank you to our published authors, who demonstrated an unwavering commitment to the quality of their papers and who were always a joy to work with despite the lengthy editing process they were subjected to.

It has been an honor and a privilege to serve as the 2020-2021 Editor-in-Chief of CUSJ. I look forward to seeing the direction of the next editorial board and the future achievements of everyone involved.

Thank you for reading CUSJ!

Sincerely,
Isabella Leite
Editor-in-Chief
Columbia Undergraduate Science Journal

COLUMBIA UNDERGRADUATE SCIENCE JOURNAL

Letter from the President

Dear Readers,

On behalf of the editorial board of the Columbia Undergraduate Science Journal, I am proud to present the 15th edition of our undergraduate publication. Over the past fifteen years we have published a wide-variety of work produced by undergraduate student-scientists. From our first edition, which featured innovative work on cell-cell communication in bone degeneration, to our present edition, which includes novel insights on the gut microbiome's contribution to epithelial barrier permeability, it is evident not only that science has made leaps, but that our young scientists have as well. As the countable infinity of scientific knowledge left to learn grows ever smaller, I am amazed by the remarkable curiosity of undergraduate student-scientists, who tackle seemingly insurmountable questions with vigor and drive.

The entire CUSJ enterprise has taken great strides over the past fifteen years. As one of the first undergraduate peer-reviewed scientific journals, we paved the way many years ago for the creation of scientific publications at other universities. Now, on our 15th anniversary, CUSJ spearheaded the formation of and currently leads the National Undergraduate Consortium of Science Journals, uniting more than 20 undergraduate scientific publications in an effort to ensure high ethical standards. At our now-annual National Undergraduate Conference on Scientific Journalism, we gathered more than 500 students from 34 countries to visualize the way forward for young scientists. As we move into the next fifteen years of CUSJ, I look forward to the continued sharing of scientific pursuits and common values.

I would like to thank all students who submitted to CUSJ, past and present. It is your commitment to thoughtful experimentation and thorough questioning that drives the young scientific world. I would like to specifically commend the authors published in our 15th edition, who have demonstrated an admirable commitment to scientific achievement and collaboration in this unusual time. I am grateful to you, your research mentors, your parents, and all who supported you for making CUSJ possible.

It has been a great honor to serve as the President and Chief Editorial Officer of the Columbia Undergraduate Science Journal for the 2020-2021 academic year. Thank you to the editorial team, our selected peer reviewers, and our esteemed Faculty Advisory Board for ensuring the growth and prosperity of the young scientific community. Congratulations to all authors, and thank you to our readers!

Arya Rao
President, Chief Editorial Officer
Columbia Undergraduate Science Journal

COLUMBIA UNDERGRADUATE SCIENCE JOURNAL

Masthead

Editors

Isabella Leite.....CUSJ Editor-in-Chief
Arya Rao.....President
Deena Shefter.....CJSJ Editor-in-Chief
Elin Hu.....Director of Communications
Hibah Vora.....Director of Events
Arjun Kudinoor.....Director of Finance
Shivali Verma.....Director of Outreach
Kate Johnson.....Director of Internal Affairs
Jason Mohabir.....President Emeritus
Ethan Chen.....Editor Emeritus
Caroline Haoud.....Editor Emeritus
Katie Long.....Editor Emeritus
Ashley Rosenberg.....Editor Emeritus
Neeraj Sakhrani.....Editor Emeritus
Ilaria Simeone.....Editor Emeritus
Maria Trifas.....Editor Emeritus
Chloe Gong.....Editor
Noah Krever.....Editor
Sophia Ladyzhets.....Editor
Mayeesa Rahman.....Editor
Ellen Ren.....Editor
Aswath Suryanarayanan.....Editor
Lydia Wu.....Editor
Shamara Yearwood.....Editor
Unal Yigit Ozulku.....Editor
Ana Beatriz Bonfim.....Associate Editor
Teodora Bratu.....Associate Editor
Gloria Charite.....Associate Editor
Nadiia Dubchak.....Associate Editor
Stan DeLaurentiis.....Associate Editor
Mehdi Elfilali.....Associate Editor
Anushka Gupta.....Associate Editor
Aaron Jackson.....Associate Editor
Shloka Janapaty.....Associate Editor
Laurelle Lee Young.....Associate Editor
Kazi Rabbe.....Associate Editor
Vanshika Sriram.....Associate Editor
Samantha Turk.....Associate Editor
Zoe Zager.....Associate Editor

Faculty Advisory Board

Hugh Ducklow.....Primary Advisor, Professor of Earth & Environmental Sciences
Ivana Hughes.....Director of Frontiers of Science & Senior Lecturer in Discipline- Chemistry
Marko Jovanovic.....Assistant Professor of Biological Sciences
Laura Kaufman.....Professor of Chemistry
Patricia Lindemann.....Director of Undergraduate Studies & Lecturer in Discipline- Psychology
Kyle Mandli.....Professor of Applied Mathematics
Gerard Parkin.....Professor of Chemistry
Ron Prywes.....Professor of Biological Sciences
Rachel Rosen.....Associate Professor of Physics
Samuel Sternberg.....Assistant Professor of Biochemistry & Molecular Biophysics

COLUMBIA UNDERGRADUATE SCIENCE JOURNAL

Microbiome Composition and Circadian Rhythm Disruption Alters Epithelial Barrier Integrity

Elisha Pinker[1], Timur Tuganbaev[2]

[1]Columbia University, New York, NY, USA

[2]Lab of Dr. Eran Elinav; Department of Immunology, Weizmann Institute of Science, Israel

KEYWORDS: Circadian rhythms, intestinal permeability, microbiome

ABSTRACT: The intestine is home to one of the most complex ecological communities, termed the human gut microbiome. The gut microbiome modulates a wide range of human diseases from diabetes to neurological disorders to cancer. Separating the host and the gut microbiome is the epithelial barrier. The intestinal epithelium serves as an adaptive interaction hub between the host and microbiome that plays an important role in deciding the outcome of host-microbiome interactions. Regulation of epithelial barrier permeability to ions, nutrients and microbiome metabolites is known to be a tightly controlled process on the host side. While previous studies have identified the microbiome as a factor for epithelial permeability, the exact mechanisms through which it mediates remains less clear. Here, we show that alterations in microbiota composition by treatment with antibiotics selectively targeting specific members of the microbiome community impacts the permeability of the intestine. Additionally, modulating the microbiome through other methods such as altering diet composition shows changes in permeability of the epithelial barrier. As daily feeding rhythm entrains diurnal fluctuations in microbiome, we have set out to measure how epithelial barrier permeability disrupts the clock. We have discovered that the permeability of the intestinal epithelial barrier exhibits circadian rhythms in mice. Disruption of these rhythms, through jet lag or genetic deficiencies in circadian machinery, alters epithelial barrier integrity. Together, these findings provide evidence that disruptions in circadian rhythms as well as alterations in microbiome composition have direct consequences in intestinal permeability, and that microbiome might serve as a tool in regulating epithelium permeability.

INTRODUCTION

The human body is colonized by a complex community of microorganisms, termed the human microbiome, that includes bacteria, archaea, viruses and fungi [1]. This ecological community exists primarily on mucosal sites, like the gastrointestinal tract, skin, lungs and urogenital system [2]. This community is such where the microbiome bacteria outnumber eukaryotic cells in the entire human body 1.3:1 [3]. The microbiota is responsible for the regulation of many physiological processes, including digestion, absorption [4], host metabolism [5], the maturation and function of the immune system [4], and even host behavior and cognitive function [6]. However, when the balanced microbial composition is disrupted, dysbiosis can cause intestinal diseases [7]. Modulating

the microbiome through the diet is one way to induce dysbiosis. Treatment with high-fat diet (HFD), containing 60% of caloric energy derived from fat (a model of a "western diet"), is one such example where the balanced gut microbial community is altered to the point of dysbiosis resulting in metabolic dysfunction consequently inducing disease, such as obesity and type 2 diabetes as well as exacerbating inflammatory bowel diseases (IBD) [7]. But, when treated with broad-spectrum antibiotics, obesity and glucose intolerance in mice fed with HFD is abrogated [8]. Previous studies show, that when microbiome from mice fed HFD were transplanted into germ-free mice (GF: free of microorganisms) significantly more weight is put on by these mice compared to GF mice transplanted with microbiome from lean donor mice fed NC (normal chow) [9]. Additionally, GF condition in mice causes significant immune system deficiency [7]. Tools like gnotobiotic animal models (GF mice) and broad-spectrum antibiotics, have enabled the discovery that microbiota contributions to health and disease span multiple organ systems.

It has previously been shown that the mammalian intestinal microbiota composition exhibits diurnal oscillations both in terms of its composition and metabolic activity [8]. The circadian clock is the top of a hierarchical internal clock system that is responsible for the circadian biological processes ranging from dictating the rhythmic gene expression in organs to behavior, metabolism and immunity [10][11]. When working with circadian rhythms, scientists devised Zeitgeber times (ZT) which measure time on a 24-hour light/dark cycle, so ZT12 and ZT0 denote "dusk" and dawn", respectively. The molecular mechanisms behind the circadian clocks in mammals is orchestrated under a transcriptional autoregulatory feedback loop comprised of the 'core' clock genes CLOCK and BMAL1, responsible for encoding activators, and PER1, PER2, CRY1 and CRY2, responsible for encoding repressors [12]. A disruption of the circadian clock in humans, environmentally or by gene deficiency, is associated with an array of diseases such as, obesity and diabetes [13] [14], cancer [15], cardiovascular disease [16], IBD (inflammatory bowel disease) exacerbation [17] and susceptibility to infection. One common feature among the diseases associated with circadian rhythm disruption, is that they appear to be triggered or promoted by inflammatory processes. Desynchronized interaction between mucosal organs and a complex community of microorganisms colonizing them have emerged as a potential source of inflammation underlining diseases promoted by circadian clock disruption. The source of this inflammation can be located at the gut epithelium [18]. The intestinal epithelium is comprised of a single-cell layer constituting the largest and most important barrier against the external environment [19]. Acting as a selectively permeable barrier, the intestinal epithelium can permit the absorption of nutrients, electrolytes and water, while simultaneously defending against toxins [19]. The epithelium maintains an effective barrier through the help of protein-protein networks forming complexes like tight junctions [19]. A compromised epithelial barrier allowing the passage of toxins, antigens and bacteria into the blood stream creates what is commonly known as "leaky gut" [20]. There is therefore an urgent need to better identify the players behind the disruption and upkeep of intestinal barrier function, to devise methods to combat negative barrier alteration. In this project we studied different factors affecting permeability in the epithelial barrier, specifically in the small intestine, the part of the intestine responsible for the majority of nutrient absorption [21]. Recent studies on type 2 diabetes and obesity have elucidated the link between microbiome composition and small intestine permeability; however, the mediators of these effects have yet to be determined [22].

Over the course of this project, we demonstrated the consequences that genetic and environmental circadian disruption have on gut barrier integrity in mice. Furthermore, we

found evidence to suggest that altering the microbiome, either with diet intervention or antibiotic treatment, can disrupt the diurnal oscillations and alter permeability. Understanding the key players behind circadian disruption and intestinal barrier maintenance has potential in therapeutic and preventative medicine interventions.

METHODS

Mice

Under normal conditions, mice had strict light-dark cycles lasting 12 hours each. Lights were turned on either at 11:30 AM or 11:30 PM, ZT0 or ZT12 respectively. For the induction of jet lag, mice were shifted between both control light conditions every 3 days for 3 weeks at a consistent but arbitrary time. Jet lag mice were moved between the different light schedules every 3 days for 3 weeks. For consistency, jet lag mice were only experimented on at 1:30 PM, which was synchronized with the ZTs of the control group (i.e., ZT14 of jet lag mice corresponded to ZT14 of control mice, as all mice were exposed to the same light-dark conditions at the onset of sample collection). HFD mice were placed in ZT2 and ZT14 light-dark cycles to measure two time points upon sacrifice. These mice were fed a strict HFD for 3 weeks. Mice receiving antibiotic treatment, either received exclusively vancomycin (1 g/l), ampicillin (1 g/l), neomycin (1 g/l), and metronidazole (1 g/l) or a combination of all four in drinking water for 3 weeks. Per 1/2-/- (KO) and Per1/2-/+ (WT) were housed under normal conditions and sacrificed at ZT 14.

Fecal Microbiome Transplantation (FMT)

Microbiome samples were collected and stored in Eppendorf tubes containing 20% glycerol. Fecal samples were homogenized and stored in dry ice before long-term storage at -80° C. For the microbiome transplantation, 0.1g of thawed fecal sample was mixed in 1mL sterile PBS and 200 µL of the diluted sample was gavaged per mouse. HFD microbiome samples were taken from mice fed ad libitum HFD for 4 weeks.

Measuring Permeability with FITC-dextran

Food was removed from mice 2 hours before gavage (starting at 9 AM). The solution was made with 4kDA fluorescein isothiocyanate (FITC)-dextran dissolved in a phosphate buffered saline (PBS) with a concentration of 40 mg/ml. At 11 AM, mice were gavaged with 200 µl dextran. After 2.5 hours (1:30 PM, ZT14), blood was drawn and centrifuged to recover the serum. The fluorescence of the serum was quantified at an excitation wavelength of 485 nm and emission wavelength of 533 nm using a microplate reader.

Ussing Chamber

The Ussing chamber is an instrument used to measure epithelial resistance which is a measure of epithelial barrier permeability. The procedure followed was in accordance with the manufacturer's instructions (Warner Instruments, P2300). Small intestine tissue is excised and immediately mounted in the chamber. Current is then applied to the system and voltage clamp recordings were taken. Small intestine was carefully cleaned and handled minimally to prevent microfracturing the tissue and compromising the results. Additionally, samples were mounted within three hours of tissue excise to limit cell death.

PRR stimulation measures degree of microbial presence at systemic sites

PRR reporter cell lines were obtained from Invivogen (HEK-Blue TLR (Toll-like Receptors) and NLR (Nod-like Receptors) reported cell lines): TLR2, TLR3, TLR4, TLR5, TLR7, TLR9, NOD1, NOD2. Extracts from spleen, liver, and serum were homogenized and added to reporter cell lines incubated with KEL-Blue detection medium according to manufacturer's instructions. Detection is a measurement of specific binding indicating extent of microbial leakage out of the gut.

Statistical Analysis

Data is presented as the mean ± standard deviation. Mann-Whitney U-tests were per-

formed to compare groups. ANOVA with post hoc test was used for comparison between multiple groups with a Bonferroni correction. $p < 0.05$ and $q < 0.1$ were the threshold for being considered significant. *$p < 0.05$, **$p < 0.01$, ***$p < 0.001$, ****$p < 0.0001$.

RESULTS

State of Small Intestinal Microbiome Determines Epithelial Barrier Function

With a GF mouse model, we initially set out to establish the role a microbiome has on the permeability of the small intestine epithelial barrier. Mice underwent fecal transplantation of either normal chow (NC) microbiome or high fat diet (HFD) fed donor specific pathogen free (SPF) microbiome, while the control group received phosphate buffered saline (PBS) (Figure 1A). Small intestine samples were taken and epithelial resistance was measured with the Ussing Chamber. Interestingly, mice with HFD microbiome showed increased permeability while mice with PBS (no microbiome) showed reduced permeability (Figure 1B). Together, this data suggests that microbiome shaped by diet is an active influencer over intestinal permeability.

We next set out to further analyze which subsets of bacteria within the microbiome community are most influential in barrier function modulation. With an antibiotic murine model, we could target specific subsets of bacteria to determine the impact the presence or lack thereof has on epithelial permeability in the intestine. We treated 5 groups of WT mice, fed with normal chow, with selective antibiotics that target specific members of microbiome: metronidazole (anaerobic bacteria), vancomycin (Gram-positive bacteria), ampicillin (broad spectrum), neomycin (Gram-negative bacteria), or a combination of all four for a duration of 3 weeks delivered in their drinking water (Figure 1C). The group containing all four antibiotics is a crude simulation of the germ-free mouse model. After 3 weeks, a FITC-dextran assay was performed, which entails orally administering mice with fluorescent dye coated 4 kDa beads and measuring fluorescence in the peripheral blood, at ZT14, as a proxy for epithelial barrier permeability. Significant reduction in optical density (OD) was observed in four of the antibiotic groups compared to the control (Figure 1D). Additionally, vancomycin treated mice had significantly higher OD than neomycin and metronidazole groups (Figure 1D). The lack of a significant reduction in permeability in the combination treatment, containing all four antibiotics, was likely due to outliers. Two days after blood was taken, and fluorescence was no longer detectable, mice were sacrificed, at ZT14, and small intestine samples were removed for the Ussing Chamber measurements. Only the jejunum region of the small intestine was used for Ussing Chamber. All five antibiotic groups showed significantly reduced permeability and vancomycin, again, showed higher permeability than two of the other antibiotic groups (Figure 1E).

Together, these results uncover that the state of microbial composition directly alters the barrier integrity in the small intestine and the entire system. Additionally, vancomycin-treated groups experienced the smallest reduction in permeability suggesting, that gram-positive bacteria play the smallest role in intestinal epithelial barrier function compared to other bacterial subtypes in the gut microbiome.

Genetic and Environmental Disruption of Circadian Clocks Impacts Epithelial Barrier Integrity

It has been shown that a functional circadian clock of a host is required for normal diurnal rhythmicity in microbiota composition and function [8]. Building off our previous observations, the next step is to examine if circadian clock disruption will likewise compromise the intestinal epithelial barrier. Testing of Per1/2-/- mice, genetically deficient in a functional host clock, has previously shown to disrupt diurnal rhythmicity in microbiota composition [8]. With our own group of Per1/2-/- mice, we ran a FITC-dextran assay.

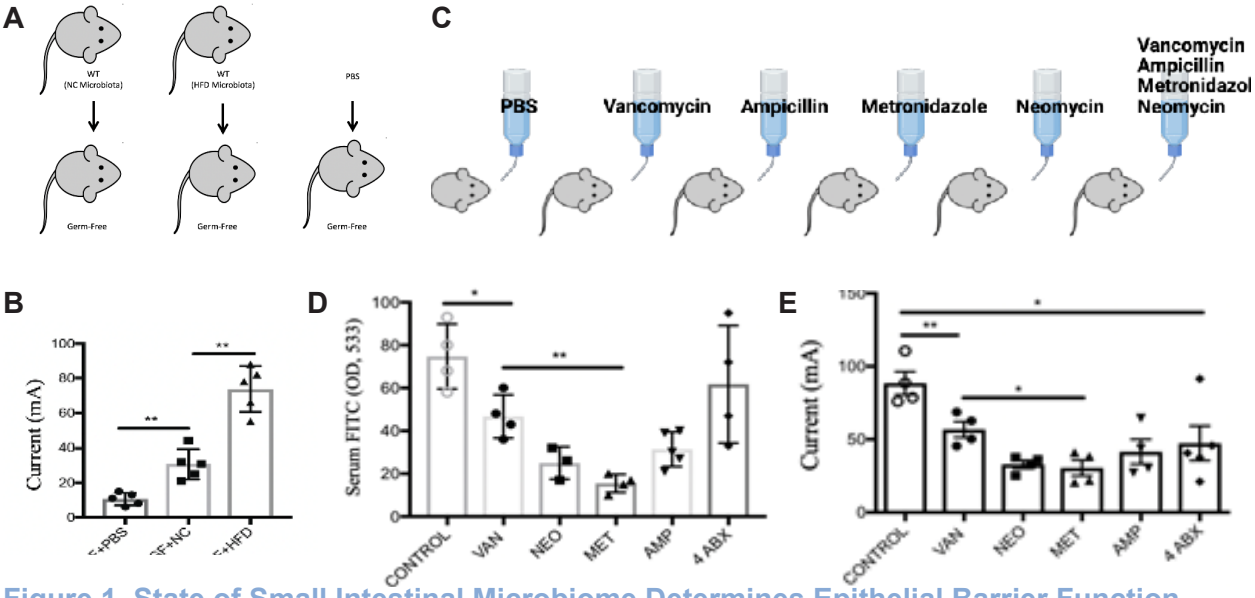

Figure 1. State of Small Intestinal Microbiome Determines Epithelial Barrier Function.
(A) Schematic summarizing transplantation of microbiota from HFD, NC and PBS into germ-free recipient mice.
(B) Ussing Chamber recording of small intestines from GF mice; measuring current (mA) as a measurement of permeability.
(C) Schematic showing a murine antibiotic treatment setup.
(D) FITC (fluorescein isothiocyanate)-dextran recovered from the serum of antibiotic treated WT mice and control.
(E) Ussing Chamber recording of small intestines from antibiotic treated WT mice and control.
Means ± SD are plotted. *p < 0.05, **p < 0.01, ***p < 0.001, ****p < 0.0001 by Mann-Whitney U test.

The OD for Per 1/2-/- was significantly higher (Figure 2A) demonstrating that circadian clock disruption results in increased intestinal permeability, a feature of a “leaky gut” syndrome.

Environmental clock disruptions such as chronic jet lag and shift work are behavioral patterns associated with an increased risk for obesity, diabetes and cardiovascular disease [23][18][14][16][24]. It has been previously established that a loss of microbiota oscillations and dysbiosis is associated with jet lag in mice [8]. So, we set out to learn if these losses of oscillations and dysbioses, in jet lag mice, also impact barrier function in the intestinal epithelial barrier. Prior to our jet lag experiment, we performed a 24-hour circadian experiment on WT mice measuring intestinal permeability with two independent methods – one measuring the electrical permeability of the epithelium to ions (the Ussing Chamber assay) and one measuring the concentration of microbial products in peripheral blood (Toll-like Receptor (TLR) assay) (Figure 2B, Figure 2C). Our findings demonstrate that just like microbial composition behaves in diurnal oscillations, so too does permeability. From this data we chose ZT2 and ZT14 as the lowest and highest points of permeability respectively and prepared control groups at each of these time points. This makes sense due to the nocturnal behaviors of mice where ZT2 is during the daylight when mice are least active while ZT14 is during the night is when mice are most active.

We then set out to mimic the situation of shift work and chronic jet lag by using a jet lag model in which mice were exposed to a 12-hour time shift every 3 days. Using a circadian cabinet, which allows us to individually control the light cycles of each compartment, a group of mice were initially started in one of two

compartments (ZT2 or ZT14) with light cycle's 12-hours apart. Every 3 days for 3 weeks the cages of mice were switched between the two compartments until they were "jet lagged". The mice were then bled for FITC-dextran assay at the same time, ZT2 and ZT14, depending on the compartment. However, if the mice were jet lagged properly, and their circadian clock was disrupted, the ZT time at which blood was drawn would not matter. The results showed that the OD from FITC-dextran between jet lag groups ZT2 and ZT14 were non-significant (Figure 2D). Additionally, compared to the controls, the jet lag groups' ODs was closer to Control ZT14 (highest measured permeability) than Control ZT2 (lowest measured permeability). When we excised small intestine samples, for Ussing chamber assay, we observed similar trends: non-significant permeability measurements between jet lag groups (sign of successful jet lag) and overall permeability levels aligned with ZT14 control levels (Figure 2E).

Altogether, these data suggest that chronic environmental (jet lag model) or genetic disruption (Per1/2-/-) of host light-dark cycles exhibits significant alterations in intestinal epithelial barrier function and as a result increasing barrier permeability. This has relevance for frequent fliers traveling across different time zones and people who perform shift work. Additionally, our data suggests an explanation for clinical observations, finding shift workers, with irregular sleep/wake schedules, to experience exacerbated inflammatory bowel disease (IBD) due to the effect endogenous misalignment of circadian rhythms has on intestinal homeostasis [26].

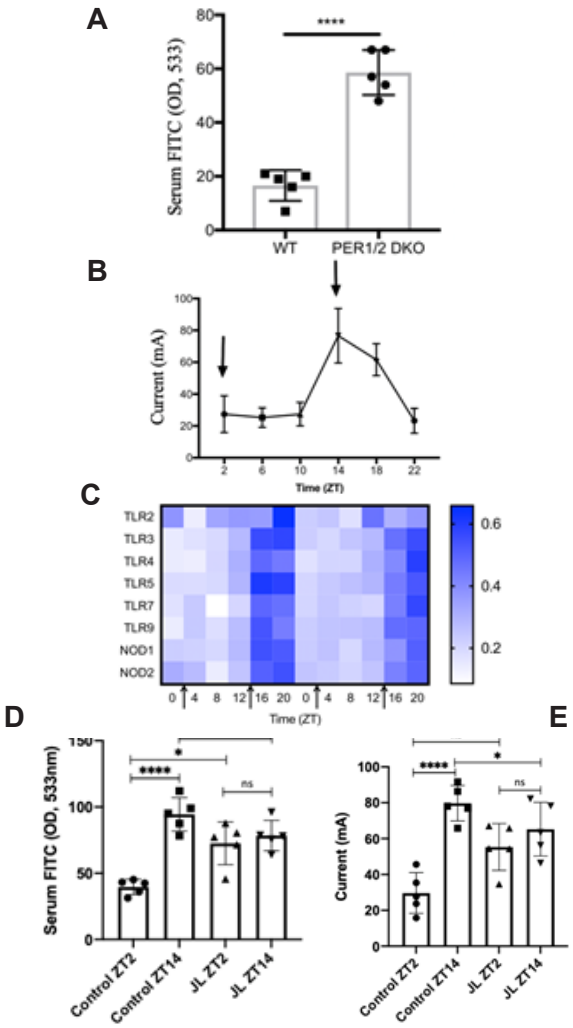

Figure 2. Genetic and Environmental Disruption of Circadian Clocks Impacts Epithelial Barrier Integrity.
(A) FITC (fluorescein isothiocyanate)-dextran recovered from the serum of Per1/2-/- and WT.
(B) Ussing Chamber recording of small intestines from naïve WT over 24 hours. Arrows mark the lowest (ZT2) and highest (ZT14) points of permeability.
(C) PRR stimulation by spleen, liver, serum extracts from naïve WT mice. Arrows mark the lowest (ZT2) and highest (ZT14) points of permeability.
(D) FITC (fluorescein isothiocyanate)-dextran recovered from the serum of jet lag mice and their respective controls.
(E) Ussing Chamber recording of small intestines from jet lag mice and their respective controls.
Means ± SD are plotted. *p < 0.05, **p < 0.01, ***p < 0.001, ****p < 0.0001 by Mann-Whitney U test. Figures 2D and 2E: 2-way ANOVA test.

Metabolic Syndrome Induced by HFD Results in Circadian Disruption and Intestinal Barrier Dysfunction

Metabolic syndromes, like obesity and diabetes, have impacted hundreds of millions of people worldwide and consequently taken the lives of millions annually [25]. Previous studies have uncovered the associations metabolic syndromes have with the functionality of the intes-

tinal barrier, specifically its state of permeability [27]. The study highlights the implications an influx of immune-stimulatory microbial ligands, leaking out of a permeable intestinal barrier can have, such as increased inflammation and risk of infection [27]. However, the tissue under scrutiny was the colon. In our studies, we focused our attention on the small intestine, which one could argue is of more significance due to it being the primary site of nutrient absorption [21]. In order to mimic human dietary habits, which would predispose one to a metabolic syndrome, we fed mice with an HFD for 3 weeks. In a previously referenced chart (Figure 1B), where germ-free mice received fecal transplantation of an HFD microbiome we saw a significant increase in small intestine permeability than mice with a normal diet (NC) microbiome, suggesting that a microbial composition associated with an HFD diet causes intestinal barrier dysfunction.

Previous studies linked circadian rhythm disruption to metabolic syndrome when they found enhanced weight gain and exacerbated glucose intolerance in jet lag mice fed HFD [8]. In an attempt to determine if an HFD would alter permeability in a circadian context we set out to perform another permeability experiment on HFD mice but under circadian conditions. We fed two groups of mice with HFD for 3 weeks. Utilizing the circadian cabinet, each group was placed in different compartments and light-dark cycles were set 12-hours apart at the previously observed lowest and highest times of permeability, ZT2 and ZT14 respectively (Figure 3A). FITC-dextran assay was run and blood was drawn at ZT2 and ZT14 depending on which compartment the mice were in. From the FITC-dextran data we see no significant difference in OD between HFD diet groups which suggests that the altered diet disrupted circadian rhythms (Figure 3B). Additionally, we see OD levels of HFD groups to be at levels closer to Control group ZT14 reaffirming previous data showing increased permeability in HFD mice (Figure 3B). When the Ussing Chamber is performed on small intestine samples, we likewise see no significance between HFD groups and overall HFD permeability levels correlate

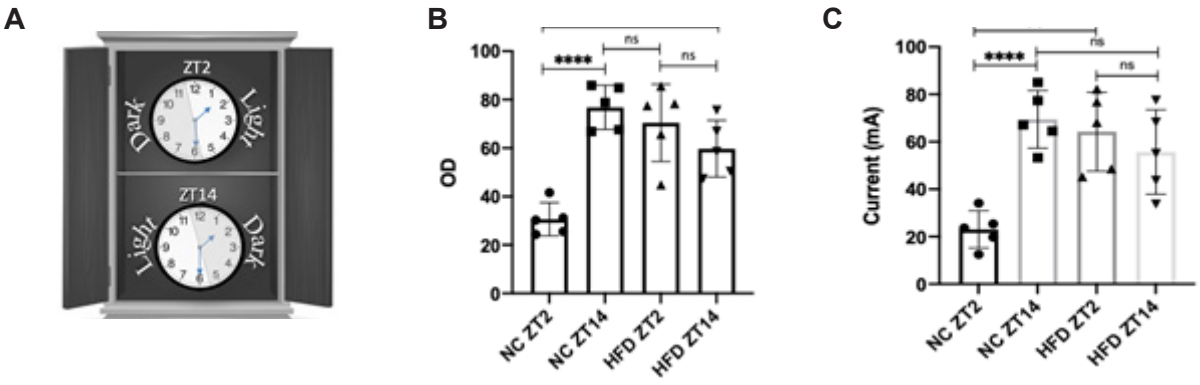

Figure 3. Metabolic Syndrome Induced by HFD Results in Circadian Disruption and Intestinal Barrier Dysfunction.

(A) Schematic showing the typical configuration of a circa-dian cabinet.

(B) FITC (fluorescein isothiocyanate)-dextran recovered from the serum of HFD mice at different ZT times and their respective controls.

(C) Ussing Chamber recording of small intestines of HFD mice at different ZT times and their respective controls.

Means ± SD are plotted. *p < 0.05, **p < 0.01, ***p < 0.001, ****p < 0.0001 by Mann-Whitney U test. Figure 3B and 3C: 2-way ANOVA test.

more strongly with ZT14 than ZT2 (Figure 3C).

Together, these observed results draw attention to a serious issue. Metabolic syndromes, which are usually onset by poor diets such as those high in fat, are only exacerbated by the same stimuli that caused the development of the disease. Our data signifies metabolic syndromes' role in both disrupting circadian rhythms and heightening intestinal barrier permeability that can lead to increased inflammation and infection.

DISCUSSION & CONCLUSION

In this study, we describe that the mammalian intestinal barrier function displays diurnal oscillations and is dependent on microbiome composition. If microbiome composition is distorted, as in the case of antibiotic treatment or HFD, we see alterations in intestinal barrier integrity as well as disruptions in the circadian rhythms of epithelial permeability. While previous studies sought to understand the consequences, diurnal disruption has on microbial composition, here we found direct evidence of the role microbial composition plays in intestinal permeability. Next, we wanted to study the direct implications distorting circadian rhythms, either with genetic clock deficiency or time-shifted induced jet lag, have on intestinal barrier function. We not only found that these conditions significantly impaired the circadian rhythms of permeability, but also, increased overall permeability resulting in greater pathobiont exposure and inflammation. Lastly, we found that inducing metabolic syndromes via HFD intervention disrupts circadian rhythms in the intestinal barrier as well as causes significant barrier dysfunction resulting in increased epithelial permeability.

Altogether, these studies have uncovered numerous future paths. While this study has broadly implicated microbiome composition as a mediator of gut permeability, in order to learn more about the key bacterial players in permeability mediation, we can perform sequencing on the microbial compositions found in our antibiotic treated groups to reveal the unique bacteria having the biggest impact on reducing or increasing permeability. Understanding which bacteria to promote and which to remove in the microbiota could be pivotal in suppressing symptoms in patients with IBD and metabolic syndromes, to name a few, caused by leakages in the intestinal epithelial. Exploiting antibiotic or probiotic treatments to target these bacteria could help combat diseases exacerbated by gut leakiness. Lastly, our observations showing intestinal permeability functioning under diurnal oscillations has applications from drug consumption to nutritional/dietary strategies. Further unravelling the roles, regulators and mechanisms of intestinal permeability could serve to one day aid therapies for illnesses affected by the "leaky gut" syndrome.

AUTHOR INFORMATION

Corresponding Author
*Elisha Pinker
ep2858@columbia.edu

Funding Sources
Columbia College Class of 1939 Fellowship

Competing Interests
The authors declare no competing financial and non-financial interests.

ACKNOWLEDGMENTS

E.P. would like to thank Columbia College and the Weizmann Institute of Science for supporting this research.

REFERENCES

[1] Marietta E, Rishi A, Taneja V. Immunogenetic control of the intestinal microbiota. Immunology. 2015;145(3):313-322. doi:10.1111/imm.12474.

[2] Neish AS. Mucosal Immunity and the Microbiome. Annals of the American Thoracic Society. 2014;11(Suppl 1):S28-S32. doi:10.1513/AnnalsATS.201306-161MG.

[3] Sender R, Fuchs S, Milo R. Revised Estimates for the Number of Human and Bacteria Cells in the Body. PLoS Biology. 2016;14(8):e1002533. doi:10.1371/journal.pbio.1002533.

[4] Clemente, J.C., Ursell, L.K., Parfrey, L.W., and Knight, R. (2012). The impact of the gut microbiota on human health: an integrative view. Cell

[5] Sommer, F., and Backhed, F. (2013). The gut microbiota—masters of host development and physiology. Nat. Rev. Microbiol

[6] Hsiao, E.Y., McBride, S.W., Hsien, S., Sharon, G., Hyde, E.R., McCue, T., Codelli, J.A., Chow, J., Reisman, S.E., Petrosino, J.F., et al. (2013). Microbiota modulate behavioral and physiological abnormalities associated with neurodevelopmental disorders. Cell

[7] Shi N, Li N, Duan X, Niu H. Interaction between the gut microbiome and mucosal immune system. Military Medical Research. 2017;4:14. doi:10.1186/s40779-017-0122-9.

[8] Thaiss C.A., Zeevi D., Levy M., Zilberman-Schapira G., Suez J., Tengeler A.C. Transkingdom control of microbiota diurnal oscillations promotes metabolic homeostasis. Cell. 2014;159(3):514–529

[9] de Groot PF, Frissen MN, de Clercq NC, Nieuwdorp M. Fecal microbiota transplantation in metabolic syndrome: history, present and future. Gut Microbes (2017)

[10] Dibner, C., Schibler, U., and Albrecht, U. (2010). The mammalian circadian timing system: organization and coordination of central and peripheral clocks. Annu. Rev. Physiol.

[11] Keller, M., Mazuch, J., Abraham, U., Eom, G.D., Herzog, E.D., Volk, H.D., Kramer, A., and Maier, B. (2009). A circadian clock in macrophages controls inflammatory immune responses. Proc. Natl. Acad. Sci.

[12] Takahashi JS. Transcriptional architecture of the mammalian circadian clock. Nature reviews Genetics. 2017;18(3):164-179. doi:10.1038/nrg.2016.150.

[13] Buxton, O.M., Cain, S.W., O'Connor, S.P., Porter, J.H., Duffy, J.F., Wang, W., Czeisler, C.A., and Shea, S.A. (2012). Adverse metabolic consequences in humans of prolonged sleep restriction combined with circadian disruption. Sci. Transl. Med

[14] Fonken, L.K., Workman, J.L., Walton, J.C., Weil, Z.M., Morris, J.S., Haim, A., and Nelson, R.J. (2010). Light at night increases body mass by shifting the time of food intake. Proc. Natl. Acad. Sc

[15] Savvidis C, Koutsilieris M. Circadian Rhythm Disruption in Cancer Biology. Molecular Medicine. 2012;18(1):1249-1260. doi:10.2119/molmed.2012.00077.

[16] Scheer, F.A., Hilton, M.F., Mantzoros, C.S., and Shea, S.A. (2009). Adverse metabolic and cardiovascular consequences of circadian misalignment. Proc. Natl. Acad. Sci

[17] Swanson, GR., Burgess, HJ. (2017). Sleep and circadian hygiene and inflammatory bowel disease. Gastroenterology Clinics of North America.46(4):881893. doi:10.1016/j.gtc.2017.08.014

[18] Koch S, Nusrat A. The life and death of epithelia during inflammation: lessons learned from the gut. Ann. Rev. Pathol. 2012;7:35–60. doi: 10.1146/annurev-pathol-011811-120905.

[19] Groschwitz KR, Hogan SP. Intestinal Barrier Function: Molecular Regulation and Disease Pathogenesis. The Journal of allergy and clinical immunology. 2009;124(1):3-22.

doi:10.1016/j.jaci.2009.05.038.

[20] Mu Q, Kirby J, Reilly CM, Luo XM. Leaky Gut As a Danger Signal for Autoimmune Diseases. Frontiers in Immunology. 2017;8:598. doi:10.3389/fimmu.2017.00598.

[21] Kiela PR, Ghishan FK. Physiology of Intestinal Absorption and Secretion. Best practice & research Clinical gastroenterology. 2016;30(2):145-159. doi:10.1016/j.bpg.2016.02.007.

[22] Chakaroun RM, Massier L, Kovacs P. Gut Microbiome, Intestinal Permeability, and Tissue Bacteria in Metabolic Disease: Perpetrators or Bystanders? Nutrients. 2020;12(4). doi:10.3390/nu12041082

[23] Archer, S.N., Laing, E.E., Mo¨ ller-Levet, C.S., van der Veen, D.R., Bucca, G., Lazar, A.S., Santhi, N., Slak, A., Kabiljo, R., von Schantz, M., et al. (2014). Mistimed sleep disrupts circadian regulation of the human transcriptome. Proc. Natl. Acad. Sci

[24] Suwazono, Y., Dochi, M., Sakata, K., Okubo, Y., Oishi, M., Tanaka, K., Kobayashi, E., Kido, T., and Nogawa, K. (2008). A longitudinal study on the effect of shift work on weight gain in male Japanese workers. Obesity

[25] Obesity and Overweight. https://www.who.int/news-room/fact-sheets/detail/obesity-and-overweight. Accessed 20 Dec. 2020.

[26] Nojkov, Borko, et al. “The Impact of Rotating Shift Work on the Prevalence of Irritable Bowel Syndrome in Nurses.” The American Journal of Gastroenterology, vol. 105, no. 4, Apr. 2010, pp. 842–47. PubMed Central, doi:10.1038/ajg.2010.48.

[27] Thaiss CA, Levy M, Grosheva I, Zheng D, Soffer E, Blacher E, et al. Hyperglycemia drives intestinal barrier dysfunction and risk for enteric infection. Science. 2018;359:1376–1

CUSJ
COLUMBIA UNDERGRADUATE SCIENCE JOURNAL

Identification of LncRNAs as Therapeutic Targets in Chronic Lymphocytic Leukemia

Simay Dolaner[1,2], Harpreet Kaur[2], Mohit Mazumder[2], Julia Panov[2,3], Elia Brodsky[2]

[1]Department of Molecular Biology and Genetics, Bahcesehir University, Istanbul, Turkey
[2]Pine Biotech, New Orleans, USA
[3]Tauber Bioinformatics Research Center, Haifa, Israel

KEYWORDS: Chronic Lymphocytic Leukemia, spontaneous regression, therapeutic targets, LncRNAs, transcriptomics

ABSTRACT: Chronic Lymphocytic Leukemia (CLL) is a type of blood cancer that has a very heterogeneous biological background and diverse treatment strategies. However, a small part of this malignancy may disappear without receiving any treatment, known as “spontaneous regression”, which occurs as a result of a poorly investigated mechanism. Exposing the underlying causes of this condition can lead to a novel treatment approach for CLL. In this article, we applied in-silico analysis on total RNA expression data from 24 CLL samples to determine possible regulatory mechanisms of spontaneous regression in CLL. These were first selected by comparing spontaneous regression with progressive samples of CLL at the transcriptional level using two unsupervised machine learning algorithms, i.e., Principal Component Analysis (PCA) and Hierarchical Clustering. Subsequently, the DESeq2 algorithm was used to scrutinize only statistically significant (adjusted p-value < 0.01) RNA transcripts that can differentiate both conditions. Here, at first, we have elucidated 870 significantly differentially expressed protein-coding genes that were involved in the biogenesis and processing of RNA. Consequently, these findings led our study to investigate non-coding RNA, and 33 long non-coding RNAs (lncRNAs) were found to be significantly differentially expressed among two conditions based on differential gene expression analysis. Further, our analysis in the current study suggested lncRNAs, PTPN22-AS1, PCF11-AS1, SYNGAP1-AS1, PRRT3-AS1, and H1FX-AS1 as potential therapeutic targets to trigger spontaneous regression. Ultimately, the results presented here reveal new insights into spontaneous regression and its relationship with non-coding RNAs, particularly lncRNAs.

INTRODUCTION

According to the American Cancer Society statistics, leukemia is the second leading blood cancer, with roughly 60,000 new cases identified in 2020 [1]. Leukemia has different subtypes, which are classified in the context of the tumor origin [2]. The most common variety in adults is chronic lymphocytic leukemia (CLL), which is a lymphoid malignancy due to failed apoptosis and aggressive proliferation of mature B cells [3]. These cells circulate through the blood as non-proliferating cells or arrested cells in the G0/G1 phase of the cell cycle and may affect the function of normal cells in other organs [4].

CLL has a highly diverse biological and clinical background for each patient that determines the stage of the disease [5]. Although there are several stages of CLL classified according to their genetic background and B cell number, one of the most intriguing concepts is known as spontaneous regression, which is the disappearance of the tumor over time either without any treatment or with treatment that is categorized as insufficient to have an impact on the tumor [6].

Spontaneous regression can be seen in 1-2% of all CLL patients, and it is a phenomenon that is poorly understood [7]. In this process, cells that proliferate uncontrollably are transmitted to the quiescent state so that the tumor disappears partially or completely with time [6]. Spontaneous regression is not a common feature of cancer cells and is regulated by mechanisms that are not well-understood. If such mechanisms can be determined, target biological molecules that have a specific role in disease progression can be identified and manipulated in vitro.

Current strategies aim to inhibit BCR signaling, which is crucial for the survival of the B-cells, and chemokine signaling that creates survival signals and attracts leukemic cells to communicate with its microenvironment [5]. Moreover, activation of apoptosis pathways via blocking BCL2 activity, an anti-apoptotic protein, which is highly expressed in leukemic cells, is included in the aforementioned strategies [8]. Although these types of targeted therapies improve the outcome of the patients, the heterogeneity of the leukemia microenvironment reinforces the necessity of new targets. As the targeted therapies may have an impact on tumor surroundings and affect the other cells found in the tumor microenvironment, triggering spontaneous regression mechanisms may improve the strategies as well as patient outcome.

In CLL, the most frequent chromosomal abnormalities and somatic mutations on the protein-coding region of the genome have been distinguished as a result of genomic sequencing, and disrupted cellular pathways are identified using next-generation sequencing of mRNA expression [9]. In spite of this progress, nearly 20% of CLL cells do not show chromosomal abnormalities or genomic variation. Therefore, researchers recently shifted their focus to the non-coding region of the genome and regulatory RNA molecules, especially long non-coding RNAs, which are deregulated in many cancers [10].

Long non-coding RNAs (lncRNAs) are a subgroup of non-coding RNAs which are longer than 200 nucleotides and encompass thousands of diverse transcripts in humans [11]. There are approximately 100,000 known lncRNAs, and this quantity is expanding each year with the new studies [12].

LncRNAs play a significant role in gene regulation, controlling multiple cellular mechanisms involved in tumor progression. They are involved in epigenetic regulation of gene expression via histone modification, DNA methylation, or acetylation. Specifically, these epigenetic regulations may include recruitment of histone remodeling complexes, interaction with histone methyltransferases and demethylases to regulate DNA methylation, or histone acetyltransferases and deacetylases to modulate the acetylation [13]. Furthermore, lncRNAs may regulate gene expression at the transcriptional level by recruiting transcription factors [14]. Moreover, lncRNAs can produce hybrids or act as scaffolds through interaction with proteins to regulate expression at the post-translational level, including regulation of phosphorylation and ubiquitination [15].

In tumor development, lncRNAs can serve as either tumor suppressors, oncogenes, or even both at the same time for some cancer types [16]. Analysis of lncRNA expression patterns had led to the identification of putative biomarkers such as HOTAIR, H19, and DLEU1/2 [17]. Specifically, HOTAIR serves as an oncogene by inducing invasiveness and metastasis in several cancers via recruiting a demethylase [13]. Since this lncRNA is highly expressed in aggressive tumors, it is considered as a bio-

marker and a possible therapeutic target for many cancers [18]. DLEU1/2 epigenetically regulate the tumor suppressors and are deleted in CLL cells, which results in the progression of the CLL. This allows it to serve as a biomarker in the diagnosis [19]. On the other hand, H19 has a dual role in different cancers by stimulating distinct mechanisms through transcription factors, which makes it a target that needs to be studied separately for each cancer [13].

Furthermore, lncRNAs are known to play an important role in cell differentiation and tissue specificity [20]. However, characterization may be compelling because lncRNAs are transcribed in different loci and localized distinctly. More importantly, lncRNA expression is generally tissue-specific and can be detected under certain conditions [21]. As the lncRNAs are differentially expressed, their roles and activities can be identified in disease conditions.

Due to the diverse functions of lncRNAs, novel studies are concentrated on the identification of lncRNAs as therapeutic targets. As the expression of these molecules is tissue and disease-specific, this specificity makes them excellent targets compared to protein-coding genes [22].

In the scope of this project, the trigger mechanism behind the spontaneous regression process is investigated at the transcriptomic level to identify a pattern of lncRNA expression that would explain cell "decision" by comparing CLL tissue at the spontaneous regression and the progressive states.

METHODS

Dataset

The dataset of this project was generated by Kwok et al. (2020) and published as a BioProject on the NCBI with the accession number PRJNA535508 (Supplementary Notes 1) [6]. Transcriptome data contains raw reads of RNA sequencing from the Illumina Nextseq 550 platform by using paired-end sequencing. In this study, the authors compared multiple samples from multiple subtypes of chronic lymphocytic leukemia that can be seen in Table I. In our project, spontaneous regression and progressive states were chosen for further analysis to investigate expression variation specifically involved in the regression mechanism in CLL cells.

Table I. Dataset of the BioProject

Disease State	Number of Samples
Spontaneous Regression	16
Progressive State	8
Indolent State	16
Unmutated State	8
Healthy Condition	3

RNA-seq Raw Data Processing

Raw reads were used to construct an RNA sequencing pipeline that contains pre-processing using Trimmomatic, mapping of reads on reference transcriptome with Bowtie2-t, and quantification using RNA-Seq by Expectation-Maximization (RSEM) algorithms with T-Bioinfo server (Supplementary Notes 1) as represented in Figure 1. Briefly, in order to get gene expression levels, duplicated sequences which resulted in PCR amplification were removed by PCR clean considering best coverage. Then, Trimmomatic was used to remove adaptor sequences and poor-quality data at the end of the sequence. Mapping of these clean reads on transcriptome was performed by using the Bowtie2-t algorithm based on the reference genome (GRCh38). Bowtie2-t is an option of the Bowtie, which is a mapping algorithm and aligns short reads according to the seed approach [23]. Finally, for the quantification of gene expression, the RSEM algorithm was used with FPKM normalization to obtain the gene expression table.

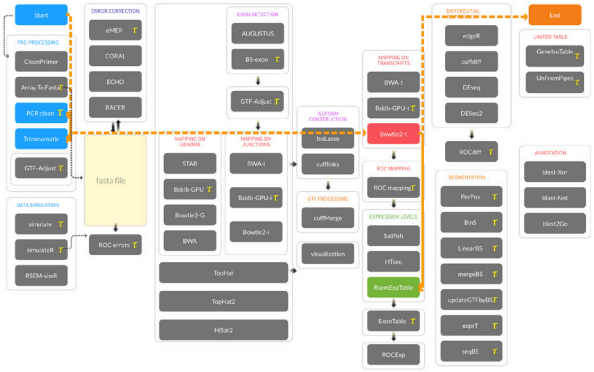

Figure 1: RNA-seq Data Processing Pipeline to generate an RNA expression table on T-Bioinfo Server

Exploratory Analysis

Exploratory analysis facilitated the examination of variation between all samples, including healthy and diseased patients, in order to select a comparison parameter for further analysis. Thus, the visual outputs were used to determine the patterns. Data was explored by using principal component analysis (PCA), which is a dimensionality reduction technique that discerns the variability between the samples [24]. PCA was performed twice, both for all the samples and for the spontaneous regression and the progressive samples to be able to observe the improvement on principle components. Hierarchical Clustering, which finds patterns among the samples using similarity measures [25], made it possible to understand the clustering aspects of spontaneous regression and progressive samples based on their gene expression, especially after the selection of statistically significant genes, which will be explained in the following section.

Differential Gene Expression Analysis

The Differential Gene Expression analysis was conducted by contrasting spontaneous regression with progressive CLL samples. Separate studies were performed for protein-coding and non-protein coding transcripts to understand the mechanisms involved in spontaneous regression. The differential gene expression (DGE) pipeline, which includes pre-processing, mapping with HiSat2, RNA expression quantification using HTseq, and differential gene expression analysis with DESeq2 algorithm was constructed by using the T-Bioinfo server (Figure 2). Here, initially, PCR cleaning was performed by considering coverage to get rid of the duplicated sequences generated via PCR amplification. To eliminate the adaptors and bad quality sequences from the data, the Trimmomatic algorithm was used. Next, the HiSat2 was utilized for the mapping of sequence reads to the reference genome (GRCh38) by taking into account the splice junctions. Then, the HTseq algorithm quantified the gene expression through overlapping reads and generated a gene expression table in the form of count values. Finally, differential gene expression analysis was performed by using the DESeq2 algorithm which gives the expression differences between two groups using the shrinkage estimators [26]. DESeq2 provides results, which include p-value, log 2-fold change, and adjusted p-value. Then, an adjusted p-value or False Discovery Rate (FDR) that is a standard statistical value utilized for multiple testing correction, is calculated to eliminate the false-positive results [26, 27].

The T-Bioinfo server uses a one-step approach for DGE analysis and combines several methods. Although DESeq2 can be used for both normalization and statistical analysis, the T-Bioinfo server provides an additional approach, which includes gene set enrichment analysis (GSEA) to discover related pathways and processes [28].

Selection of Significant Genes

The significant genes were identified by their p-adjusted values and log2 fold change. The determined threshold for the adjusted p-value was 0.01 and the log2 fold change was ±1 in non-coding RNAs and ±1.5 in protein-coding genes.

Figure 2: Differential Gene Expression Analysis Pipeline Using the T-Bioinfo Server

Gene Ontology Analysis

The enrichment analysis was done via using the Enrichr platform for the protein-coding genes [29]. Respectively, the GO and KEGG pathways were considered for the observed upregulated and downregulated genes in spontaneous regression samples.

Data Visualization

The gene expression patterns were observed by heatmaps. Furthermore, PCA and H-Clustering were repeated with the selected significant RNA transcripts to make a comparison as before and after, and see an improvement on the basis of variance. Visualization was performed independently for protein-coding genes and non-protein coding genes.

RESULTS

Variation is Detected Between Spontaneous Regression and the Progressive Samples

The exploratory analysis using the PCA revealed that there was a variation between the spontaneous regression and the progressive state.

Based on Figure 3A, it can be seen that healthy samples and the diseased samples are well separated, which means there is significant variation between these groups. When the spontaneous regression and progressive samples were examined in a specific scatter plot, it was obvious that there was an improvement in principal components, and the two groups were clearly separated from each other (Figure 3B). After the observed variation between the two groups, the reason for this difference and its impacts could be investigated at the level of gene regulation.

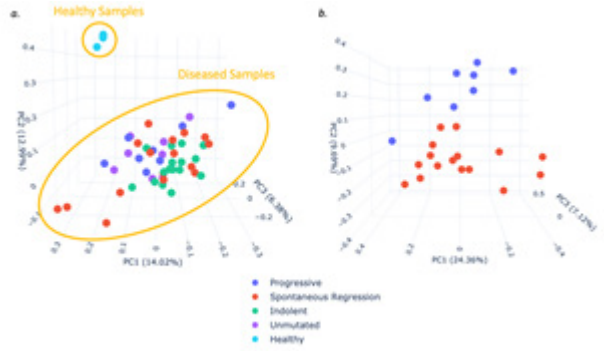

Figure 3. Principal Component Analysis, (A) Healthy samples versus Diseased samples (B) Spontaneous Regression (Red) versus Progressive Samples (Purple)

Revealed Pathways Involved in Biogenesis and Processing of RNA

Based on DESeq2 analysis, expression levels of 870 protein-coding genes were identified as significantly different between the two groups with p-adjusted values (<0.01) and log2 fold change (+/- 1.5) (Supplementary Table 1). The heatmap of the protein-coding genes shows the gene expression patterns between spontaneous regression and progressive samples (Figure 4A). It is obvious that most of the genes were upregulated in spontaneous regression while they downregulated in progressive ones. To understand the biological importance of pathways, gene ontology analysis was performed. Interestingly, although there were different pathways in upregulated genes, many represented biological pathways involved in biogenesis and processing of RNA, and mRNA translation (Figure 4B). In addition, identified pathways also included ribosome-related pathways, which imply translation of protein-coding RNAs is affected. The same concept could be detected with

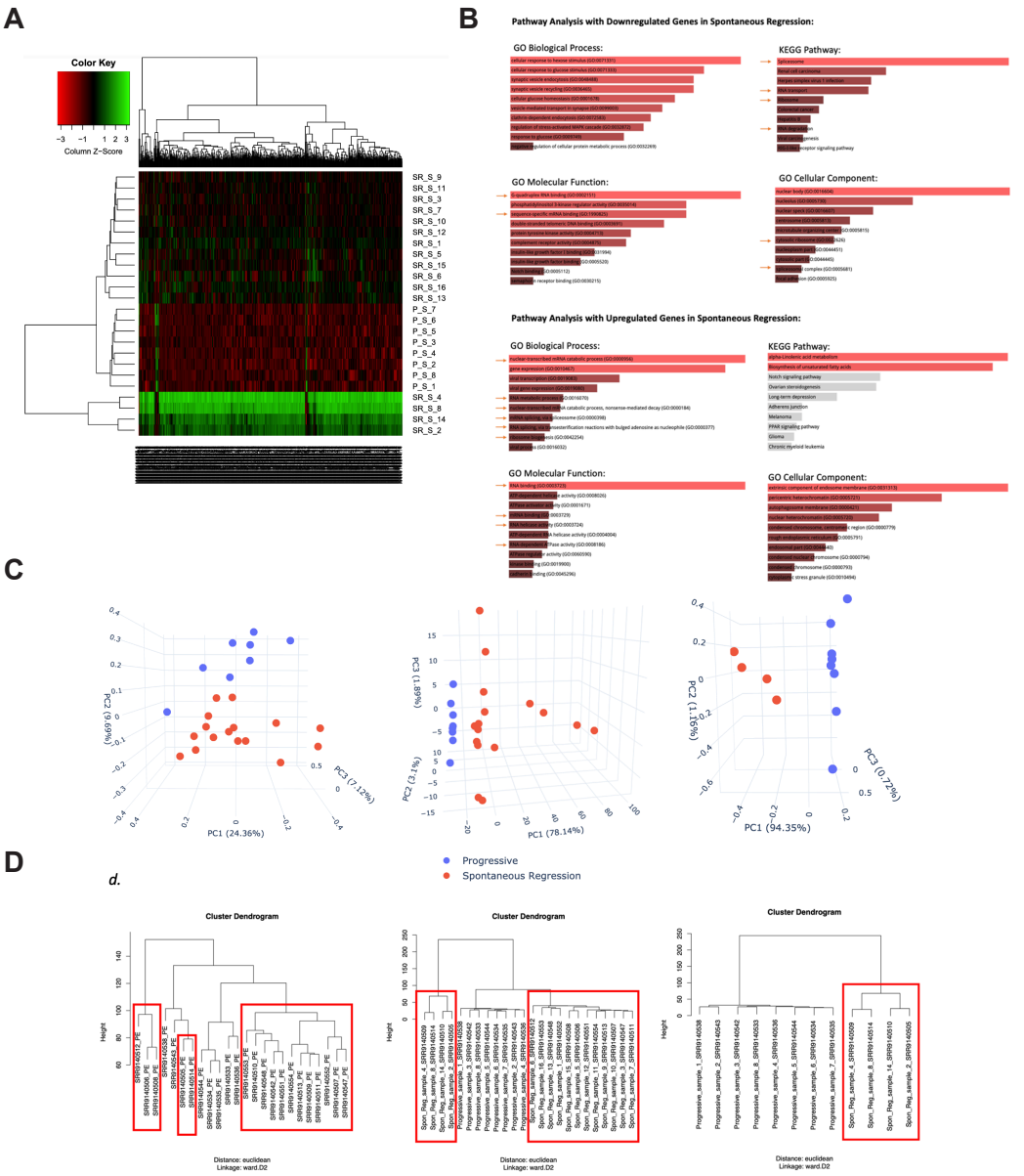

Figure 4. Data visualization of protein-coding genes

(A) Gene expression patterns of protein-coding genes. Heatmap exposes the downregulated and upregulated genes among the samples

(B) Gene ontology analysis of protein-coding genes. Pathway analysis shows the downregulated and upregulated pathways in the spontaneous regression samples, respectively. Arrows indicate the RNA related pathways

(C) Representation of principal component analysis with 3D scatter plots. First PCA shows the separation of spontaneous regression (SR) and progressive (P) samples before the selection of the protein-coding genes, second PCA represents the separation of SR and P samples after the selection of the protein-coding genes, and last PCA indicates the true variability source considering four outliers

(D) Hierarchical Clustering results as dendrograms. Each dendrogram point out the related scatter plots that are placed above and reveal the clustering perspective. Red boxes indicate the SR samples, and the other ones are the P samples

the downregulated genes as presented in Figure 4B. Consequently, these findings led this research to investigate the non-coding RNAs, which was the second branch of this study.

There was a Diversity Among the Spontaneous Regression Samples

According to the first principal component, spontaneous regression had a lot of variability within its own group (Figure 4C). This variation could be observed from the dendrograms in Figure 4D. Correspondingly, spontaneous regression samples had two diverse groups. The clinical data of these samples, therefore, needed to be examined to interpret them as outliers or true variability sources. However, no difference was detected between the four outliers and the other samples. This meant the difference had to be in their biological background. That is why these four diverse samples were selected in comparison with progressive samples to see the most significant difference between the two groups in the context of expression patterns.

As a result, it can be seen in Figure 4C that there was a significant improvement with the well-separated two groups after the selection of true variability source. Additionally, better separation could also be observed from the dendrogram in Figure 4D that four samples and the progressive samples have distinct branches compared to the remaining twelve samples.

Identified Non-Coding RNAs were Novel Transcripts

Based on differential gene expression analysis, 33 lncRNAs, which are significantly expressed, were identified with the specific parameters (Supplementary Table 2). Each lncRNA was investigated by their Ensembl ID and identified as novel transcripts. When the PCA was repeated with selected lncRNAs, clear separation could be seen among the spontaneous regression and the progressive samples (Figure 5A). Even though there was no dramatic improvement in principal components, hierarchical clustering results were highly distinctive. It can be seen in Figure 5B that the two groups cluster separately in the dendrogram, which implies these significant genes might predict tumor characteristics.

To be able to observe the gene expression pattern of the lncRNAs, a heatmap was generated. As shown in Figure 5C, most of the genes were upregulated in progressive samples compared to spontaneous regression.

So far, pathway analysis of differentially expressed protein-coding genes in spontaneous regression samples has demonstrated that global gene expression in these samples might be modulated at the transcriptional and post-transcriptional level, and non-protein coding genes have shown that lncRNAs are differentially expressed in these samples. To make a biologically relevant interpretation, the analysis will regard lncRNAs identified as statistically most significant.

DISCUSSION

Although spontaneous tumor regression is rare, it is a phenomenon that can be observed in some types of cancer, such as neuroblastoma, renal cell carcinoma, lung cancer, lymphoma, and leukemia [30]. To be able to increase the occurrence rate of this mechanism, detailed studies should be conducted, and the related pathways should be examined.

In summary, we used RNA-seq datasets from CLL patients containing a total of 16 spontaneous regression and 8 progressive state samples. First of all, we looked for variation and pattern among these two groups by using PCA and H-Clustering based on gene expression. After the detection of variation, we hypothesized that the reason for this difference should be at the gene expression level. Therefore, we applied differential gene expression analysis by comparing spontaneous regression and progressive tumor states. We identified 870 protein-coding genes which were significantly differentially expressed and also were associated with RNA-related pathways based on gene ontology analysis. Depending on these findings, we also investigated non-coding RNAs and

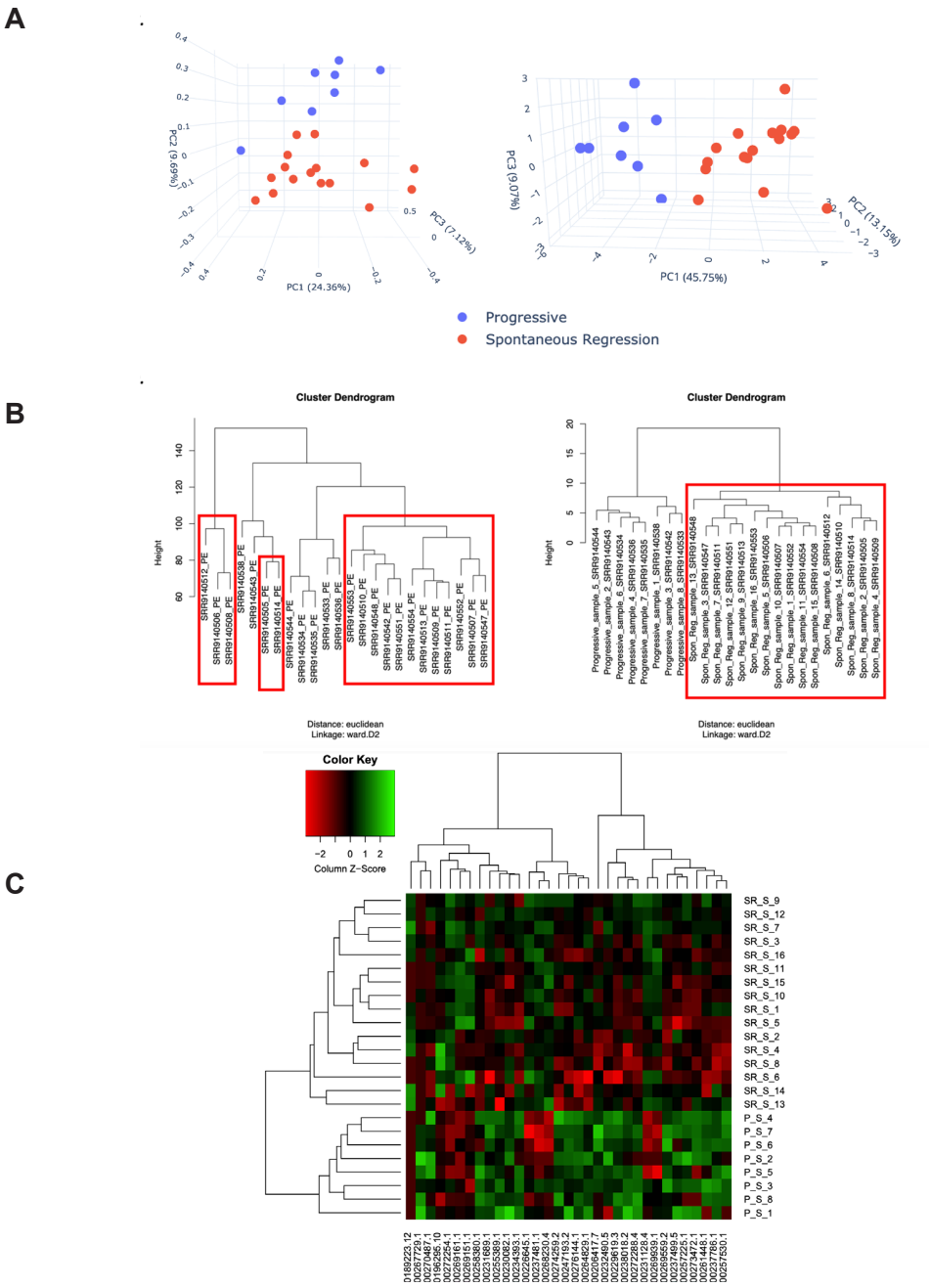

Figure 5. Data visualization of non-coding RNAs

(A) Representation of principal component analysis with 3D scatter plots. Initial PCA indicates the separation of spontaneous regression (SR) and progressive (P) samples before the selection of the non-coding RNAs and second PCA shows the separation of SR and P samples after the selection of the non-coding RNAs

(B) Hierarchical Clustering results as dendrograms. Each dendrogram specify the related scatter plots that are located above and expose the clustering perspective. Red boxes demonstrate the SR samples, and the other ones are the P samples

(C) Gene expression patterns of non-coding RNAs. Heatmap represents the downregulated and upregulated genes between the samples

identified significantly expressed 33 lncRNAs. This paper has highlighted that new therapeutic strategies may involve lncRNAs to trigger the spontaneous regression phenomena in cancer cells. Since the lncRNAs can regulate the important cellular mechanisms during cancer progression, identification of disease-specific lncRNAs may enlighten the way of new treatment strategies. Therefore, a detailed literature review for each lncRNA and their sense mRNAs had been done. Even though the detailed explanation can be found in Supplementary Table 2, identified lncRNAs are involved in several pathways including tumor growth, metastasis, cell survival, and regulation of the tumor microenvironment such as the immune system.

Previous studies showed that identified two lncRNAs, the PRRT3-AS1 and H1FX-AS1, were focused on cancer progression [31, 32, 33, 34]. Both lncRNAs were upregulated in the progressive state compared to spontaneous regression, which indicates that these lncRNAs were functioning as tumor enhancers in CLL cells. Li et al. (2020) showed that the lncRNA PRRT3-AS1 is upregulated in prostate cancer and targets the PPARγ gene by binding its 3' end, which leads to regulation of the Akt/mTOR signaling pathway [31]. The same study also revealed that the down-regulation of PRRT3-AS1 inhibits prostate cancer progression by regulating cell proliferation, migration, and apoptosis. Moreover, knocking down this lncRNA triggers autophagy via the mTOR pathway [31]. Another study suggested that PRRT3-AS1 is estimated as an immune-related lncRNA involved in PPAR signaling and can be used as a potential target in glioblastoma [32]. In light of these findings, it can be said that the PRRT3-AS1 functions as a tumor promoter gene in prostate cancer and glioblastoma. Since it is revealed that this lncRNA is highly expressed in the progressive state of CLL, further studies may clarify the related pathways and novel targets. Moreover, downregulation of this lncRNA might promote spontaneous regression by repressing cell proliferation and inducing apoptosis.

According to Shi et al. (2020), lncRNA H1FX-AS1 is downregulated in cervical cancer, and low expression is correlated with poor prognosis and linked to tumor size as well as metastasis. In silico analysis predicted that the possible target of the H1FX-AS1 was the miR-324-3p, and it was binding and regulating the DACT1 [33]. Furthermore, the same research included overexpression studies, which revealed that the high expression levels of this lncRNA significantly reduced the proliferation and invasiveness, and activated the apoptosis pathways. H1FX-AS1, therefore, is identified as a tumor suppressor gene in cervical cancer [33]. On the contrary, high expression levels of lncRNA H1FX-AS1 are associated with a poor prognosis in gastric cancer. It is predicted that this lncRNA was related to epithelial to mesenchymal transition (EMT) and metastasis pathways [34]. Additionally, in-silico prediction analysis indicated several targets of the H1FX-AS1 lncRNA, such as H1FX, COPG1, and MIR6826 that can be used as potential therapeutic targets in gastric cancer [34]. Since H1FX-AS1 is upregulated in the progressive state of CLL, the precise roles of this lncRNA should be examined for CLL cells. Besides, considering the studies on gastric cancer, downregulation of H1FX-AS1 may trigger the spontaneous regression through inactivation of metastasis.

As the other 31 lncRNAs were novel transcripts, several examples could be considered by examining the sense protein-coding genes of the lncRNAs to reveal the significance and possible functions of these lncRNAs. Thereby, the specified lncRNAs and their sense protein-coding genes can be targeted for further analysis and treatment strategies.

The first one is the lncRNA PTPN22-AS1 that was upregulated in the spontaneous regression samples. It is known that the B cell receptor signaling is vital for the growth and survival of the leukemic cells [35]. These signaling pathways can be stimulated with diverse tyrosine kinases as well as phosphatases. PTPN22 is a protein tyrosine phospha-

tase specifically expressed in immune cells. It can function as an enhancer or suppressor of BCR and TCR signaling by regulating phosphorylation status [36]. According to studies, the PTPN22 gene is upregulated in CLL cells, and this upregulation results in attenuation of the apoptosis signals produced by the BCR and stimulation of the AKT activity that generates a survival signal [35]. This regulation reveals that the cancer cells which express autoreactive BCRs can escape from apoptosis by upregulating the PTPN22 gene. Therefore, downregulation of this gene through the lncRNA PTPN22-AS1 at multiple levels may trigger the spontaneous regression in CLL by eliminating autoreactive B cells in the context of immune tolerance. So, if the upregulation of this lncRNA can be induced by an external factor, it could be used as a therapeutic target for CLL cells.

The next lncRNA would be PCF11-AS1, and it is also upregulated in spontaneous regression. Alternative polyadenylation (APA) leads to transcription of diverse isoforms at the RNA 3' end that affects the functioning of encoded proteins. This mechanism needs multicomponent protein complexes, and one of the protein complexes is called CFII [37]. This complex comprises the PCF11 gene that is a cleavage and polyadenylation factor subunit, and regulates the transcription termination and RNA 3' end maturation. Studies show that this gene particularly regulates the alternative polyadenylation of the genes associated with the WNT pathway as an oncogene in neuroblastoma cells [38]. Accordingly, the downregulation of this gene results in diminished cell growth as well as invasiveness. Interestingly, one of the studies indicates that spontaneously regressed neuroblastomas express the PCF11 gene at low levels compared to highly progressive neuroblastomas [39]. Basically, downregulation of this gene at the epigenetic or post-transcriptional level through the lncRNA PCF11-AS1 may induce the spontaneous regression in CLL via ceasing the cell growth. Thus, the upregulation of this lncRNA can be used as a therapeutic strategy.

Another lncRNA is the SYNGAP1-AS1 which is upregulated in progressive samples. Mutant RAS genes stimulate the GTP-bound state which constitutively activates RAS signaling in metastatic cells [40]. RasGAPs inactivate RAS signaling by converting active GTP-bound into its inactive state [41]. SYNGAP1, also known as RASA5, is a member of the RasGAP family and functions as a tumor suppressor gene [42, 43]. Studies proved that the RASA5 gene is epigenetically disrupted in multiple cancer types by promoter methylation, and gain of function assays exposed that RASA5 expression leads to a reduction in metastasis by regulating EMT and cell stemness [43]. As it is known that the lncRNAs can regulate gene expression at the epigenetic level through methylation, this epigenetic silencing may be due to the lncRNA SYNGAP1-AS1. So, the upregulation of the SYNGAP1-AS1 can knock down this gene at the epigenetic level by methylating the promoter region leading to aggressive tumor progression in CLL patients. Even though further studies are essential, targeting this lncRNA may also trigger spontaneous regression through metastasis and cell stemness pathways, and enhance our understanding of this mechanism. As a result, the deduction that can be made from these exemplary lncRNAs is that the detailed examination of the identified novel transcripts can be used to reveal the mechanisms that lead to spontaneous regression, as well as to identify these lncRNAs as targets for small molecule inhibitors or activators so that the spontaneous regression mechanism can be triggered in other cancer types.

CONCLUSION

These findings suggest that regulation through the lncRNAs might have a major role in cells' fate, and their detailed examination can enlighten the way of discovery of the possible therapeutic targets. In prospective studies, each lncRNA should be investigated to perceive their functional pathways by over-expression and suppression studies in various cancer types

in order to understand their specific roles. Additionally, the following study which considers these findings should combine the protein-coding genes and non-protein coding genes. Since these two groups revealed significant results independently, their combination can lead to future selection and determination of particular pathways which affected each other.

This study had certain limitations that need to be overcome to conduct more efficient studies. Spontaneous regression samples had diverse biological backgrounds, which increased the demand for the detailed investigation of these samples. Furthermore, it was problematic to identify the significant pathways through differential gene expression algorithms due to this variability. Finally, as the amount of the samples was limited, more comprehensive research is required to verify these findings and make a distinctive interpretation.

AUTHOR INFORMATION

Corresponding Author
*Simay Dolaner (College of Engineering and Natural Sciences, Department of Molecular Biology and Genetics, Bahcesehir University, Istanbul, Turkey)
simay.dolaner@bahcesehir.edu.tr

Author Contributions
Simay Dolaner performed the data analysis and produced the figures and manuscript. Dr. Harpreet Kaur provided technical assistance with analysis and pipelines. Elia Brodsky and Dr. Mohit Mazumder added project direction and provided guidance. Dr. Julia Panov provided expert feedback for the project.

Competing Interests
The authors declare no competing financial and non-financial interests.

SUPPLEMENTARY DOCUMENTS

Supplementary Notes 1, which includes external sources and related links mentioned in the Methods section, can be found in the following link.
https://www.dropbox.com/s/mlo17y1yjdxfekm

The list of the significantly differentially expressed protein-coding genes can be found in Supplementary Table 1 through the following link.
https://www.dropbox.com/s/zc1oaryr3zyhxlf

Supplementary Table 2, which contains the name, Ensembl ID, and the possible functions of the 33 significant lncRNAs, can be found in the following link.
https://www.dropbox.com/s/4p67jf4d54if2b8

ACKNOWLEDGMENTS

This research was performed within the framework of a research fellowship program and was supported by Pine Biotech. Data processing and visualization pipelines were run with the T-Bioinfo Server. I would like to thank Elia Brodsky, Dr. Harpreet Kaur, Dr. Mohit Mazumder, and Dr. Julia Panov for their expertise and guidance throughout the project.

ABBREVIATIONS

CLL: Chronic Lymphocytic Leukemia
NCBI: National Center for Biotechnology Information
BCR: B Cell Receptor
TCR: T Cell Receptor
PCA: Principal Component Analysis
H-Cluster: Hierarchical Clustering
GO: Gene Ontology
KEGG: Kyoto Encyclopedia of Genes and Genomes
lncRNA: Long Non-Coding RNA
PRRT3-AS1: Antisense to PRRT3
H1FX-AS1: Antisense to H1FX
PTPN22-AS1: Antisense to PTPN22
PCF11-AS1: Antisense to PCF11
SYNGAP1-AS1: Antisense to SYNGAP1
EMT: Epithelial to Mesenchymal Transition

REFERENCES

[1] American Cancer Society. Cancer Statistics Center. https://cancerstatisticscenter.cancer.

org. 2020

[2] A. A. Ferrando, C. López-Otín, Clonal evolution in leukemia. Nature Medicine, 23(10), 1135–1145. doi:10.1038/nm.4410 (2017).

[3] M. V. Haselager, A. P. Kater, E. Eldering, Proliferative Signals in Chronic Lymphocytic Leukemia; What Are We Missing? Frontiers in Oncology, 10(), 592205–. doi:10.3389/fonc.2020.592205 (2020).

[4] G. Fabbri, R. Dalla-Favera, The molecular pathogenesis of chronic lymphocytic leukaemia. Nature Reviews Cancer, 16(3), 145–162. doi:10.1038/nrc.2016.8 (2016).

[5] D. L. Longo, J. A. Burger, Treatment of Chronic Lymphocytic Leukemia. New England Journal of Medicine, 383(5), 460–473. doi:10.1056/NEJMra1908213 (2020).

[6] M. Kwok et al., Integrative analysis of spontaneous CLL regression highlights genetic and microenvironmental interdependency in CLL. Blood, 135 (6): 411–428. doi: https://doi.org/10.1182/blood.2019001262 (2020).

[7] J. Delgado, F. Nadeu, D. Colomer, E. Campo, Chronic lymphocytic leukemia: from molecular pathogenesis to novel therapeutic strategies. Haematologica, 105:xxx doi:10.3324/haematol.2019.236000 (2020).

[8] T. J. Kipps, M. Y. Choi, Targeted Therapy in Chronic Lymphocytic Leukemia. Cancer journal (Sudbury, Mass.), 25(6), 378–385. https://doi.org/10.1097/PPO.0000000000000416 (2019).

[9] F. Bosch, R. Dalla-Favera, Chronic lym-phocytic leukaemia: from genetics to treatment. Nat Rev Clin Oncol, 16, 684–701 https://doi.org/10.1038/s41571-019-0239-8 (2019).

[10] L. Fabris, J. Juracek, G. Calin, Non-Coding RNAs as Cancer Hallmarks in Chronic Lymphocytic Leukemia. Interna-tional Journal of Molecular Sciences, 21(18), 6720–. doi:10.3390/ijms21186720 (2020).

[11] J. Fernandes, et al., Long Non-Coding RNAs in the Regulation of Gene Expres-sion: Physiology and Disease. Non-coding RNA, 5(1), 17. https://doi.org/10.3390/ncrna5010017 (2019).

[12] L. Nobili, D. Ronchetti, E. Taiana, A. Neri, Long non-coding RNAs in B-cell malig-nancies: a comprehensive overview. On-cotarget, 8(36), –. doi:10.18632/oncotarget.17303 (2017).

[13] M. Aprile, V. Katopodi, E. Leucci, V. Cos-ta, LncRNAs in Cancer: From garbage to Junk. Cancers, 12(11), 3220. https://doi.org/10.3390/cancers12113220 (2020).

[14] M. Gourvest, P. Brousset, M. Bousquet, Long Noncoding RNAs in Acute Myeloid Leukemia: Functional Characterization and Clinical Relevance. Cancers, 11(11), 1638. https://doi.org/10.3390/cancers11111638 (2019).

[15] X. Zhang, et al., Mechanisms and Functions of Long Non-Coding RNAs at Multi-ple Regulatory Levels. International jour-nal of molecular sciences, 20(22), 5573. https://doi.org/10.3390/ijms20225573 (2019).

[16] M. A. Diamantopoulos, P. Tsiakanikas, A. Scorilas, Non-coding RNAs: the riddle of the transcriptome and their perspectives in cancer. Annals of translational medi-cine, 6(12), 241. https://doi.org/10.21037/atm.2018.06.10 (2018).

[17] J. Gao, F. Wang, P. Wu, Y. Chen, Y. Jia, Aberrant LncRNA Expression in Leuke-mia. Journal of Cancer, 11(14), 4284–4296. https://doi.org/10.7150/jca.42093 (2020).

[18] Q. Tang, S. S. Hann, HOTAIR: An Onco-genic Long Non-Coding RNA in Human Cancer. Cellular Physiology and Biochem-istry, (), 893–913. doi:10.1159/000490131 (2018).

[19] Y. Chi, D. Wang, J. Wang, W. Yu, J. Yang, Long Non-Coding RNA in the Pathogene-sis of Cancers. Cells, 8(9), 1015. https://doi.org/10.3390/cells8091015 (2019).

[20] J. Iwakiri, G. Terai, M. Hamada, Computa-tional prediction of lncRNA-mRNA inter-actions by integrating tissue specificity in human transcriptome. Biology Direct 12, 15 https://doi.org/10.1186/s13062-017-0183-4 (2017).

[21] G. M. Cruz-Miranda, et al., Long Non-Coding RNA and Acute Leuke-mia. International journal of molecular sciences, 20(3), 735. https://doi.org/10.3390/ijms20030735 (2019).

[22] G. Arun, S. D. Diermeier, D. L. Spector, Therapeutic Targeting of Long Non-Coding RNAs in Cancer. Trends in molecu-lar medicine, 24(3), 257–277. https://doi.org/10.1016/j.molmed.2018.01.001 (2018).

[23] B. Langmead, S. Salzberg, Fast gapped-read alignment with Bowtie 2. Nat Meth-ods 9, 357–359 (2012). https://doi.org/10.1038/nmeth.1923

[24] J. Lever, M. Krzywinski, N. Altman, Points of Significance: Principal component analysis. Nature Methods, 14(7), 641–642 (2017). doi:10.1038/nmeth.4346

[25] N. Altman, M. Krzywinski, Points of Sig-nificance: Clustering. Nature Methods, 14(6), 545–546 (2017). doi:10.1038/nmeth.4299

[26] M. I. Love, W. Huber, S. Anders, Moderat-ed estimation of fold change and dis-per-sion for RNA-seq data with DESeq2. Ge-nome Biol 15, 550 (2014). https://doi.org/10.1186/s13059-014-0550-8

[27] Y. Benjamini, Y. Hochberg, Controlling the False Discovery Rate: A Practical and Powerful Approach to Multiple Testing. Journal of the Royal Statistical Society: Series B (Methodological), 57: 289-300 (1995). https://doi.org/10.1111/j.2517-6161.1995.tb02031.x

[28] A. Subramanian, et al., Gene set enrich-ment analysis: A knowledge-based approach for interpreting genome-wide ex-pression profiles. Proceedings of the Na-tional Academy of Sciences, 102(43), 15545–15550. doi:10.1073/pnas.0506580102 (2005).

[29] M. V. Kuleshov, et al., Enrichr: a compre-hensive gene set enrichment analysis web server 2016 update. Nucleic acids re-search, 44(W1), W90–W97. https://doi.org/10.1093/nar/gkw377 (2016).

[30] P. Ghatalia, C. J. Morgan, G. Sonpavde, Meta-analysis of regression of advanced solid tumors in patients receiving placebo or no anti-cancer therapy in prospective trials. Critical Reviews in Oncolo-gy/Hematology, 98(), 122–136. doi:10.1016/j.critrevonc.2015.10.018 (2016).

[31] L. Fan, H. Li, W. Wang, Long noncoding RNA PRRT3-AS1 silencing inhibits pros-tate cancer cell proliferation and promotes apoptosis and autophagy. Experimental Physiology, (), EP088011–. doi:10.1113/ep088011 (2020).

[32] X. Li, M. Yutong, Immune-Related lncRNA Risk Signatures Predict Survival of IDH Wild-Type and MGMT Promoter Unmethylated Glioblastoma, BioMed Re-search International, vol. 2020, Article ID 1971284, 11 pages, https://doi.org/10.1155/2020/1971284 (2020).

[33] X. Shi, et al. A newly identified lncRNA H1FX-AS1 targets DACT1 to inhibit cervi-cal

cancer via sponging miR-324-3p. Can-cer Cell Int 20, 358 https://doi.org/10.1186/s12935-020-01385-7 (2020).

[34] E. Delshad, et al. In-silico identification of novel lncRNAs with a potential role in di-agnosis of gastric cancer, Journal of Bio-molecular Structure and Dynamics, (), 1–9. DOI: 10.1080/07391102.2019.1624615 (2019).

[35] R. Negro, et al., Overexpression of the au-toimmunity-associated phosphatase PTPN22 promotes survival of antigen-stimulated CLL cells by selectively activat-ing AKT. Blood, 119(26), 6278–6287. https://doi.org/10.1182/blood-2012-01-403162 (2012).

[36] R. Cubas, et al., Autoimmunity linked protein phosphatase PTPN22 as a target for cancer immunotherapy. Journal for Im-munoTherapy of Cancer, 8(2), e001439–. doi:10.1136/jitc-2020-001439 (2020).

[37] S. W. Yang, et al., A Cancer-Specific Ubiq-uitin Ligase Drives mRNA Alternative Pol-yadenylation by Ubiquitinating the mRNA 30 End Processing Complex, Molecular Cell, 77(6), 1206–1221.e7. https://doi.org/10.1016/j.molcel.2019.12.022 (2020).

[38] J. Nourse, S. Spada, S. Danckwardt, Emerging Roles of RNA 3′-end Cleavage and Polyadenylation in Pathogenesis, Di-agnosis and Therapy of Human Disorders. Biomolecules, 10(6), 915. doi:10.3390/biom10060915 (2020).

[39] A. Ogorodnikov, et al., Transcriptome 3′end organization by PCF11 links alterna-tive polyadenylation to formation and neu-ronal differentiation of neuroblasto-ma. Nature communications, 9(1), 5331. https://doi.org/10.1038/s41467-018-07580-5 (2018).

[40] M. H. Berryer, et al., Decrease of SYNGAP1 in GABAergic cells impairs in-hibitory synapse connectivity, synaptic in-hibition and cognitive function. Nature communications, 7, 13340. https://doi.org/10.1038/ncomms13340 (2016).

[41] O. Maertens, K. Cichowski, An expanding role for RAS GTPase activating proteins (RAS GAPs) in cancer. Advances in Bio-logical Regulation, 55(), 1–14. doi:10.1016/j.jbior.2014.04.002 (2014).

[42] M. Berryer, et al. Decrease of SYNGAP1 in GABAergic cells impairs inhibitory syn-apse connectivity, synaptic inhibition and cognitive function. Nature Communica-tions 7, 13340 https://doi.org/10.1038/ncomms13340 (2016).

[43] L. Li, et al., Tumor Suppression of Ras GTPase-Activating Protein RASA5 through Antagonizing Ras Signaling Perturbation in Carcinomas. iScience, 21, 1–18. doi:10.1016/j.isci.2019.10.007 (2019).

CUSJ
COLUMBIA UNDERGRADUATE SCIENCE JOURNAL

Effect of Eccentricity in Microwave Imaging of Multiple Composite Pipes

Yuki Gao*[1], Noshin Raisa[1], and Reza K. Amineh[1]

[1]Department of Electrical and Computer Engineering, New York Institute of Technology, New York, NY, USA

KEYWORDS: Eccentricity effect, microwave imaging, non-destructive testing, non-metallic pipes

ABSTRACT: The use of non-metallic composites that are durable, low cost, and lightweight is growing fast in various industries. In the oil and gas industry, a commonly used form of these materials is in the shape of pipes. Such pipes can be damaged due to material loss (defects and holes), erosions, and more which may cause major production failures or environmental mishaps. To prevent these issues, non-destructive testing (NDT) methods need to be employed for regular inspections of such components. Since traditional NDT methods are mainly used for metallic pipes, microwave imaging has recently been proposed as a promising approach for examination of non-metallic pipes. While microwave imaging can be employed for inspection of multiple layers of pipes, the effect of undesired eccentricity of the pipes (undesired distance between the centers of multiple pipes which are supposed to be concentric) can impose additional imaging errors. In this paper, for the first time, we study the effect of eccentricity of the pipes on the images reconstructed using near-field holographic microwave imaging on double pipes through simulations. To have a realistic study, we add artificial noise to the simulated data.

INTRODUCTION

Recently, non-metallic pipes and composite components such as fiber reinforced plastic (FRP), glass reinforced epoxy resin (GRE), high density polyethylene (HDPE), reinforced rubber expansion joints (REJs), carbon fiber reinforced plastics (CFRP), and polyvinyl chloride (PVC) are replacing metallic pipes throughout different industries due to advantages such as durability, low cost, light-weight, resistance to corrosion, etc. The growing demand for these materials necessitates the use of proper non-destructive testing (NDT) techniques for material integrity inspections.

In general, NDT methods such as ultrasonic testing, radiography, eddy current, and magnetic flux leakage have been widely applied in different industries for inspection of metallic components. However, these NDT methods cannot fulfill the demand for testing certain materials and components such as non-metallic composite pipes. For example, due to the complex structure of composite materials such as FRP/GRE [1] and the nature of defects and failure morphology in HDPE thermal fusion joints, ultrasonic testing fails to perform NDT for these mediums [2, 3]. On the other hand, radiography relies on the use of X-ray [4] which requires extra safety measures. Besides, it is incapable of detecting de-

lamination and planar cracks for defects when the local density remains nearly the same.

Thus, to fulfill the growing demand for NDT of non-metallic materials, microwave measurement techniques have been proposed (e.g., see [5, 6]). The usage of microwave imaging helps detecting defects, cracks, holes, and more in such components. In particular, microwave holographic imaging is a fast and robust imaging technique that has been successfully applied in various applications such as the security screening of airport passengers [7], etc. Originally, microwave holographic imaging techniques were developed based on synthetic aperture radar (SAR) imaging techniques [7] which employ far-field assumptions, i.e., the imaging distance which is the distance between the measuring antennas and the imaged object is assumed to be much larger than the wavelength. Wide-band SAR imaging has been used to produce three-dimensional (3D) images of the vertical cracks/flaws in fat and curved HDPE pipes [8]. Recently, SAR-based imaging techniques have been extended to the near-field applications where the distance between the measuring antennas and the imaged object is small (e.g., see [9, 10]). Thus, these techniques can be called near-field holographic imaging techniques where the information related to a specific imaging system is obtained *a priori* through the measurement of the so-called point-spread functions (PSFs) [11]. This offers several advantages such as: the reduction of modeling errors (as the modeling of the antennas and the imaging setup is not required), the reduction of errors due to uncertainties in the material properties, and the reduction of errors due to the size of antennas (measuring the PSFs directly instead of having assumption-based point-wise antennas). Although analytical expressions for the PSF (instead of direct measurement of them) can still be used in near-field holographic imaging, the material selection and the ignored near-field terms for the antennas may degrade the image reconstruction quality.

It is common to use multiple pipes in concentric configuration, as illustrated in Figure 1, to improve the efficiency and increase the lifetime of the wellbore production in oil and gas industry [12] or to separate the flow in the fluid transfer pipeline [13]. Near-field holographic imaging has been extended to the application of multiple non-metallic pipe imaging in [14, 15] where the pipes are assumed to be perfectly concentric. In this paper, we study the performance of the near-field holographic imaging of double pipes with different eccentricity values, i.e., the centers of the two pipes are not perfectly aligned. Although, in industry, normally centralizers are employed for making the multiple pipes concentric, the small misalignment of the centers, called eccentricity, can impose errors in image reconstruction when using techniques that have been developed based on the zero-eccentricity assumption. Thus, here, we consider this important factor for the first time and we use a quantitative measure, called reconstruction error (RE), to evaluate the degradation of the images of the defects on the inner and outer pipes of a double-pipe configuration due to various eccentricity values. It is worth noting that the effect of other important parameters for the considered microwave imaging setup such as thickness, radius, and permittivity of the pipes as well as angular separation of the antennas have been already studied in [15] and will be excluded here. Although the study is performed through simulations, we add artificial noise to the simulated data to have realistic results.

METHODS

In this section, we review the near-field holographic imaging approach for imaging of multiple pipes using an array of receiver antennas and multiple frequency data. Figure 1 illustrates the microwave imaging setup. It consists of a transmitter antenna to illuminate the pipes and an array of N_A receiver antennas measuring the scattered fields. The transmitter and receiver antennas scan a circular aperture with radius of r_A. It is assumed that the defects and

pipes are infinite along the longitudinal direction (z). The scattered field is recorded at N_ϕ angles along the azimuthal direction ϕ (within [0,2π]). The complex-valued scattered field $E^{SC}(\phi)$ is measured, at each sampling position, at N_ω frequencies within the band of ω_1 to ω_{N_ω} by each receiver. Such scattered response is obtained from subtracting the response of the pipes without defects from the response of the same pipes with defects. The image reconstruction process then provides one-dimensional (1D) images of the pipes with radii r_i, where $i=1,\ldots,N_r$. Please note that the imaging along the z direction can be implemented using similar concepts discussed here. The imaging system is assumed to be linear and space-invariant (LSI) which allows us to use the convolution theory. The convolution theory allows to write the response to an unknown input to the system as the convolution of the point-spread functions (PSF) (also known as impulse responses) of the system with that unknown input function.

For implementation of the near-field holographic imaging, first, the PSFs of the LSI imaging system are acquired. These PSFs are approximated by measuring small defects, called calibration defects (CDs) placed on each pipe one at a time, representing impulse functions as the inputs to the imaging system. In other words, the PSFs are measured by the same imaging system that will be later used for imaging test objects. These CDs are the smallest defects that can be measured by the system. To provide more data for image reconstruction, measurements can be implemented at multiple frequencies, ω_n, n=1,…, N_ω and by multiple receivers, a_m, m=1,…, N_A. We denote the measured PSF function for the i-th pipe measured by the receiver antenna a_m at frequency ω_n by $E^{SC,CD}_{i,a_m}(\phi,\omega_n)$. We also denote the measured scattered field by the receiver antenna a_m at frequency ω_n by $E^{SC}_{a_m}(\phi,\omega_n)$. Let's first consider the spatially-sampled versions of $E^{SC}_{a_m}(\phi,\omega_n)$, $E^{SC,CD}_{i,a_m}(\phi,\omega_n)$, and $f_i(\phi)$ denoted by $\mathbf{E}^{SC}_{a_m}(n_\phi,\omega_n)$, $\mathbf{E}^{SC,CD}_{i,a_m}(n_\phi,\omega_n)$, and $\mathbf{f}_i(n_\phi)$, $n_\phi=1,\ldots,N_\phi$, with the angular interval denoted by $\Delta\phi$. Using the convolution theory and discrete Fourier transforms (DFT) along ϕ direction, it can be shown that the unknown shape functions of the defects on the pipes $f_i(\phi)$, $i=1,\ldots,N_r$, can be found by solving the following system of equations at each spatial frequency k_ϕ [15]:

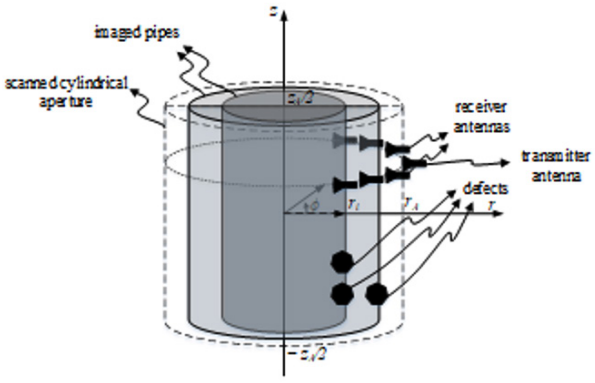

Figure 1: Illustration of the simulation setup in FEKO for the case that the defects are on the inner pipe.

$$\underline{\tilde{\tilde{\mathbf{E}}}}^{SC}=\underline{\underline{\tilde{\tilde{\mathbf{D}}}}}\,\underline{\tilde{\tilde{\mathbf{F}}}} \tag{1}$$

where

$$\underline{\tilde{\tilde{\mathbf{E}}}}^{SC}=\begin{bmatrix}\underline{\tilde{\tilde{\mathbf{E}}}}^{SC}_1\\ \vdots\\ \underline{\tilde{\tilde{\mathbf{E}}}}^{SC}_{N_A}\end{bmatrix}\quad \underline{\underline{\tilde{\tilde{\mathbf{D}}}}}=\begin{bmatrix}\underline{\tilde{\tilde{\mathbf{D}}}}_1\\ \vdots\\ \underline{\tilde{\tilde{\mathbf{D}}}}_{N_A}\end{bmatrix}\quad \underline{\tilde{\tilde{\mathbf{F}}}}=\begin{bmatrix}\tilde{\tilde{\mathbf{f}}}_1(k_\phi)\\ \vdots\\ \tilde{\tilde{\mathbf{f}}}_{N_r}(k_\phi)\end{bmatrix} \tag{2}$$

and

$$\underline{\tilde{\tilde{\mathbf{E}}}}^{SC}_{a_m}=\begin{bmatrix}\tilde{\tilde{\mathbf{E}}}^{SC}_{a_m}(k_\phi,\omega_1)\\ \vdots\\ \tilde{\tilde{\mathbf{E}}}^{SC}_{a_m}(k_\phi,\omega_{N_\omega})\end{bmatrix}$$

$$\underline{\tilde{\tilde{\mathbf{D}}}}_{a_m}=\begin{bmatrix}\tilde{\tilde{\mathbf{E}}}^{SC,CD}_{1,a_m}(k_\phi,\omega_1) & \cdots & \tilde{\tilde{\mathbf{E}}}^{SC,CD}_{N_r,a_m}(k_\phi,\omega_1)\\ \vdots & \ddots & \vdots\\ \tilde{\tilde{\mathbf{E}}}^{SC,CD}_{1,a_m}(k_\phi,\omega_{N_\omega}) & \cdots & \tilde{\tilde{\mathbf{E}}}^{SC,CD}_{N_r,a_m}(k_\phi,\omega_{N_\omega})\end{bmatrix} \tag{3}$$

where $\tilde{\tilde{\mathbf{E}}}^{SC}_{a_m}(k_\phi,\omega_n)$, $\tilde{\tilde{\mathbf{E}}}^{SC,CD}_{i,a_m}(k_\phi,\omega_n)$, and $\tilde{\tilde{\mathbf{f}}}_i(k_\phi)$ denote DFT along ϕ axis of $\mathbf{E}^{SC}_{a_m}(n_\phi,\omega_n)$, $\mathbf{E}^{SC,CD}_{i,a_m}(n_\phi,\omega_n)$, and $\mathbf{f}_i(n_\phi)$, respectively. These systems of equations are solved at each spatial frequency k_ϕ to obtain the values for $\tilde{\tilde{\mathbf{f}}}_i(k_\phi)$, $i=1,\ldots,N_r$. Then, inverse DFT along ϕ is applied to reconstruct images $\mathbf{f}_i(n_\phi)$ over all the pipes with radii $r=r_i$, $i=1,\ldots,N_r$. At the end, the normalized modulus of $\mathbf{f}_i(n_\phi)$

$|\mathbf{f}_i(n_\phi)|/M$, where M is the maximum of $|\mathbf{f}_i(n_\phi)|$ for all r_i, is plotted versus ϕ to obtain a 1D image of the defects on the i-th pipe. We call $|\mathbf{f}_i(n_\phi)|/M$ the normalized image.

In [15], inspired by standardized low-resolution brain electromagnetic tomography, the systems of equations in (1) are solved using standardization of the minimum norm. Using this concept, the objective function to be minimized is constructed as:

$$J = \left\| \tilde{\tilde{\mathbf{E}}}^{SC} - \tilde{\tilde{\mathbf{D}}}\tilde{\tilde{\mathbf{F}}} \right\|^2 + \alpha \left\| \tilde{\tilde{\mathbf{F}}} \right\| \quad (4)$$

where $\alpha \geq 0$ is a regularization parameter. The detailed solution has been explained in [15].

As discussed earlier, the PSF data is collected beforehand for the configuration of the pipes under inspection assuming that they are concentric. A non-zero eccentricity, however, affects the measured data for the inspected pipes leading to errors in the reconstructed images. To evaluate the quality of reconstructed images, we define a reconstruction error (RE) parameter as:

$$\mathrm{RE} = \sum_{i=1}^{N_r} \left\| |\mathbf{f}_i(n_\phi)|/M - \mathbf{f}_{i,ideal}(n_\phi) \right\| \quad (5)$$

where $\mathbf{f}_{i,ideal}(n_\phi)$ is the ideal image for which the values are all 0 except being 1 at the true positions of the defects.

RESULTS

To study the effect of eccentricity on imaging of the multiple non-metallic composite pipes, we conduct a study using simulation data provided by Altair's FEKO software [16] which is a high frequency modeling software. The study was done by 1D scanning and image reconstructions along the azimuthal direction. In order to have a more realistic simulation study, white Gaussian noise with signal-to-noise ratio (SNR) of 20 dB is added to the simulated responses by using the *awgn* command in MATLAB.

Figure 2 illustrates the configuration of the imaging setup in FEKO. We study the performance of the system where the antenna array is placed on the outside of two concentric pipes. There are 13 resonant dipole antennas separated by $\Delta\phi_a = 10^\circ$ angles along the ϕ direction. Thus, all the antennas are used as receivers except the center element which acts as both transmitter and receiver. The radii of the inner and outer pipes, namely, R_{out1} and R_{out2} are 20 mm and 40 mm, respectively, and the thickness of both pipes is D = 2 mm. The pipes have a relative permittivity ε_r of 2.25 and a tangent loss of 0.0004. The defects have semi-cylindrical shape and their parameters are L_d = 1.5D and W_d = 0.75D. In addition, the models are simulated with two identical defects on the pipes. The studied scenarios are: (1) both defects on the outer pipe only and (2) both defects on the inner pipe only. The eccentricity parameter, denoted by E_{cc}, represents the distance between the centers of the inner and outer pipes (the outer pipe is assumed to be concentric with the circular path scanned by the antennas known as measurement aperture).

For data acquisition, we perform scanning of a circular aperture to get the complex-valued transmission scattering parameters (in microwave, these are the parameters representing the coupling of the transmitter to

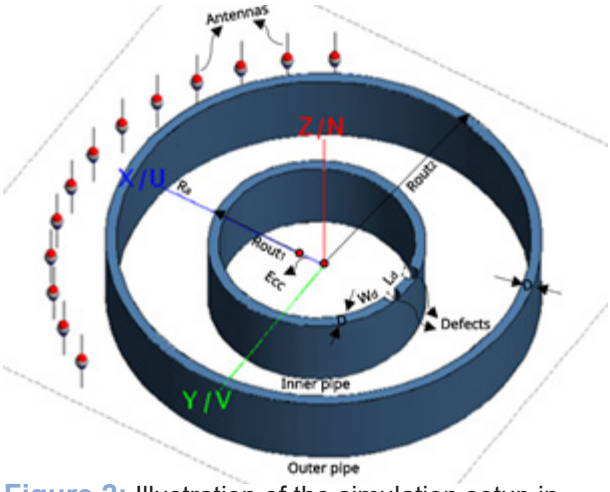

Figure 2: Illustration of the simulation setup in FEKO for the case that the defects are on the inner pipe.

the receiver which here takes into account the field scattered back from the objects as well) by rotating the antennas along the azimuth angle (ϕ) from 0° to 360° every 2° (181 grid points) in FEKO. For each scenario, the simulated responses without the presence of the defects are subtracted from the simulated responses with the presence of the defects to acquire the scattered responses only due to the defects. Also, white Gaussian noise with SNR of 20 dB is added to each defect response to imitate real-world measurement data.

First, we study the effect of eccentricity when E_{cc} = 0.5 mm (along the x axis) and both defects are on the inner pipe or on the outer pipes at various azimuthal angles from $\phi = \pm 10^{\circ}$ to $\phi = \pm 170^{\circ}$.

After applying near-field holographic imaging as described in the previous section along with the PSF data collected for concentric pipes, the values of REs are computed for each scenario. Figures 3A and 3B show the variations of the computed REs versus the angle of defects for the cases that both defects are on the outer pipe and inner pipe, respectively. From both figures, it is observed that there is no clear correlation between the angles of the defects and the values of the REs. In general, the error seems to be larger for the defect angles between $\phi = \pm 20^{\circ}$ to $\phi = \pm 140^{\circ}$. Furthermore, the values of REs are larger when the defects are on the inner pipe indicating that the image of the inner pipe is more affected by the adverse effects of eccentricity.

Next, we study the effect of value of eccentricity on the quality of the reconstructed images when the defects are on the outer and inner pipes by visually comparing the quality of the reconstructed images to the ideal images. For this study, the eccentricity parameter E_{cc} varies from 0.1 mm to 0.9 mm with steps of 0.1 mm and we choose constant angles of $\phi = \pm 170^{\circ}$ for the defects one time when they are on the outer pipe and another time when the defects are on the inner pipes.

Figure 4 shows the reconstructed images of the two pipes when the eccentricity parameter is 0.1 mm. Figures 4A and 4B show the images when the defects are on the outer and inner pipes respectively. In general, we notice that the image deteriorates is more for the inner pipe than the outer pipe. The reconstructed image in Figure 4A for which the defects are on the outer pipe clearly shows the

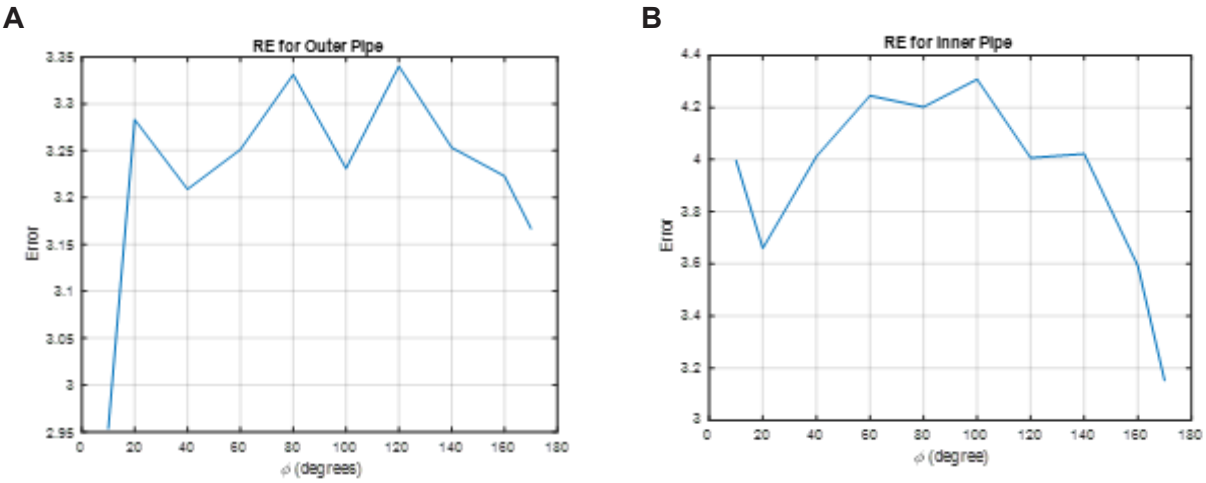

Figure 3: Variation of computed RE when E_{cc} = 0.5 mm and the angular positions of two identical defects are varying from $\phi = \pm 10^{\circ}$ to $\phi = \pm 170^{\circ}$:
(A) defects are on outer pipe
(B) defects are on inner pipe.

presence of the defects and it is close to the ideal image. However, the image for the inner pipe in Figure 4A shows artifacts around 0.3 level. The reconstructed images in Figure 4B in which the defects are on the inner pipe, still show the presence of the defects on the inner pipes but again contains large artifacts with maximum of 0.5 level. In this case, the image on the outer pipe also contains some small level (around 0.1 level) of artifacts with some shadows of the defects on the inner pipe.

In the following, we demonstrate that as we continue to increase the value of eccentricity parameter in this study, the quality of the reconstruction images deteriorates significantly. Figure 5 shows the reconstructed images when

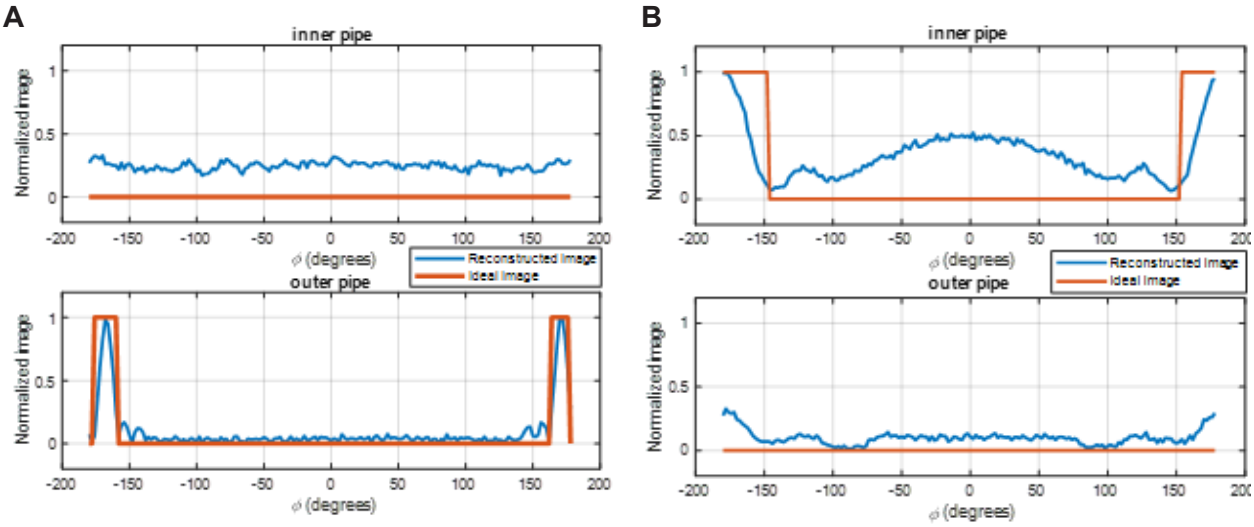

Figure 4: Reconstructed 1D images when the defects are at $\phi = \pm 170^{\circ}$ and eccentricity = 0.1 mm for:
(A) defects on the outer pipe
(B) defects on the inner pipe.

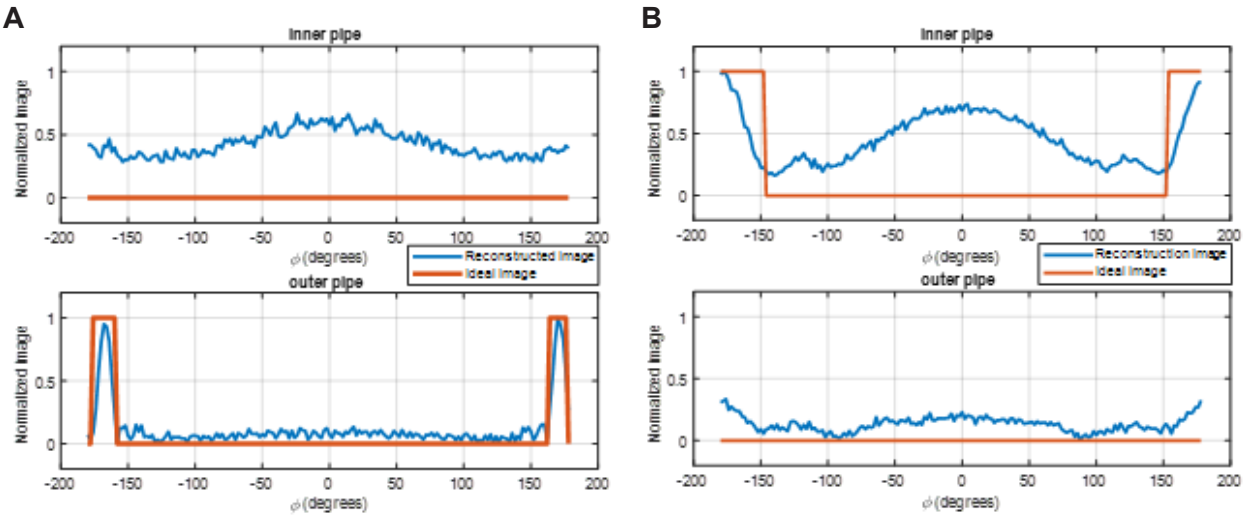

Figure 5: Reconstructed 1D images when the defects are at $\phi = \pm 170^{\circ}$ and eccentricity = 0.5 mm for:
(A) defects on the outer pipe
(B) defects on the inner pipe.

the value of E_{cc} is increased to 0.5 mm. Compared to Figure 4, images in Figure 5 are more distorted. As expected, the increase in the value of E_{cc} leads to larger image reconstruction errors. Next, we increase the value of E_{cc} even further. Figure 6 displays the high deterioration of the images when the value of E_{cc} is 0.9 mm. From these figures, it can be easily deduced that the reconstructed image is far off from the ideal image due to high error caused by eccentricity.

As a final step, we compute the variation of REs as the value of E_{cc} increases and when the defects are at on the outer pipe or on the inner pipe. Figure 7A shows this variation when the defects are on the outer pipe. It is observed that the value of RE increases sharply as E_{cc} increases. A similar trend is observed in Figure 7B when the defects are on the inner pipe.

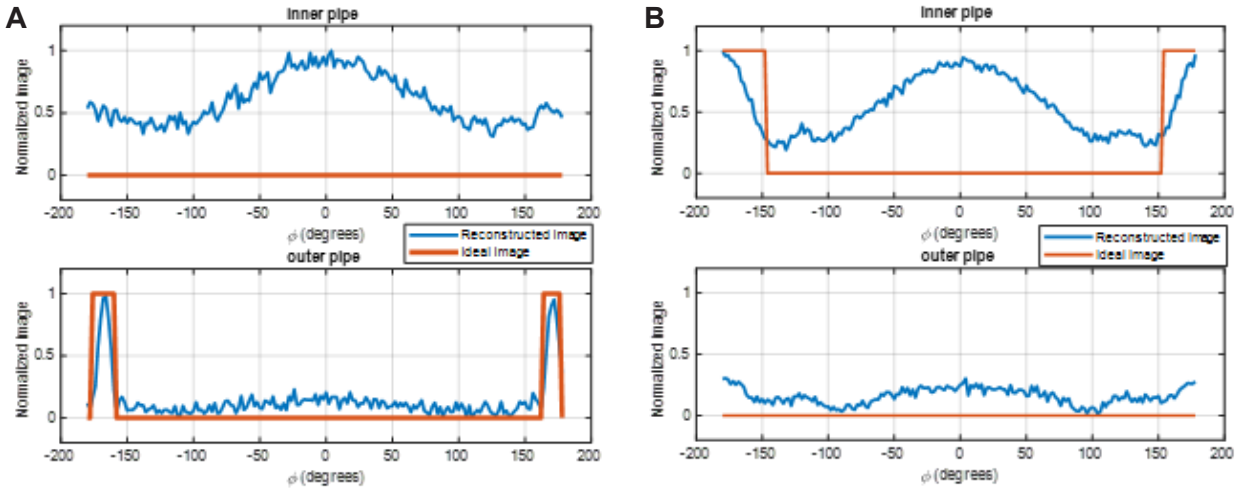

Figure 6: Reconstructed 1D images when the defects are at $\phi = \pm 170^{\circ}$ and eccentricity = 0.9 mm for:
(A) defects on the outer pipe
(B) defects on the inner pipe.

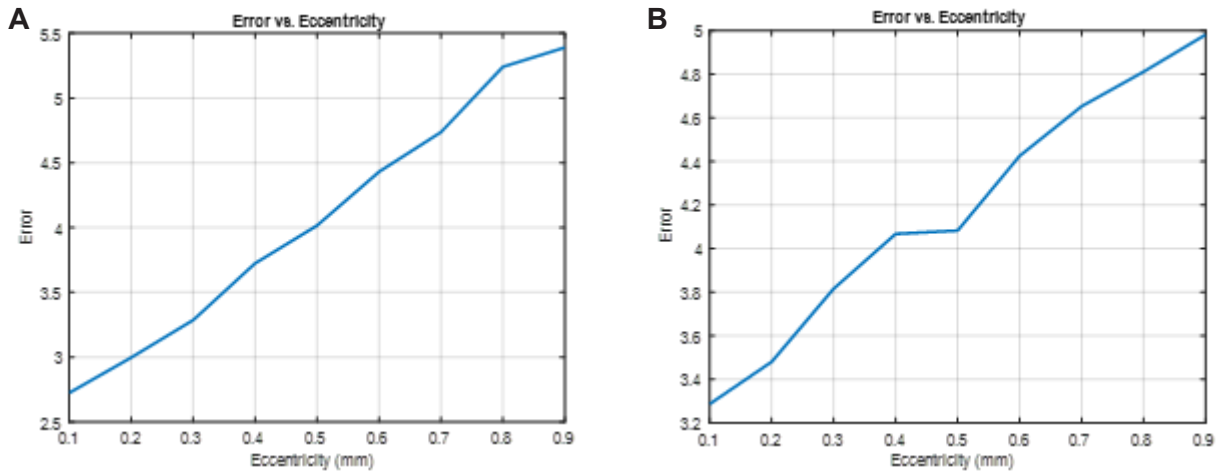

Figure 7: Variation of computed RE vs. eccentricity when defects are at $\phi = \pm 170^{\circ}$ and both defects are on
(A) outer pipe
(B) inner pipe.

DISCUSSION & CONCLUSION

In this paper, we studied the effect of eccentricity of the pipes on the results of the holographic microwave imaging of multiple non-metallic pipes. Microwave imaging is a non-contact method that can be used for inspection of multiple pipes and it is also safe due to the use of low-level microwave power.

In general, the results indicate that the quality of the reconstructed images is highly sensitive to non-zero eccentricity values such that even an eccentricity of 0.5 mm imposes image quality deteriorations. Besides, it was observed that the images of the defects on the inner pipes would be affected more seriously by non-zero eccentricity effects.

Although we employed simulated results from Altair FEKO software, we applied additive white Gaussian noise to the simulated responses to mimic real-world measurements and have a more realistic study.

Here, the study was conducted with two scenarios: (1) changing the angles of the defects while the eccentricity value is fixed and (2) changing the value of eccentricity while the positions of defects are fixed. It is worth noting that the effect of other important parameters for the considered microwave imaging setup such as thickness, radius, and permittivity of the pipes as well as angular separation of the antennas have been already studied in [15] and have been excluded here.

Due to serious adverse effects of eccentricity, we plan to develop a technique to estimate the value of unknown eccentricity parameter and then reduce the effect of that on the reconstructed images. Ultimately, the goal is to develop a robust tool for NDT of non-metallic pipes that promote using these components in various industries.

AUTHOR INFORMATION

Corresponding Author
*Email: ygao21@nyit.edu

Author Contributions

Yuki Gao and Noshin Raisa have contributed in performing the parametric analysis of the eccentricity effect. Reza K. Amineh has provided the original FEKO simulation models and MATLAB codes for applying the near-field holographic imaging. All authors have contributed in preparation of this manuscript.

Funding Sources

U.S. National Science Foundation (NSF) under Award 1920098 and the New York Institute of Technology's Institutional Support for Research and Creativity (ISRC) Grants

Competing Interests

The authors declare no competing financial and non-financial interests.

ACKNOWLEDGEMENTS

The authors thank New York Institute of Technology's Undergraduate Research and Entrepreneurship Program (UREP).

ABBREVIATIONS

CD – Calibration Defect
CFRP – Carbon Fiber Reinforced Plastic
DFT – Discrete Fourier transform
DTFT – Discrete Time Fourier Transform
FRP – Fiber Reinforced Plastic
GRE – Glass Reinforced Epoxy Resin
HDPE – High Density Polyethylene
NDT – Non-Destructive Testing
PSF – Point-Spread Function
PVC – Polyvinyl Chloride
RE – Reconstruction Error
REJ –Rubber Expansion Joint
SAR – Synthetic Aperture Radar

REFERENCES

[1] L. Tong, A. P. Mouritz, M. K. Bannister, 3D Fiber Reinforced Polymer Composites. 1st ed. (2002).

[2] K. Murphy, D. Lowe, Evaluation of a novel microwave based NDT inspection method for polyethylene joints. in Proc. ASME Pressure Vessels Piping Conf., Baltimore, MD, U.S.A. 321-327 (2002).

[3] X. W. Zhu, J. P. Pan, L. J. Tan, Microwave scan inspection of HDPE piping thermal fusion welds for lack of fusion defects. Appl. Mech. Mater. 333-335, 1523-1528 (2013).

[4] R. Pincu, “Digital radiography and its advantages in field NDT inspections today” 17th World Conf. on Nondestructive Testing, Shanghai, China (2008).

[5] R. Zoughi, Microwave Non-Destructive Testing and Evaluation. (2000).

[6] S. Kharkovsky, R. Zoughi, Microwave and millimeter wave nondestructive testing and evaluation - Overview and recent advances. IEEE Instr. and Meas. Mag., 10(2), 26-38 (2007).

[7] D. M. Sheen, D. L. Mcmakin, T. E. Hall, Three-dimensional millimeter-wave imaging for concealed weapon detection. IEEE Trans. Microw. Theory Techn., 49(9), 1581-1592 (2001).

[8] M. T. Ghasr, K. Ying, R. Zoughi, 3D millimeter wave imaging of vertical cracks and its application for the inspection of HDPE pipes. AIP Conf. Proc., 1581(1), 1531–1536 (2014).

[9] R. K. Amineh, N. K. Nikolova, M. Ravan, Real-Time Three-Dimensional Imaging of Dielectric Bodies Using Microwave/Millimeter Wave Holography. Wiley & IEEE Press, ISBN: 978-1-119-53886-8, (2019).

[10] R. K. Amineh, M. Ravan, H. Wu, A. Kasturi, Three-dimensional holographic imaging using data collected over cylindrical apertures. Microwave and Optical Technology Letters, 61(4), 907–911 (2019).

[11] R. K. Amineh, J. McCombe, A. Khalatpour, N. K. Nikolova, Microwave holography using point-spread functions meas-ured with calibration objects. IEEE Trans. on Inst. and Meas., 64(2), 403−417 (2015).

[12] L. E. S. Martin, A. E. Fouda, R. K. Amineh, I. Capoglu, B. Donderici, S. S. Roy, F. Hill, New high-definition frequency tool for tubing and multiple casing corrosion detection. SPE Abu Dhabi Int. Petroleum Exhibition & Conference, (2017).

[13] Y. Renardy, D. D. Joseph, Couette flow of two fluids between concentric pipes. J. of Fluid Mechanics, 150, 381–394 (1985).

[14] R. K. Amineh, M. Ravan, R. Sharma, Nondestructive testing of nonmetallic pipes using wideband microwave measurements. IEEE Trans. Microwave Theory and Techniques, 65w(5), 1763-1772 (2020).

[15] H. Wu, M. Ravan, R. Sharma, J. Patel, R. K. Amineh, Microwave holographic imaging of nonmetallic concentric pipes. IEEE Trans. Instrumentation & Measurement, 69(10), 7594-7605 (2020).

[16] Altair FEKO, https://www.altair.com/feko/

CUSJ
COLUMBIA UNDERGRADUATE SCIENCE JOURNAL

Neural Oscillations as Predictors of Variability in Second Language Proficiency

Victoria Ogunniyi[1]*, David Abugaber[2], Irene Finestrat[2], Alicia Luque[4], Kara Morgan-Short[2,3]

[1]Department of Biological Sciences, University of Illinois at Chicago, Chicago, IL
[2]Department of Hispanic Linguistics, University of Illinois at Chicago, Chicago, IL
[3]Department of Psychology, University of Illinois at Chicago, Chicago, IL
[4]Department of Language and Culture, UiT The Arctic University of Norway, Tromsø (Norway)

KEYWORDS: Second language acquisition, language proficiency, quantitative EEG, psycholinguistics, resting-state studies

ABSTRACT: Understanding what traits facilitate second language (L2) learning has been the focus of many psycholinguistic studies for the last thirty years. One source of insight comes from quantitative electroencephalography (qEEG), i.e., electrical brain activity recorded from the scalp. Using qEEG, [1] found that functional brain connectivity is predictive of language learning ability. This study extends Prat et al. in investigating the association of qEEG measures for two measures of L2 proficiency, namely: 1. a grammaticality judgment task, wherein participants read and identified Spanish sentences as either correct or incorrect based on possible grammar violations, and 2. a standardized Spanish proficiency test (DELE). Participants were low-intermediate L2 learners recruited from third- and fourth-semester university Spanish classes. Spectral power and coherence within and across six different regions were analyzed for correlations with either scores on the grammaticality judgment task or on the DELE. Follow-up linear regression models based on significant qEEG correlates explained up to 11% of variance in DELE scores but none of the variance in grammaticality judgment task performance. Negative correlations were found between theta frequency coherence and the DELE. Because theta activity has been associated with episodic and working memory performance, these findings suggest that less proficient learners might utilize memory-based strategies more often to compensate for their lack of familiarity with the L2.

INTRODUCTION

Understanding what characteristics underlie successful learning is not only pedagogically important but also intriguing from a cognitive standpoint. In the study of linguistics, this question has frequently been examined in regard to second language (L2) acquisition (for a review, see [2]). Researchers have used a variety of approaches to investigate which cognitive abilities are correlated with higher L2 proficiency. Going beyond behavioral measures for psycholinguistic and cognitive constructs

[2], neuroimaging techniques such as electroencephalography (EEG) allow us to directly quantify and connect brain activity to the processes involved in language processing [3].

This study addresses the question of whether EEG can explain variance on outcomes of L2 proficiency. We first review the literature on qEEG and its use as a neurocognitive measure in L2 studies, focusing on the studies that examine resting-state qEEG as a potential factor in language learning ability and language proficiency. Then, in a conceptual replication and extension of [1], we describe the results of our study in which EEG measures of resting-state brain rhythms were explored for relationships with behavioral measures of L2 proficiency. The potential neurocognitive and pedagogical implications of these findings are expounded on in the discussion section.

Through our conceptual replication of [1], which focused on measures of L2 learning, we aimed to examine whether prior research on resting-state qEEG and L2 learning rate would extend to the construct of L2 proficiency, that is, whether a learner's intrinsic pattern of brain rhythms is associated with their L2 abilities.

Background on qEEG

EEG is an electrophysiological technique that utilizes electrodes placed on the scalp to measure changes in voltage between electrodes [4, 5]. These transient shifts in electric potential are caused by the electrical activity of neurons. Due to their proximity to the scalp, pyramidal neurons, which project information to neurons in local regions, produce most of the postsynaptic potentials recorded by EEG [5]. Although EEG data cannot attribute the electrical activity to specific brain regions, its temporal resolution allows researchers to track changes in brain activity to the millisecond. Thus, since the 1960s, EEG has been a widely used tool in cognitive studies [6].

There are various methods that can be used to analyze EEG data. The analysis of raw EEG, or qEEG, data yields useful information via neural oscillations, that is, rhythmic or repetitive patterns of neural activity. In contrast to more common methods that analyze voltage amplitudes within given time windows tied to a stimulus, such as event related potentials, qEEG has the advantage of providing information about neural activity occurring before and after the onset of a stimulus, or even in the absence of any particular stimulus. In prior literature, qEEG has been used in disparate domains, such as serving as evidence of mental dysfunction in criminal cases [7], providing neurofeedback for therapy patients with ADHD [8], and predicting learners' aptitude for learning computer programming languages [9].

Neural oscillations can be quantified through three measures: synchrony, amplitude, and coherence. The first measure, synchrony, describes whether neural oscillations are increasing or diminishing during a cognitive process [6]. By measuring the phase synchronization and desynchronization of the neural oscillations in this way, researchers can map larger interactions among the brain's networks and demonstrate patterns of activation. This may provide insight into a possible solution to the binding problem, which asks how the brain integrates separate streams of information into one cohesive mental representation [5]. The second measure, amplitude, describes local changes in synchrony. Amplitude within a certain frequency band is also often referred to as power. Though an increase in power does not always reflect the presence of oscillations, sustained power increases within a narrow frequency range is usually a good indicator that oscillations are likely present at that frequency [6]. The third measure, coherence, describes the similarity in waveform properties and the stability of phase differences between two oscillations across brain regions [6]. Though these three measures do not encompass all possible properties of oscillations, they can describe how oscillations represent activation and suppression of different neural networks, how wave amplitude is related

to increased general activation, and how oscillations communicate over long distances.

Though their specific ranges vary between studies, there are five primary frequency bands that neural oscillations can be divided into [5, 6, 10]: delta (1-2 Hz), theta (3-7 Hz), alpha (8-12 Hz), beta (13-30 Hz), and gamma (30-200 Hz). These bands have been implicated in a variety of cognitive processes. For instance, prior research has suggested a relationship between oscillation frequency and the range of neural network interactions: the lower frequencies, alpha and below, represent local interactions, whereas higher frequencies represent interactions between more distant brain regions [10].

In regard to the more general applications of qEEG, all of the frequency bands have been shown to play a role in memory. For instance, the delta band, which is the predominant frequency found in slow wave sleep, has been associated with memory consolidation [5]. In particular, delta oscillations facilitate the formation of declarative memory, the memory of one's experiences and explicit knowledge. Similarly, theta oscillations have been implicated in both working memory and long-term memory retrieval [5, 11]. Theta oscillations have primarily been observed in the cortex, further echoing these memory functions [10, 11]. Alpha oscillations, which are the most prominent in the adult brain, are related to attention paid to external stimuli [5, 6]. More importantly, alpha plays a role in blocking irrelevant information in working memory. Additionally, alpha desynchronization and reductions in alpha power result in more successful information encoding [10]. Recent studies have shown that the beta band, which is mostly generated in the fronto-central region of the brain, also plays a role in regulating information stored in working memory [12]. The gamma band, which has been observed in the cortex [5], has been associated with short- and long-term memory maintenance [6]. Additionally, increases in gamma activity is anti-correlated with beta activity levels [12].

Additionally, the bands have been shown to play significant roles in stimulus-based language tasks. For instance, increased power in the theta band, which occurs during grammatical violations and sentence contexts that are difficult to interpret, reflects its involvement in lexical-semantic memory retrieval. Similarly, the alpha band helps organize information stored in short-term memory during sentence comprehension [10]. Regarding the higher frequency bands, gamma and beta have been associated with unifying related word meanings and similar grammatical forms, respectively. More specifically, the gamma band has been attributed to semantic unification [6, 10], which is supported by the observed decreases in gamma power in response to phrases with unclear meanings and idiomatic expressions [10]. Conversely, the beta band is involved in syntactic unification [5, 6, 10]. Beta oscillations sentence to lower processing regions [10]. By reflecting both domain-general and stimulus-specific cognitive functions, qEEG has proven to be a useful neurocognitive measure in psycholinguistic studies.

The Use of qEEG in L2 Studies

Several L2 studies have tested the relationship between qEEG measures and L2 constructs. These studies have generally addressed two issues: L2 proficiency [13-16], which describes a learner's language abilities at a given point in time, and L2 grammatical learning [17-19], which describes how learners better understand the rules of a language with increasing proficiency. Regarding L2 proficiency studies, results have shown that highly proficient L2 learners differ in qEEG measures from less proficient L2 learners [14-16]. When comparing differently proficient participant groups, significant differences are found in the timing and location of oscillatory activity, especially regarding lateralization of the location of the oscillations between the right and left hemisphere. Though the delta band is not frequently analyzed in these studies, one study found no significant group differences [13]. For grammatical learning studies, in both natural and ar-

tificial grammar learning tasks, higher relative power and coherence in the higher frequency bands (>8 Hz) were associated with higher proficiency and increased in prevalence over time, whereas higher relative power and coherence in the lower frequency bands were associated with lower proficiency and decreased over time [16, 17, 19]. Gauging learning by assessing oscillatory responses to grammatical violations, other research has also found that the higher frequency bands were elicited in both semantic and syntactic conditions [17].

A relatively new approach in L2 studies is to examine whether resting-state qEEG measures (i.e., that are taken when the brain is "idling" in the absence of any explicit task, as opposed to stimulus-related qEEG measures) are associated with the rate at which an individual acquires second language abilities, or L2 learning, and proficiency. As of now, very few studies have tested the correlation between neural activity occurring in the absence of a stimulus, or resting-state qEEG, and L2 learning rates [1, 20]. In these studies, native-English speakers learned a second language over the span of a few months. Prior to this learning period, resting-state EEG was performed, and various behavioral measures were collected as additional outcome measures. In the first of these studies, [20] found that, when entered as predictors into a regression model, resting-state qEEG measures explained up to 60% of the variance observed in L2 learning rates, meaning that learning rate accounted for more than half of the variability in the data. Though the most predictive frequency range was found to be the low-beta range (13-14.5 Hz), power in the beta and gamma frequency bands recorded primarily over right hemisphere electrode regions were found to be the strongest predictors of L2 learning ability in general. The authors also found that alpha power over frontal and temporal electrodes and low-beta power over temporal regions were indicative of better language learning ability. As with other studies, greater activation in left hemisphere electrode sites was associated with lower L2 proficiency.

In a later study conducted by [1] with a higher sample size, the authors tested whether resting-state qEEG measures were significant predictors of different L2 learning measures. Similar to their earlier study, the results implicated the qEEG activity in the right hemisphere with greater L2 learning ability. Simultaneous regression analyses were run on three outcome variables: L2 learning rate, total speech attempts, and performance on a declarative memory posttest. Mean right posterior beta power was found to be a significant predictor of L2 learning rate and total speech attempts. Frontotemporal to posterior coherence in the right hemisphere was found to be a significant predictor of performance on the declarative memory posttest, whereas mean within left posterior coherence across all frequencies was a significant predictor of total speech attempts. Altogether, these results indicate that mean beta power over posterior electrode regions plays a significant role in L2 ability.

In all, due to their potential advantages over stimulus-locked measures, qEEG measures have been increasingly used in L2 studies. Though some frequency bands have been more frequently studied than others, all five of the classic bands have been implicated in various language functions in some way. Across various research designs, qEEG has been used to illustrate large-scale patterns of brain activation during language processing. However, relatively little research has explored the potential of resting-state paradigms for qEEG in L2 psycholinguistics. For example, although [1, 20] have examined whether qEEG can predict individual differences in L2 learning rate, speech attempts during learning, and L2 declarative knowledge, no study has yet examined whether or how resting-state qEEG measures may be predictive of L2 proficiency, which is the desired final outcome of L2 learning.

Purpose of Research

The goal of this study is to investigate the

potential association between resting-state qEEG and L2 proficiency. The current study expands on the research design of previous resting-state L2 studies. At present, resting-state qEEG studies have involved extensive training sessions with participants in the initial stages of L2 learning. However, the participant population utilized in this study comprised L2 learners at a low-intermediate stage who were recruited from third- and fourth-semester university-level Spanish courses. In connecting the qEEG measures with observed variability in language proficiency, we reasoned that second-year Spanish learners with the qEEG profiles most conducive to effective processing (e.g., through memory functions and other related cognitive processes) would have gained the most Spanish proficiency from their classes. Additionally, this study has the advantage of analyzing a greater number of electrodes than prior research [1, 20], providing higher spatial resolution for measuring electrical activity on the scalp. As with prior resting-state studies, a variety of qEEG measures were analyzed, including spectral power and coherence. Considering the issues above, this study specifically investigated two research questions:

Research Question 1: Is mean spectral power calculated from resting-state qEEG data associated with L2 proficiency, as assessed by two Spanish proficiency tasks?

Research Question 2: Is mean within- and between-network coherence calculated from resting-state qEEG data associated with L2 proficiency, as assessed by two Spanish proficiency tasks?

Following the results of [1], we predicted that the qEEG measures that were most likely to show a relationship with the two L2 proficiency tasks were mean beta power and frontotemporal-to-posterior coherence. In spite of these tentative predictions, we sought to replicate [1]'s methods as closely as possible in reproducing their two-step exploratory analysis strategy (i.e., pairwise correlations followed by multiple regression using significant correlates as predictors) on all frequency bands. As we intended our analysis itself to be strictly exploratory rather than confirmatory, we included all frequency bands in the analysis. In order to assess L2 proficiency, we decided to administer two assessments, one that reflects specific grammatical knowledge acquired through the learners' class (the grammaticality judgment task), and one that is a more general and widely measure in the L2 literature (Diplomas de Español como Lengua Extranjera), see Methods. Given that prior research [21] has found a distinction between automatic and controlled language processing, using both a timed and untimed L2 proficiency measure would allow us to examine the application of L2 knowledge in two distinct ways.

METHODS

Participants

Forty-nine participants (29 female; 20 male; mean age = 21.54; age SD = 4.14; range = 18-38) were initially recruited for participation in a two-part EEG study in which they were tested in English and in Spanish in separate testing sessions. Participants were recruited at a large, public urban university in Chicago from third- and fourth-semester Spanish language courses, which centered on developing communicative abilities and aimed to help students obtain low-intermediate proficiency by the end of the fourth-semester course. Thirteen of these participants were recruited from the third-semester Spanish course, while twenty-two of these participants were recruited from the fourth-semester Spanish course; thirteen participants did not report their course level. The recruitment process involved advertising to these language courses, after which participants self-selected whether to participate. Regarding the racial distribution of the participant population, nineteen participants identified as White/Caucasian, fourteen participants identified as Asian, six participants identified as Black/Af-

rican-American, four participants identified as multiracial, and six participants' races were unreported. All the participants reported having English as a native language (even if they were simultaneous bilinguals with early exposure to other languages) and having no Spanish exposure growing up. Additionally, per our EEG criteria, all participants were right-handed as assessed by the abridged version of the Edinburgh Handedness Inventory [22], with normal or normal-to-corrected vision. This was done to ensure that our results were not confounded by uncorrected vision or differing brain activity in those who are left-handed. None of the participants reported having psychiatric, neurological, or learning disorders. All participants gave informed consent according to the standards of the University of Illinois at Chicago institutional review board and were financially compensated for their participation based on the number of hours spent participating in the study, receiving $5 for every hour spent on completing the proficiency measures, $15 for every hour spent during the EEG recording process, and a $45 bonus for completing both sessions.

Participants were only included in the analysis if they completed the resting state EEG recording along with at least one of our Spanish proficiency measures. The final number of participants included in the current analysis is 47, with 44 of these participants having completed both Spanish proficiency measures (see Table I below). A similar EEG recording procedure was performed for an L1 English reading task (not reported here). The participant data included in this study was collected over the span of two years, from 2018 to 2020.

Table I. Participant Language Characteristics

	M (SD) [Range]
Number of native languages	1.29 (0.45) [1-2]
Number of L2s	1.44 (0.53) [1-3]
Age of acquisition Spanish (years)	14.53 (4.88) [0-29]
Self-rated Spanish listening proficiency[a]	4.88 (2.01) [1-9]
Self-rated Spanish reading proficiency	5.42 (1.72) [1-8]

Note: [a]Self-rated proficiency on 0 ('none) to 10 ('perfect) scale.

Grammaticality Judgment Task

Participants read various Spanish sentences and were asked to determine whether they followed Spanish grammatical rules. The grammaticality judgment task consisted of three experimental conditions: phrase structure, subject-verb agreement, and noun-phrase violations (see Table II for examples). The phrase structure condition, wherein word order violations were introduced into a sentence by presenting a noun instead of a verb or vice-versa, consisted of 60 correct and 60 violation sen-

Table II. Examples of stimulus sentences

Item Type	Example
Phrase Structure	Ella tiene mucho dinero/*gastar que gastar/dinero en ropa. [She has a lot of money/*spend to spend/money on clothes.]
Subject-Verb	La mujer dibuja/*-dibujan en su habitación. [The lady draws/*draw in her bedroom.]
Noun Phrase	El hombre prepara estas papas/ *papa para su esposa. [The man prepares these pota-toes/*potato for his wife.]

Note: * = violation word. Italics indicate the critical correct/violation word in each sentence.

tence frames, totaling 120 sentences overall. The subject-verb agreement condition, for which the verb ending did not agree with the plurality of the subject, consisted of 60 correct sentences with a singular subject, 60 correct sentences with a plural subject, and 120 violation sentences, totaling 240 sentences. The noun-phrase condition, for which either the singular/plural status or the grammatical gender of an article (e.g., los, "the [MASC. PLURAL]"; esta, "this [FEM. SINGULAR]") did not match the noun, consisted of 124 number violation frames, 124 gender violation frames, and 248 correct sentence frames, for a total of 496 sentences. In total, 856 sentences were used across all three conditions. The sentences ranged from 5 to 12 words in length. None of the sentences contained violations in initial or final sentence positions, so as to avoid sentence "start-up" and "wrap-up" effects in the EEG [23-24], and none of the critical words were repeated between frames. To ensure that the participants would be familiar with the vocabulary contained in the sentence frames, all the words for this task were taken from a Spanish textbook used at the university at the time that data collection began [25].

Sentences were presented one word at a time on the computer screen (see Figure 1) using E-Prime 2.0 software. Instructions for the task were read orally to the participants by the experimenter. Preceding each sentence, there was a screen that read, "Rest your eyes." After three seconds, the sentence was then visually presented one word at a time. Each word was displayed in the center of the screen for 350 ms, with a 150 ms interval of blank screen before the onset of the subsequent word. Once the entire sentence was presented, a screen followed that said, "Good/Bad?" In response to this prompt, participants pressed a keyboard button to categorize the sentence as either grammatical or ungrammatical. Participants first completed a short practice block containing 8 sentences. The stimuli sentences were then presented over 4 experimental blocks. There were three 3-minute breaks during the experiment, one at the end of each block. Another EEG recording was performed over the duration of this task but was not analyzed in the current study. Participants' responses were used to calculate a d-prime (d') score, which is a metric for signal detection that accounts for response bias by comparing how often a participant correctly identifies a signal to their false-alarm rate [26].

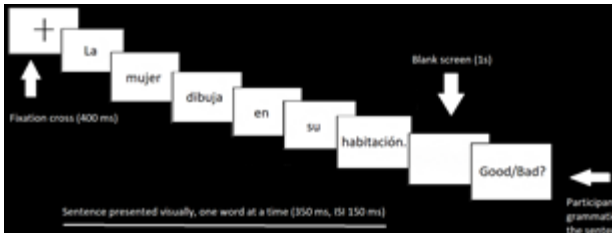

Figure 1: Diagram of a typical trial in the grammaticality judgment task.

Diplomas de Español como Lengua Extranjera (Diploma of Spanish as a Foreign Language):

A modified version of the Diplomas de Español como Lengua Extranjera (DELE, [27]) was used to assess Spanish proficiency. The three-part test was completed on a computer in the laboratory through a Qualtrics survey form. Participants were asked to read through the DELE questions and answer them at their own pace. In the first section, participants were required to read through a passage in Spanish and answer 20 fill-in-the-blank questions. Each question had 3 possible answer choices. In the second section, participants were given 10 sentences and asked to choose the answer choice that best defines the bolded word in the sentence. Each sentence also had 3 possible answer choices. The third section consisted of 19 grammatical questions . Participants were asked to select the answer choice that fit best in the context of each of the sentences. Eight of these questions had 2 possible answer choices, and the remaining questions had 4 possible answer choices. In total, participants answered 49 questions.

Procedures

Prior to testing, all participants completed pre-testing questionnaires that verified their eligibility and provided more detailed information about their language history. This included a language background questionnaire, a test-session questionnaire, and a handedness questionnaire. The language background questionnaire assessed each participant's demographic background and language history and experience (LEAP-Q, [28]). The test-session questionnaire assessed how much sleep a participant had and whether they had taken any psychoactive substances that may affect their ability to perform the task. The handedness questionnaire was used to gauge left-/right-handedness by assessing hand preference during various activities, following the standard Edinburgh Handedness Inventory [22]. The items were read to participants, who provided their answers verbally to the experimenter. Answers were recorded in computer-based survey forms.

In replicating [1]'s procedure, we collected five minutes of eyes-closed resting-state EEG following completion of the pre-testing surveys. Participants sat in a chair inside of a sound-attenuating booth. After fitting the participants for an EEG cap and placing eye electrodes, an electrolyte solution was applied to the scalp electrodes to minimize electrical impedances. Participants were then instructed to close their eyes and remain still and awake during the recording. While recording, the lights were turned off and the door of the sound booth was closed.

The EEG data was recorded using asa™ software with an ANT Neuro waveguard™ elastic cap with 32 Ag/AgCl electrodes distributed in standard and extended 10-20 system locations. Scalp impedances were lowered to 10 kΩ or below. Scalp electrodes were referenced to the common average of all the electrodes. To detect artifacts caused by eye movements, electrodes were placed above and below the right eye and on the left and right outer canthi to record a vertical electrooculogram and a horizontal electrooculogram, respectively. Using an ANT Neuro bioamplifier system (AMP-TRF40AB Refa-8 amplifier), the EEG signal was amplified to 22 bits. The signal was also recorded in DC mode, digitized with a 512 Hz sampling rate, and filtered online using a low-pass filter with a cutoff of 138.24 Hz.

Following the resting-state EEG session, the grammaticality judgment task was implemented in the sound booth (see above), and after disassembly of EEG equipment and a short break the DELE task was performed on a computer outside of the sound booth (see above).

Analyses

The qEEG data was pre-processed using the EE-GLab toolbox [29] for MATLAB [30]. To ensure that the resting-state recording was exactly five minutes, each recording was limited to 300 seconds. Seven participants had recordings that were slightly less than 300 seconds (minimum = 283 seconds) but were still included in the analysis. Each participant's recording was divided into epochs of two-second duration, with 50% overlap across epochs. These epochs were then cleaned for artifacts (e.g., from muscle movements, eyeblinks, faulty electrodes, etc.) using the pop_autorej() function from EEGLab. Participant datasets with less than 75 seconds of epoch-free recording were omitted from the final analysis, which resulted in the loss of 6 participants (12% of the data). The mean number of samples per participant was 144.44 (S.D. = 39.73).

The pre-processed data were subsequently analyzed using a modified version of the script used in the Prat et al. study [1] (available at: https://github.com/UWCCDL/QEEG) for the R scripting language [31]. Six electrode networks were defined (Figure 2): medial frontal (electrodes FP1, FPz, FP2, and Fz), left hemisphere fronto-temporal (electrodes F7, FC5, T7, C3), right hemisphere frontotemporal (F8, FC6, T8), left hemisphere posterior (CP5, CP1, P7, P3, O1), right hemisphere posterior (Cz, CP6, CP2, C4, P4, Pz), and right hemisphere posterior occipital (Oz, O2, POz, P8).

In defining the electrode clusters, we aimed to replicate Prat et al. (2019), in which qEEG channels were collapsed into networks based on phase synchrony results from an earlier L2 qEEG study. Prat et al. 2019's network definitions are technically slightly different from ours in that they used 14 electrodes rather than a 32-electrode cap, but our network definitions were aligned as closely with theirs as possible based on visual inspection of scalp maps (and in fact having a higher spatial resolution is a point in our favor in a sense). As data-driven results in favor of our network definitions (which we left out due to space limits), we replicated [1] (2019, Table I) in that independent samples t tests found that all within-network qEEG coherence values in our networks were significantly greater than all between-network coherence values, with all independent samples t-tests at $p < .001$. We then extracted the qEEG measures of interest, which were power and within- and between-network coherence for each of the frequency bands: theta (4-7.5 Hz), alpha (8-12.5 Hz), beta (13-29.5 Hz), and gamma (30-40 Hz).

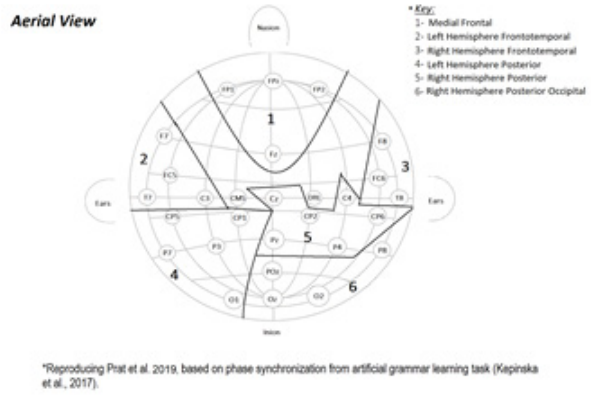

Figure 2: Diagram of the six network regions analyzed

Finally, to address the research questions, we first conducted correlations between mean power and performance on the grammaticality judgment task and the DELE, followed by correlations between mean coherence and performance on the grammaticality judgment task and the DELE. Here we report statistically significant correlations. These exploratory correlations were not corrected for multiple comparisons following the main analyses reported by [1]. For power and coherence measures that showed statistically significant correlations for either proficiency variable, we then entered them as predictors into two, separate regression analyses.

RESULTS

Individual Differences in Indicators of L2 Proficiency

Before examining the qEEG measures, descriptive statistics were examined for the two outcome measures of Spanish proficiency (see Figures 3 and 4 and Table III). With respect to the DELE, the group mean was 19 out of 49, which illustrates that the participants were overall low proficiency speakers [27]. The most proficient participant scored twice as much as the least proficient participant. With respect to the grammaticality judgment task, participants were given two scores: mean accuracy and d'. The average accuracy on the grammaticality judgment task was 76%. The average d' was 0.91. A bootstrapped simulation of chance-level d' values on 244 trials with 10,000 iterations performed using the psycho package for R [32] found a 95% confidence interval of -0.26 to 0.26. This suggests that our participants' d' values were above chance at $\alpha = 0.05$. DELE scores did seem to be above chance, as indicated by a mean accuracy of 39.5%. Considering that most of the DELE test items had 2, 3, or 4 answer choices, a minimum accuracy of 25% would at least reflect chance levels on the items with the most answer choices. DELE scores and grammaticality judgment task d' scores were not significantly correlated with one another, $r(44) = 0.27$, $p = 0.069$. As per [21], our results suggest that the grammaticality judgment task and DELE might capture somewhat different facets of L2 proficiency.

Table III. Performance on the two proficiency tasks

Performance measure	M (SD) [Range]
DELE score	19.3 (3.15) [0.13-0.26]
Grammaticality judgment task d' score	0.91 (0.74) [-0.27-2.88]
Grammaticality judgment task accuracy	0.76 (0.10) [0.51-0.98]

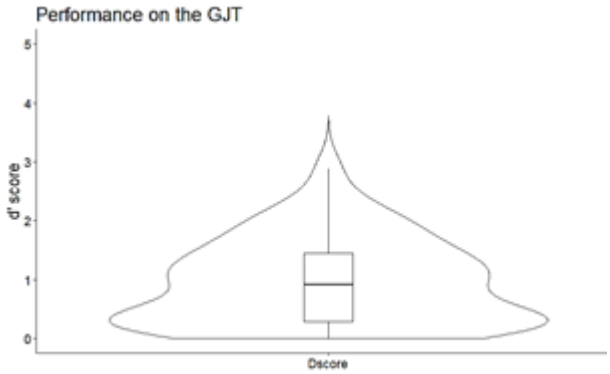

Figure 3: Participant performance on the grammaticality judgment task. The maximum possible d'score on the grammaticality judgment task was effectively 4.9.

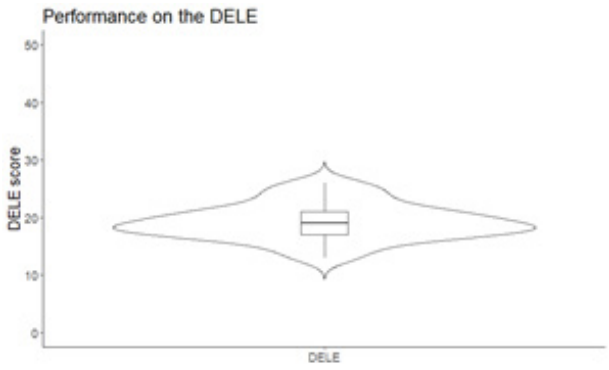

Figure 4: Participant performance on the Spanish proficiency test (DELE). The maximum possible score on the DELE was 49.

Relating Individual Differences in Resting-state qEEG Power to L2 Proficiency Variables

In order to determine the relationship between resting-state qEEG power and performance on the two proficiency tests, we performed correlation analyses between either the grammaticality judgment task or DELE scores (in separate analyses) and mean power across six electrode networks. The frequency bands of interest were theta (3-7 Hz), alpha (8-12 Hz), beta (13-30 Hz), and gamma (30-200 Hz). After conducting these analyses, none of the correlations were found to be significant. However, two positive correlations were approaching significance: medial frontal alpha power and DELE scores, $r(47) = 0.28$, $p = .052$; and left hemisphere frontotemporal alpha power and DELE scores, $r(47) = 0.27$, $p = 0.057$.

Relating Individual Differences in Resting-state qEEG Coherence to L2 Proficiency Variables

In order to determine the relationship between resting-state qEEG coherence and performance on the two proficiency tests, we performed correlation analyses between the L2 proficiency variables and mean within- and between-coherence across six electrode networks. The frequency bands of interest were theta, alpha, beta, and gamma. For the between-coherence values, each of the networks were paired together and coherence across the four frequency bands was calculated for every pair. Regarding the DELE, two significant negative correlations were found: theta coherence within the right hemisphere posterior occipital network, $r(47) = -0.31$, $p = 0.028$; theta coherence between the me-dial frontal and right hemisphere posterior occipital networks, $r(47) = -0.35$, $p = 0.012$. Regarding the grammaticality judgment task, there were no signif-icant correlations (all $p > 0.05$).

Simultaneous Linear Regression Analyses

When the two predictors of performance on the DELE (theta coherence within the right hemi-

sphere posterior occipital network and theta coherence between medial frontal and right hemisphere posterior occipital) were entered into a simultaneous regression analysis, the overall model was found to be statistically significant, $F(2, 46) = 3.97$, $p = 0.026$, explaining up to 11% of the observed variance. However, neither theta coherence within the right hemisphere posterior occipital network ($\beta = -13.91$, $t = -1.07$, $p = 0.290$) nor theta coherence between medial frontal and right hemisphere posterior occipital ($\beta = -41.78$, $t = -1.61$, $p = 0.114$) were found to independently predict performance on the DELE (see Figures 5 and 6).

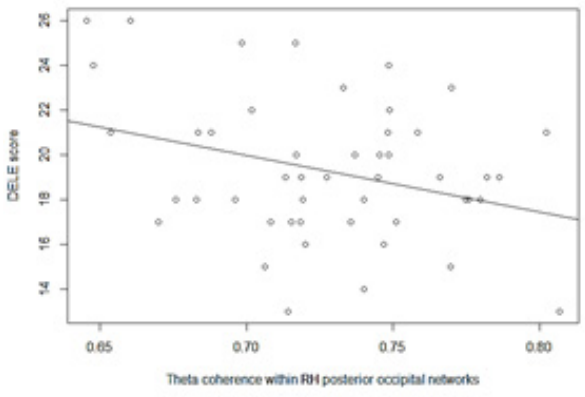

Figure 5: Regression line between the DELE and theta coherence within right hemisphere posterior occipital networks.

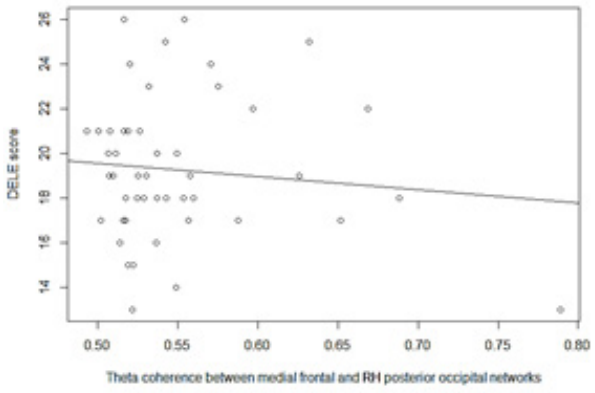

Figure 6: Regression line between the DELE and theta coherence between the medial frontal and right hemisphere posterior occipital networks.

DISCUSSION

Our results suggest that certain resting-state qEEG measures, particularly over the theta frequency band, are associated with L2 proficiency. Regarding the first research question, none of the correlations run between resting-state mean power and L2 proficiency reached significance. However, the two correlations that did approach significance were related to alpha power: the positive correlation between medial alpha power and the DELE, and the positive correlation between left hemisphere frontotemporal alpha power and the DELE. Regarding the second research question, two significant negative correlations were found between resting-state within- and between-network coherence and the DELE, one within right hemisphere posterior networks and another between medial frontal and right hemisphere posterior networks. Both significant correlations were found over the theta frequency band. After performing regressions on the significant qEEG predictors for DELE performance, the model was found to explain up to 11% of the variance. None of the variance in grammaticality judgment task performance was explained by qEEG measures.

In relating our results with those of previous studies, the correlations found between the theta frequency band and L2 proficiency were anticipated, although the direction of the relationship varied by study. In [1], theta coherence within frontal electrode regions was positively correlated with several outcome measures of L2 learning. In [16], highly proficient speakers experienced increased theta synchronization in right frontal regions during a grammar learning task. However, in the L2 proficiency study conducted by [13], lower theta coherence in frontal and occipital electrodes was observed among highly proficient speakers. In our study, the relationship between theta coherence measures and L2 proficiency was also negative. Why do we see these contradictory patterns among studies? This may be explained by the differences in language learning and language proficiency. For instance, the participant

population used for language learning studies consists of speakers who were just beginning to learn an L2, whereas proficiency studies involve participants who have already had experience learning the additional language.

We understand activity in the theta frequency band to reflect several memory functions, including specifically short- and long-term memory maintenance and memory retrieval [5, 10, 33, 34]. Additionally, the theta frequency is believed to originate from the cortex [5], which plays a role in the formation of new memories. Generally, studies have found positive relationships between theta activity and learning rate in earlier stages of learning, negative relationships between theta and L2 ability in later stages [1, 16, 19]. The negative relationship found in this study may signify that more proficient participants are good at applying and retrieving grammar rules and no longer need to rely on working memory, which would result in a decreased prevalence of theta oscillations. Altogether, as suggested by [16], the negative correlations found between theta coherence and DELE performance suggest that less proficient L2 speakers have a greater reliance on memory-based strategies to compensate for their lack of familiarity with the language.

Even though the alpha frequency band was not significant, it was approaching significance, which reflects the inverse theta-alpha relationship expressed in the literature [5]. Increases in the alpha frequency have been associated with diminished attention paid to a linguistic task [10]. Interpreting the negative correlation between theta and proficiency to be the consequence of decreased working memory load, a positive correlation with alpha would suggest that more proficient participants were able to pay less attention to the task and still be successful. This may signify that the more automatic a language task is to a participant, the more likely they are to be more proficient.

The results of this study need to be considered in light of its limitations. One limitation was the proficiency measures that were employed. As mentioned in the results section, our participants did not score statistically above chance on average on the DELE. Thus, it is somewhat surprising that significant results were found for the DELE and not for the grammaticality judgment task. Perhaps the more difficult DELE test, which had been developed to test up to near-native speaker status, allowed us to detect a role related to which learners are more successful on a more challenging task. Conversely, the grammaticality judgment task was designed to reflect specific grammatical structures taught in intermediate-level Spanish courses, so we would expect participants to perform more successfully on this task overall, which they did, as evidenced by above-chance performance. More generally, because the DELE and grammaticality judgment task both reflect performance accuracy on grammatical tasks, it is important to note that they are not holistic measures. As a multidimensional construct, language proficiency encompasses all the skills necessary to engage with the language in a real-life context [2]. Thus, it would be beneficial for future research to include more time-pressured proficiency measures in future research, such as an oral elicited imitation (EIT) task. Unlike the DELE and grammaticality judgment task, which are both primarily prescriptive grammar tasks, the EIT can assess more implicit language knowledge by asking participants to listen to sentences and repeat them [35, 36]. This testing method has been found to engage long-term memory and require a higher level of language comprehension.

It is also worth noting that, while we found significant correlations with theta coherence, the majority of the qEEG measures were not associated with L2 proficiency. Though we interpreted theta to reflect the engagement of working memory, one difficulty in interpreting the results of this study, is in interpreting what cognitive processes may be reflected by the different frequency bands. Although previous research does suggest associations between activity in the frequency bands and different

cognitive processes, future research will need to strengthen the validity of these claims regarding theta. In regard to the lack of a relationship between L2 proficiency and the other frequency bands, null results can be difficult to explain, but the results could be at least partially due to our processing procedures where a certain amount of the data was not included. For future analyses, we plan on implementing independent component analyses performed to correct for eye and muscle artifacts in EEG data (using ICLabel; [37]), which is expected to lead to lead to cleaner data, higher sample sizes, and improved model fits for both DELE and grammaticality judgment task.

We note three further limitations in our study that should be addressed in future research. First, future research might want to analyze data from a particular semester rather than data spanning participants from two Spanish course levels, or the course level could be included as a covariate in analyses. Second, regarding the analysis, a more precise way to define the frequency ranges of the specific frequency bands is to use individual alpha frequency (IAF) peaks. For each person, the IAF peaks at a different number, which affects the ranges of the other frequency bands [38]. Finally, given the highly exploratory nature of this study, we did not correct for multiple correlation analyses, and we entered regression predictors based on significance from the correlational analyses. Future research should conduct more conservative, confirmatory analyses on a dataset with higher statistical power to mitigate possible Type I errors. Indeed, post hoc analyses for our dataset showed that the significant correlations reported above did not survive correction for Type I error inflation using the family-wise discovery rate, which further suggests that a confirmatory study would need to be conducted to validate any of the exploratory findings reported in this study. Using this method in future research may further solidify the validity of our results or may lead to different findings.

CONCLUSION

The purpose of the current study was to investigate whether mean qEEG power and coherence are significant predictors of L2 proficiency. Based on our results, within- and between-network coherence over the theta frequency band is closely related to Spanish L2 proficiency. Because the theta frequency has been associated with memory retrieval and load, these results suggest that there is an inverse relationship between L2 proficiency and reliance on memory-based strategies for interpreting linguistic inputs. Additionally, increased theta activity may be characteristic of individuals in earlier stages of language learning. More research is needed to further validate the significance of theta in L2 proficiency, as well as to determine the importance of the other frequency bands. Ultimately, this study adds to growing literature of resting-state L2 qEEG studies, echoing the implication of intrinsic patterns of neural activity as sources of individual variation in linguistic ability. Over time, qEEG may help to reveal individual neurophysiological variations among students within a classroom, enabling educators to develop language learning strategies that will be most conducive to successful L2 outcomes for them. In other words, from the conclusions of this body of research, we might be able to identify particular cognitive processes that are associated with L2 learning and proficiency. With such information, further research could then examine how to leverage these processes in instruction.

AUTHOR INFORMATION

Corresponding Author
Victoria Ogunniyi
*vogunn2@uic.edu

Author Contributions

Victoria Ogunniyi assisted with data collection and performed the analyses along with Irene Martinez and David Abugaber. Victoria Ogunniyi wrote the manuscript. Kara

Morgan-Short, David Abugaber, Irene Finestrat, and Alicia Luque reviewed the manuscript and devised the experimental plan.

Competing Interests
The authors declare no competing financial and non-financial interests.

ACKNOWLEDGMENTS

Thank you to Kinsey Bice for her help with performing the qEEG analyses. Thank you also to all undergraduate research assistants affiliated with the Cognition of Second Language Acquisition laboratory who contributed towards data collection for this project, including Hannah Chaddah, Sarah Hassan, Gayatri Chavan, Will Camacho, Ana Hernandez, Anahi Gaytan, Krishna Bhatia, Amber Lewis, Mallory Webber, Evelyn Delgado, Daniel Henreckson, Yasiel Lacalle, and Nethaum Mizyed. We would also like to thank Sarah Malone, Christopher Powell, Crystal Galvan, and Allen Bryson of the University of Illinois at Chicago's Summer Research Opportunities Program for Undergraduates for their support in the development of this manuscript.

ABBREVIATIONS

DELE- Diplomas de Español como Lengua Extranjera
EEG – Electroencephalography
L2 – Second Language
qEEG – Quantitative Electroencephalography

REFERENCES

[1] C.S. Prat, B.L. Yamasaki, E.R. Peterson, Individual Differences in Resting-state Brain Rhythms Uniquely Predict Second Language Learning Rate and Willingness to Communicate in Adults. J Cogn Neurosci 31(1), 78-94 (2019).

[2] P. Leclercq, A. Edmonds, H. Hilton, Eds. Measuring L2 proficiency: Perspectives from SLA (Multilingual Matters, 2014).

[3] C. J. Doughty, M.H. Long, "The scope of inquiry and goals of SLA" in The handbook of second language acquisition (John Wiley & Sons, 2003), pp. 3-16.

[4] S. J. Luck, An introduction to the event-related potential technique (MIT press, 2014).

[5] K. Majumdar, A brief survey of quantitative EEG, 2nd ed. 2018 (CRC Press, 2018).

[6] M. Bastiaansen, A. Mazaheri, O. Jensen, "Beyond ERPs: Oscillatory neuronal dynamics" in The Oxford Handbook of event-related potential components, S. Luck & E. Kappenman, Eds. (Oxford University Press, 2012), pp. 31-50.

[7] G. Gluck, QEEG accepted in death penalty trial in Florida v. Nelson. Biofeedback 39(2), 74-77 (2011).

[8] M. Arns, W. Drinkenburg, J. Leon Kenemans, The effects of QEEG-informed neurofeedback in ADHD: an open-label pilot study. Appl Psycho-physiol Biofeedback 37(3), 171-180 (2012).

[9] C.S. Prat, T.M. Madhyastha, M.J. Mottarella, C.H. Kuo, Relating Natural Language Aptitude to Individual Differences in Learning Programming Languages. Sci Rep 10(1), 1-10 (2020).

[10] Y. Prystauka, A.G. Lewis, The power of neural oscillations to inform sentence comprehension: a linguistic perspective. Lang Linguist Compass 13(9), e12347 (2019).

[11] L. Meyer, The neural oscillations of speech processing and language comprehension: state of the art and emerging mechanisms. Eur J Neurosci 48(7), 2609-2621 (2018).

[12] M. Lundqvist, P. Herman, M.R. Warden,

S.L. Brincat, E.K. Miller, Gamma and beta bursts during working memory readout suggest roles in its volitional control. Nat Commun 9(1), 1-12 (2018).

[13] S. Reiterer, C. Hemmelmann, P. Rappels-berger, M.L. Berger, Characteristic functional networks in high- versus low-proficiency second language speakers detected also during native language processing: an explorative EEG coherence study in 6 frequency bands. Brain Res Cogn Brain Res 25(2), 566-578 (2005).

[14] S. Reiterer, E. Pereda, J. Bhattacharya, Measuring second language proficiency with EEG synchronization: how functional cortical networks and hemispheric involvement differ as a function of proficiency level in second language speakers. Second Lang Res 25(1), 77-106 (2009).

[15] S. Reiterer, E. Pereda, J. Bhattacharya, On a Possible Relationship between Linguistic Expertise and EEG Gamma Band Phase Synchrony. Front Psychol 2, 334 (2011).

[16] O. Kepinska, E. Pereda, J. Caspers, N.O. Schiller, Neural oscillatory mechanisms during novel grammar learning underlying language analytical abilities. Brain Lang 175, 99-110 (2017).

[17] A. Kielar, J.A. Meltzer, S. Moreno, C. Alain, E. Bialystok, Oscillatory responses to semantic and syntactic violations. J Cogn Neurosci 26(12), 2840-2862 (2014).

[18] A.G. Lewis, K. Lemhöfer, J.M. Schoffelen, H. Schriefers, Gender agreement violations modulate beta oscillatory dynamics during sentence comprehension: A comparison of second language learners and native speakers. Neuropsychologia 89, 254-272 (2016).

[19] Z.R. Cross, A. W. Corcoran, M. Schlesewsky, M.J. Kohler, I. Bornkessel-Schlesewsky, Oscillatory and aperiodic neural activity jointly predict grammar learning. BioRxiv (2020).

[20] C.S. Prat, B.L. Yamasaki, R.A. Kluender, A. Stocco, Resting-state qEEG predicts rate of second language learning in adults. Brain Lang 157, 44-50 (2016).

[21] A. Godfroid, S. Loewen, S. Jung, J. H. Park, S. Gass, R. Ellis, Timed and untimed grammaticality judgments measure distinct types of knowledge: Evidence from eye-movement patterns. Studies in Second Language Acquisition 37(2), 269-297 (2015).

[22] R.C. Oldfield, The assessment and analysis of handedness: the Edinburgh inventory. Neuropsychologia 9(1), 97-113 (1971). Available at: https://www.psytoolkit.org/survey-library/handedness-ehi.html.

[23] V. Kuperman, M. Dambacher, A. Nuthmann, R. Kliegl, The effect of word position on eye-movements in sentence and paragraph reading. Q J Exp Psychol (Hove) 63(9), 1838-1857 (2010).

[24] L.A. Stowe, E. Kaan, L. Sabourin, R.C. Taylor, The sentence wrap-up dogma. Cognition 176, 232-247 (2018).

[25] J.A. Blanco, P.R. Donley, Vistas: Introduccion a la lengua española, 5th ed. 2016 (Vista Higher Learning, Inc., 2016).

[26] N.A. Macmillan, C.D. Creelman, Detection theory: A user's guide (Psychology press, 2004).

[27] S. Montrul, Second language acquisition and first language loss in adult early bilinguals: exploring some differences and similarities. Second Lang Res 21(3), 199-249 (2005).

[28] V. Marian, H.K. Blumenfeld, M. Kaushanskaya, The Language Experience and Proficiency Questionnaire (LEAP-Q): assessing language profiles in bilinguals and multilinguals. J Speech Lang Hear Res 50(4), 940-967 (2007). Available at: https://bilingualism.northwestern.edu/leapq/.

[29] A. Delorme, S. Makeig, EEGLAB: an open source toolbox for analysis of single-trial EEG dynamics including independent component analysis. J Neurosci Methods 134(1), 9-21 (2004). Available at: https://sccn.ucsd.edu/eeglab/index.php.

[30] MathWorks, Inc., MATLA8B 8.0 and Statistics Toolbox 8.1, Natick, Massachusetts, United States (2020). Available at: https://www.mathworks.com/downloads/.

[31] R Core Team, R: A language and environment for statistical computing. R Foundation for Statistical Computing, Vienna, Austria (2020). Available at: https://www.r-project.org/.

[32] D. Makowski, The Psycho Package: An Efficient and Publishing-Oriented Workflow for Psychological Science. Journal of Open Source Software 3(22), 470 (2018). Available at: https://github.com/neuropsychology/psycho.

[33] W. Klimesch, EEG alpha and theta oscillations reflect cognitive and memory performance: a review and analysis. Brain Res Brain Res Rev 29(2-3), 169-195 (1999).

[34] N.A. Herweg, E.A. Solomon, M.J. Kahana, Theta Oscillations in Human Memory. Trends Cogn Sci 24(3), 208-227 (2020).

[35] R. Erlam, Elicited imitation as a measure of L2 implicit knowledge: an empirical validation study. Applied Linguistics 27(3), 464–491 (2006).

[36] N. Spada, J.L.J. Shiu, Y. Tomita, Validating an elicited imitation task as a measure of implicit knowledge: comparisons with other validation studies. Lang Learn 65(3), 723-751 (2015).

[37] L. Pion-Tonachini, K. Kreutz-Delgado, S. Makeig, ICLabel: An automated electroencephalographic independent component classifier, dataset, and website. Neuroimage 198, 181-197 (2019).

[38] O.M. Bazanova, Alpha EEG activity depends on the individual dominant rhythm frequency. J Neurother 16(4), 270-284 (2012).

CUSJ
COLUMBIA UNDERGRADUATE SCIENCE JOURNAL

The Effects of APOBEC3G's Cytidine Deaminase Activity on Retroviral Evolution

Mary-Benedicta Obikili[1]

[1]Department of Microbiology and Immunology, University of Illinois at Chicago College of Medicine, Chicago, IL, USA

KEYWORDS: APOBEC3G, cytidine deamination, retroviral evolution

ABSTRACT: Apolipoprotein B editing complex (APOBEC3/A3) genes are found in mammalian cells. In primates, there are 7 APOBEC3 genes, namely, 3A, 3B, 3C, 3DE, 3F, 3G, and 3H. Previous research has shown that A3 proteins help to inhibit viral infection via their cytidine deaminase activity. However, it has also been found that A3 proteins could lead to viral evolution, where retroviruses such as HIV (Human Immunodeficiency Virus), acquire beneficial mutations that enable them to overcome the antiviral activity of A3 proteins, gain resistance to certain drugs used for treating viral infections and escape recognition by the immune system. This paper is a review article summarizing the role of A3G on viral infection and evolution, and the potential impact viral evolution could have in treatment of retroviral infections such as HIV.

INTRODUCTION

Apolipoprotein B- Editing Complex 3 (APOBEC3/A3) genes encode enzymes that prevent viral infection through their cytidine deaminase activity [1]. There are seven APOBEC3 genes found in humans, namely: A3A, A3B, A3C, A3DE, A3F, A3G, and A3H. Most of these proteins play a role in inhibiting viral infection, however, A3G, A3F, A3D, and A3H are best known for their antiviral role [2, 3]. A3 proteins can be found in human and mouse dendritic and myeloid cells, and they are usually expressed at different levels in hematopoietic cell populations, which include B cells, CD4+ and CD8+ T cells [1]. When a host cell is infected, interferons, and other chemokines and cytokines are released and stimulate the expression of A3 proteins in other cells which help to fight off the infection [1]. It has been found that A3 proteins, specifically A3G, is the main antiviral protein in CD4+ T cells. Therefore, when a cell is infected, A3G levels increase, hence inhibiting viral replication by introducing more G to A hypermutations in the virus [1]. These A3 proteins are packaged into the virion, which lead to viral inhibition through their cytidine deaminase activity. The cytidine deaminase activity of A3 proteins refers to the conversion of cytosine to uracil in single-stranded DNA (Fig. 1A). During the process of retrovirus infection, the virion enters the cell cytoplasm and uncoats its viral RNA (Fig. 1B). The viral enzyme reverse transcriptase then uses the RNA as a template for making DNA. However, during the process of reverse transcription, the A3 protein deaminates the cytidine residues of the (-) strand vi-

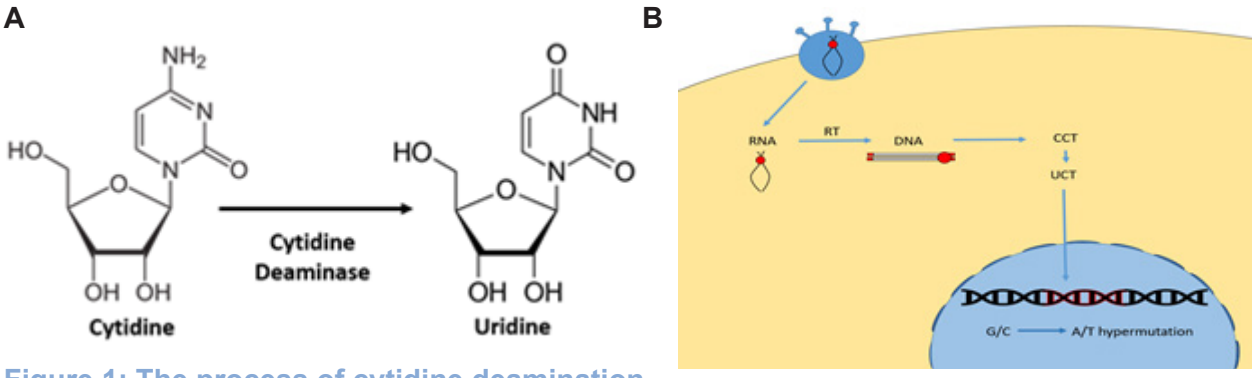

Figure 1: The process of cytidine deamination.
(A) The enzyme APOBEC3, which is a cytidine deaminase, deaminates cytidine to uridine in the single-stranded retroviral DNA before its integration into the host cell
(Source: National University of Singapore, Faculty of Science, Special Programme in Science and iGEM 2018, Yuhui Deborah Fong (used with permission))
(B) The virus enters the cell. After uncoating of the RNA genome, the viral enzyme, reverse transcriptase makes a double-stranded DNA copy of the genome, which then enters the nucleus and integrates into the host chromosomes. During reverse transcription, A3 enzymes (red ball), which are packaged in the virion deaminates cytidine to uracil in the single-stranded viral DNA before its replication and integration into the chromosomes, resulting in G-to-A changes in the viral genome. The red DNA in the nucleus is the integrated viral DNA.

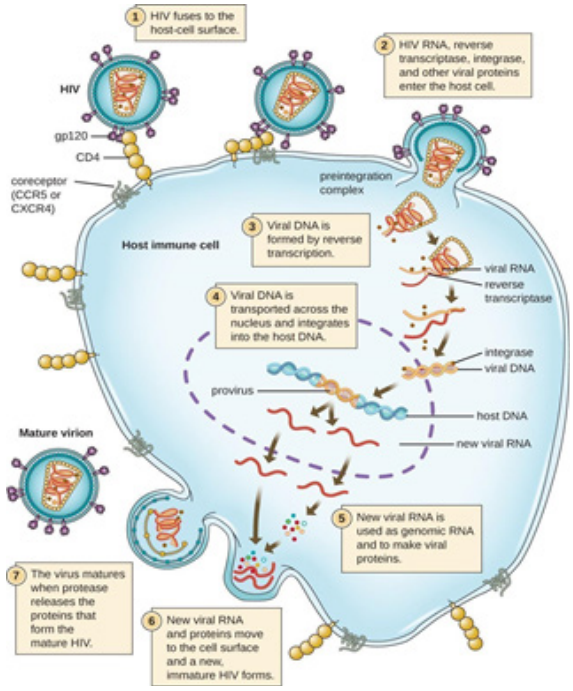

Figure 2: Retrovirus Life Cycle
This shows the process of retroviral integration and replication in the host cell.
(Figure obtained and used with permission from OpenStax Microbiology textbook [7]) (Access at https://openstax.org/books/microbiology/pages/1-introduction)

ral DNA to uracil residues, resulting in G-to-A mutations in the viral coding (+) strand DNA. In other words, because cytidine is converted to uracil, which reverse transcriptase reads as thymidine, guanosine is replaced with adenine in the viral coding strand DNA. After the synthesis of a double stranded DNA molecule, the viral DNA goes into the host cell's nucleus and becomes integrated in the chromosomes (Fig. 1B). The A3-induced mutations inhibit the synthesis of virus proteins and virions because they inactivate the virus, which prevents it from infecting and replicating in other cells.

Although APOBEC3 proteins help inhibit viral infection through their cytidine deaminase activity, A3D, A3F, A3G, and A3H may also play a role in viral evolution, where viruses such as HIV gain beneficial mutations that enable them to overcome the antiviral activity of A3 proteins [5, 6]. This paper will highlight the role of A3 proteins, specifically A3G, on retroviral evolution.

RETROVIRUS REPLICATION

Viruses are infectious pathogens that require a host cell for their growth and replication. Al-

though they do not have the ability to grow on their own, once inside a cell they use its machinery to grow and multiply and have the potential to cause diseases in the host organism.

Retroviruses are viruses that use their viral RNA-dependent enzyme, reverse transcriptase, to synthesize viral DNA in a host cell which is then inserted into the chromosomal DNA (Fig. 1B). HIV is a lentivirus that infects CD4+ T cells, macrophages, and dendritic cells in humans [1]. The process of retrovirus infection is shown in Fig. 2. Once a retrovirus encounters a host cell, it binds to a cell surface receptor, hence enabling its fusion with the cell. After it fuses with the cell, it uncoats its RNA genome and enzymes, such as reverse transcriptase (RT), which then synthesize a new copy of the viral DNA from the RNA template. Then the viral DNA enters the nucleus and the viral enzyme integrase, along with several host proteins, splices the viral DNA into the cell's genome. Cellular RNA polymerase is then used to transcribe the viral DNA into mRNA which is then translated into viral protein. The new virions made are assembled at the host membrane and bud off from the cell membrane.

The final stage consists of the retrovirus protease enzyme cleaving the precursor proteins into mature viral proteins leading to the maturation of the virus and the start of a new cycle [8].

RETROVIRAL EVOLUTION

The cytidine deaminase activity of A3 proteins may also lead to retroviral evolution, where the virus gains beneficial mutations that help the virus to counteract A3 antiviral activity [5, 6]. A3G has been shown to preferentially deaminate CC motifs, resulting in AG motifs in the coding strand, whereas the other A3 proteins have been shown to preferentially deaminate TC motifs, resulting in AA motifs [5, 6]. However, HIV-1 encodes a protein the viral infectivity factor (Vif), which leads to the degradation of A3 proteins in virus-producing cells [5]. Vif has two motifs that bind to A3 proteins: DRMR which binds to and degrades A3F and A3D, and the other motif, YRHHY, which binds to A3G, leading to its degradation [5]. Fig. 3 shows the structure of the Vif complex [5]. When Vif binds to A3, it prevents it from entering the budding virion by targeting it for degradation. It does this by binding to CBFB co-factor and Cullin 5 E3 – Ubiquitin Ligase (ELOB-ELOC-CUL5), via the sites diagrammed in Fig. 3B, which then targets the A3 protein for proteasomal degradation [5].

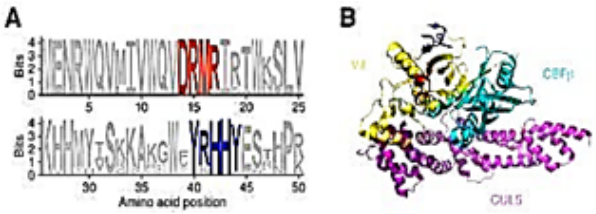

Figure 3: The structure of Vif
(A) Shows the two Vif motifs that bind to A3 proteins. DRMR (red) binds to A3D and A3F, whereas YRHHY (blue) binds to A3G
(B) Shows the Vif complex. The blue and red correspond to the Vif binding motifs in A where Vif binds to A3D, A3F and A3G, respectively. The yellow, cyan and pink colors represent the Vif protein, CBFB co-factor and CUL5 ligase respectively
(Fig. obtained from Sato K. et al. 2014, with permission to reprint from PLOS pathogens).

Viral evolution can occur when there are defective (mutant) Vif proteins. The defective proteins do not cause complete A3 degradation and therefore allow some A3 proteins to enter the virion, resulting in mutations in the viral genome. Since A3G prefers to deaminate TGGG – TAGG motifs, it often converts the codon encoding for the amino acid tryptophan (TGG) into a stop codon (TAG), which renders the virus defective and unable to synthesize its proteins. This prevents it from `assembling at the host cell's membrane and infecting other cells. Sato et al. found that A3 proteins lead to mutations in the env region of the HIV-1 genome, which codes for the viral glycoprotein [5]. This protein is important for enabling the virus to bind to cellular receptors and fuse with the host cell's membrane. Mutations caused by

A3 proteins inhibit the virus from synthesizing its glycoprotein, which in turn prevents it from infecting the cell. These defective viruses may later get degraded. Occasionally, the resulting G-to-A mutations may also be sub-lethal (depending on the levels of A3G present in the cell, which may be due to genetic factors, such as different polymorphisms in A3G genes in humans [9], and the context of the TG motif), resulting in missense mutations. In other words, lower levels of A3G expression, would result in more sub-lethal mutations, compared to higher levels of A3G expression, which would mostly result in lethal mutations. Moreover, other A3 proteins such as A3D and A3F, respectively prefer deaminating the GA – AA and GAA – AAA motifs [5], resulting in sub-lethal missense mutations. These missense mutations may result in viral evolution and diversification. For example, the Sato study showed that A3 mutations in env also changed the co-receptor specificity of the glycoprotein, enabling it to preferentially infect different cell types.

It has been found that some A3 proteins may indirectly contribute to retroviral evolution, where the cytidine deaminase activity of the A3 protein helps the virus to acquire mutations that will make it more fit. Studies by Kim et al., Sato et al., and Fourati et al. showed that retroviruses, such as HIV, can sometimes gain beneficial mutations that enable them to replicate better [3, 5, 6]. Sato et al., Fourati et al., and Borzooee et al., also demonstrated that A3 proteins such as A3D, A3F, A3G and A3H can sometimes lead to retroviral evolution [3, 5, 10]. It was also shown that A3 proteins can mutate viruses so that they can use different receptors on the cell surface for entry into the host cell [5]. Moreover, in the Sato study [5], where humanized mice models were used to study different Vif mutants that were initially mutated via A3-independent means, it was found that A3D and A3F highly suppressed one mutant, A3G highly suppressed another mutant, and the other was a double mutant, that was suppressed by A3D, A3F, and A3G [5]. It was demonstrated that although a wild type Vif protein can target A3 for proteasomal degradation, a defective Vif protein, could be suppressed by A3 proteins. However, sometimes these A3-dependent mutations may benefit the virus. In the study, they found that A3F and A3D led to more viral diversification compared to A3G (for reasons previously described).

These studies suggest that A3 proteins could benefit the virus by leading to mutations that will help the virus to overcome A3's antiviral activity, and evade antiretroviral drugs detection, leading to viral escape. This will enable them to continue to undergo replication and infection in additional cells. In other words, the A3 proteins assist the virus by enabling them to gain diversity, which in turn may help the virus to acquire mutations that make it gain drug resistance.

DRUG RESISTANCE

Drug resistance refers to the ability of a pathogen to overcome the effects of a drug. This usually occurs when a certain drug is continuously used to treat a particular infection, and due to constant exposure of the disease pathogen to the drug, the drug becomes less effective, usually because the pathogen acquires drug-resistance gene mutations. To minimize the possibility of disease pathogens gaining resistance, multiple drugs could be used for the treatment of that disease. This is usually seen in the treatment of certain diseases, such as HIV, where a combination of different drugs (such as highly active antiretroviral therapy, HAART) are used simultaneously to prevent the emergence of drug-resistant virus. However, G-to-A mutations caused by A3 proteins in the retrovirus may cause the retrovirus to gain mutations that enable it to become drug-resistant. As shown in the study by Fourati et al., peripheral blood mononuclear cells (PBMCs) and other body fluids/tissues obtained from 30 HAART-treated patients were examined for possible drug-resistance mutations. It was found that A3-dependent hypermutations in addition to viral recombination could lead to viral evolution [6].

Additionally, in a study by Mulder et al., it was found that G-to-A hypermutations caused by A3G reduces the viral infectivity and could also lead to viral diversification [11]. In this study, it was demonstrated that defective Vif mutants with suboptimal anti-A3G activity could lead to the production of proviruses resistant to the drug lamivudine (3TC) (which inhibits the retroviral reverse transcriptase) before drug exposure. Although the proviruses were not able to replicate, when they recombined with wild-type HIV-1, they produced competent viruses that were resistant to the drug 3TC [11].

In a similar study by Hernandez et al., it was found that sublethal mutations induced by A3G could lead to viral diversification. They infected humanized mice with different variants of HIV (that were mutated via A3-independent means), and they found that the wild type HIV strain had a higher fitness compared to the mutant strains prior to its treatment with 3TC [12]. However, when they started the treatment with the drug, they found that the mutant strain was less susceptible to the antiretroviral drug's effect because of its defectiveness. In other words, because the mutant HIV strain is less fit, the drug has a decreased effect on it compared to the wild type, hence the mutant strains become resistant to the drug [12]. Thus, these studies show that sublethal mutations caused by A3G, increase viral diversification which could make the virus gain resistance to certain drugs. These mutations could also enable the virus to undergo immune escape.

IMMUNE ESCAPE

Immune escape refers to a situation where a pathogen evades detection by the host's immune system. In the case of retroviruses, this immune escape can be aided by A3 proteins [1, 10, 13]. As mentioned earlier, A3 proteins may sometimes cause sublethal mutations, which could help the virus to avoid detection by cytotoxic T cells (CTL), which kill infected cells [1, 10, 13]. These sublethal mutations may alter CTL epitopes or lead to mutations that alter peptide degradation and its presentation by the human leukocyte antigen (HLA) proteins on the cell surface [10, 13]. HLA proteins are human major histocompatibility complex (MHC) proteins that present peptides to CTLs, thereby allowing recognition of infected cells [10, 13].

In a study by Grant and Larijani, it was found that A3G/A3F could cause mutations in HIV peptides that prevented the virus from being detected by CTLs, hence enabling it to escape the host cell's immune response [13]. Similarly, a study by Borzooee et al. showed that A3G-dependent mutations could lead to decreased binding affinity of HLA to the peptide epitopes, which also enables viral immune escape [10]. In this study, it was observed that the sequences that encode CTL epitopes in HIV are rich in A3G-preferred deamination motifs, which preferentially mutate the C in CC<u>C</u>, TC<u>C</u>, and AC<u>C</u> [10]. This could result in missense mutations that alter CTL epitopes. Thus, these mutations could help the virus evade detection by the host cell's immune response, which enables it to continue to spread in an individual.

These studies show that although A3G could result in lethal mutations in the virus, sublethal mutations could cause viral immune escape, where CTLs are no longer able to recognize infected cells to target them for killing. This could lead to natural selection and viral evolution, where the viruses are able to acquire beneficial mutations that enable them to become more fit and harmful/difficult to treat.

CONCLUSION

In conclusion, many studies have shown the effects of the cytidine deaminase activity of the A3 genes on retroviral evolution. APOBEC3 proteins are known to inhibit viral infection through their cytidine deaminase activity [1, 2, 3, 14]. However, lower expression of A3 proteins in cells could also lead to viral evolution [3, 5, 6]. When A3 proteins such as A3G and A3F are expressed at lower levels, they are likely to introduce nonsense mutations in the virus, which instead of inhibiting the virus, helps it ob-

tain beneficial mutations that allow it to become more fit and able to evade the cells' immune response [10, 13] and develop drug resistance [6, 11, 12]. Also, many studies show that HIV can evolve to overcome A3's cytidine deaminase activity by encoding Vif's variants that more effectively target A3 for proteasomal degradation [1, 3, 5, 14]. Moreover, Fourati et al. and Mulder et al., both showed that in addition to A3-dependent mutations, viruses could also evolve via recombination, where defective viruses after recombination gain drug resistance [6, 11].

These studies collectively suggest that A3 proteins play an important role in the host cells' immune response and help the cells to combat viral infection. Although, these studies highlight the importance of A3 proteins, they also show the limitations of its use in preventing viral infection, since HIV-1 Vif protein inhibits A3 proteins' antiviral activity. Future studies should focus on developing drugs that would inhibit HIV-1 Vif's ability to bind and degrade A3 proteins, or enable A3 proteins, specifically A3G, to overcome Vif activity, so that they could better inhibit retroviral infection and evolution.

AUTHOR INFORMATION

Corresponding Author
*Mary-Benedicta Obikili
mobiki2@uic.edu

Funding Sources
This research was supported by the NIH/NIAID grant R01AI085015 and the L@s GANAS project (HSI STEM grant from Dept. of Education P031C160237).

Competing Interests
The author declares no competing financial and non-financial interests.

ACKNOWLEDGMENTS

I would like to thank L@s Ganas Research Fellowship and the Chancellor's Undergraduate Research Award (CURA) for funding my research. I would also like to thank the entire Ross lab, for their support during my research. I especially want to thank Dr. Karen Salas Briceno, for all her mentorship and guidance during my research. Finally, I am especially grateful to Dr. Susan R. Ross, who provided me with immense knowledge and guidance during my time at her lab. I am truly grateful for the opportunity of doing research at the Ross lab.

REFERENCES

[1] Stavrou S, Ross SR (2015) APOBEC3 Proteins in Viral Immunity. The Journal of Immunology 195(10):4565–4570.

[2] Armitage AE, et al. (2014) Possible Footprints of APOBEC3F and/or Other APOBEC3 Deaminases, but Not APOBEC3G, on HIV-1 from Patients with Acute/Early and Chronic Infections. Journal of Virology 88(21):12882–12894.

[3] Kim E-Y, et al. (2014) Human APOBEC3 Induced Mutation of Human Immunodeficiency Virus Type-1 Contributes to Adaptation and Evolution in Natural Infection. PLoS Pathogens 10(7). doi:10.1371/journal.ppat.1004281.

[4] Sousa MM, Krokan HE, Slupphaug G (2007) DNA-uracil and human pathology. Molecular Aspects of Medicine 28(3-4):276–306.

[5] Sato K, et al. (2014) APOBEC3D and APOBEC3F Potently Promote HIV-1 Diversification and Evolution in Humanized Mouse Model. PLoS Pathogens 10(10). doi:10.1371/journal.ppat.1004453.

[6] Fourati S, et al. (2014) Differential impact of APOBEC3-driven mutagenesis on HIV evolution in diverse anatomical compartments. Aids 28(4):487–491.

[7] Parker N, Schneegurt M, Tu A-HT, Forster BM, Lister P (2016) Microbiology (OpenStax, Houston, TX).

[8] Herron JC, Freeman S (2014) Evolutionary analysis (Pearson). 5th Ed.

[9] An P, et al. (2004) APOBEC3G genetic variants and their influence on the progression to AIDS. Journal of Virology 78: 11070–11076.

[10] Borzooee F, Joris KD, Grant MD, Larijani M (2019) APOBEC3G Regulation of the Evolutionary Race Between Adaptive Immunity and Viral Immune Escape Is Deeply Imprinted in the HIV Genome. Frontiers in Immunology 9. doi:10.3389/fimmu.2018.03032.

[11] Mulder LCF, Harari A, Simon V (2008) Cytidine deamination induced HIV-1 drug resistance. Proceedings of the National Academy of Sciences 105(14):5501–5506.

[12] Hernandez MM, et al. (2019) Impact of Suboptimal APOBEC3G Neutralization on the Emergence of HIV Drug Resistance in Humanized Mice. Journal of Virology 94(5). doi:10.1128/jvi.01543-19.

[13] Grant M, Larijani M (2017) Evasion of adaptive immunity by HIV through the action of host APOBEC3G/F enzymes. AIDS Research and Therapy 14(1). doi:10.1186/s12981-017-0173-8.

[14] Cadena C, et al. (2016) The effect of HIV-1 Vif polymorphisms on A3G anti-viral activity in an in vivo mouse model. Retrovirology 13(1). doi:10.1186/s12977-016-0280-y.

The Columbia Undergraduate Science Journal takes great pride in having the honor of hosting the annual Columbia Spring Research Symposium. This year, the 2021 Symposium was held virtually for the first time, and we are happy to have celebrated undergraduate research and retained the lively spirit of the event despite the unprecented circumstances. Below are the winning presentations selected by our esteemed faculty judges!

First Place: "*Can we use next-generation gravitational wave detectors for terrestrial precision measurements of Shapiro time delay?*" by Andrew Sullivan

Abstract: Shapiro time delay is an effect predicted by Einstein's theory of general relativity whereby the travel time of light is delayed as light passes by massive objects. Shapiro time delay is related to the parameterized post-Newtonian formalism parameter γ, which quantifies spacetime curvature produced by a unit mass. Consequently, the measurement of Shapiro time delay can be used as a method of measuring the accuracy of the theory of general relativity. To date, all measurements of Shapiro time delay have been conducted in space over astronomical scales. We propose an experiment that will allow Shapiro time delay measurements to be conducted on Earth, in which we use a rotating mass unit and a next-generation gravitational wave detector. With this scheme, we find that Shapiro time delay and γ may be measured with sub-percent precision. This is the most precise scheme proposed for measuring Shapiro time delay on Earth to date.

About the Author: "Andrew is a junior physics major at Columbia University from Yonkers, New York. Andrew has performed research with Columbia's Experimental Gravity group for the last two years and his research interests lie in the field of gravitational physics and gravitational wave astronomy. Andrew hopes to obtain a PhD in physics and become a professional researcher. For fun, Andrew enjoys watching baseball and running."

Second Place: "*Neural oscillations as predictors of second language learning*" by Victoria Ogunniyi

The full body of this work can be found on page 39 of this issue of the Columbia Undergraduate Science Journal.

About the Author: "Victoria Ogunniyi is a third-year undergraduate student majoring in Neuroscience with a minor in Professional Writing at the University of Illinois at Chicago. After college, she plans to apply to medical school and pursue a residency in psychiatry. In her free time, she enjoys improving her fictional writing skills and hopes to one day become a published novelist."

Third Place: "*Probing the Statistical Relationship Between Binary Black Hole Mergers and Active Galactic Nuclei Hosts*" by Amanda Beck

Abstract: Since 2015, LIGO/Virgo has detected many Binary Black Hole merger Gravitational Wave signals. Identifying the origins of these is key to discover more about these mergers. Rare host galaxies, like AGN, present a favorable environment for these events due to the possible dynamical interactions in their accretion disks. In this project we will probe the statistical relationship between BBH mergers and AGN hosts by analyzing the overlap in localization, as outlined in Bartos et. al. 2017. To do that, we developed a python-based framework that can get the volume overlap between AGN catalogs and LIGO/Virgo 90% probability density volume of BBH mergers. It can be used to establish the fraction of BBH GW detections that come from AGN and to inform real-time EM follow-up.

About the Author: "My name is Amanda Beck, and I am a Brazilian Junior at Columbia University, Columbia College, majoring in Astrophysics. I am mainly interested in high energy astrophysics, and anything that deals with relativity and statistical analysis, as well as STEM education, but am open to any field of research. I plan on obtaining a PhD in Astronomy or Astrophysics, and engage in research and teaching. My favorite pastime is reading, specially fantasy or sci-fi!"

Fourth Place: "*The Diagnosis of Median Arcuate Ligament Syndrome and Postural Orthostatic Tachycardia Syndrome and the effect upon the Presentation of Clinical Depression*" by Jessica Eddy

Abstract: Median Arcuate Ligament Syndrome is a rare, congenital condition where the diaphragm sits too low and the median arcuate ligament crushes the celiac artery. Postural Orthostatic Tachycardia Syndrome often presents as a co-occurring condition. The presentation of these conditions impacts the solar plexus, celiac ganglion, autonomic nervous system dysregulation, and neuropathy. My research was conducted in order to see if patients with median arcuate ligament syndrome and orthostatic intolerance as a comorbidity present with higher levels of clinical depression. Furthermore, if the severity of the chronic condition increased, would clinical depression increase, as well? This research utilized methods such as peak systolic velocities from color duplex ultrasound technology, tilt table results to test for orthostatic intolerance, and the Beck Depression Inventory-II to seek to understand the connection between median arcuate ligament syndrome and orthostatic intolerance caused by dysregulation of the autonomic nervous system, which works in some level of conjugation with the solar plexus, sympathetic nervous system, dopamine and serotonin pathways, and dopamine receptor agonists and antagonists.

About the Author: "My name is Jessica Eddy. I am from Grand Rapids, Michigan and am currently studying at the University of Oxford. My current research includes the impact of rare vascular/gastrointestinal diseases and the role of endothelial cells in HIV latency. I plan to attend medical school for a joint MD/PhD and hope to research genetic biomarkers in rare vascular conditions. For fun, I love dancing and own my own dance studio, running with my puppy, and traveling the world!"

Figure: First place poster from Andrew Sullivan

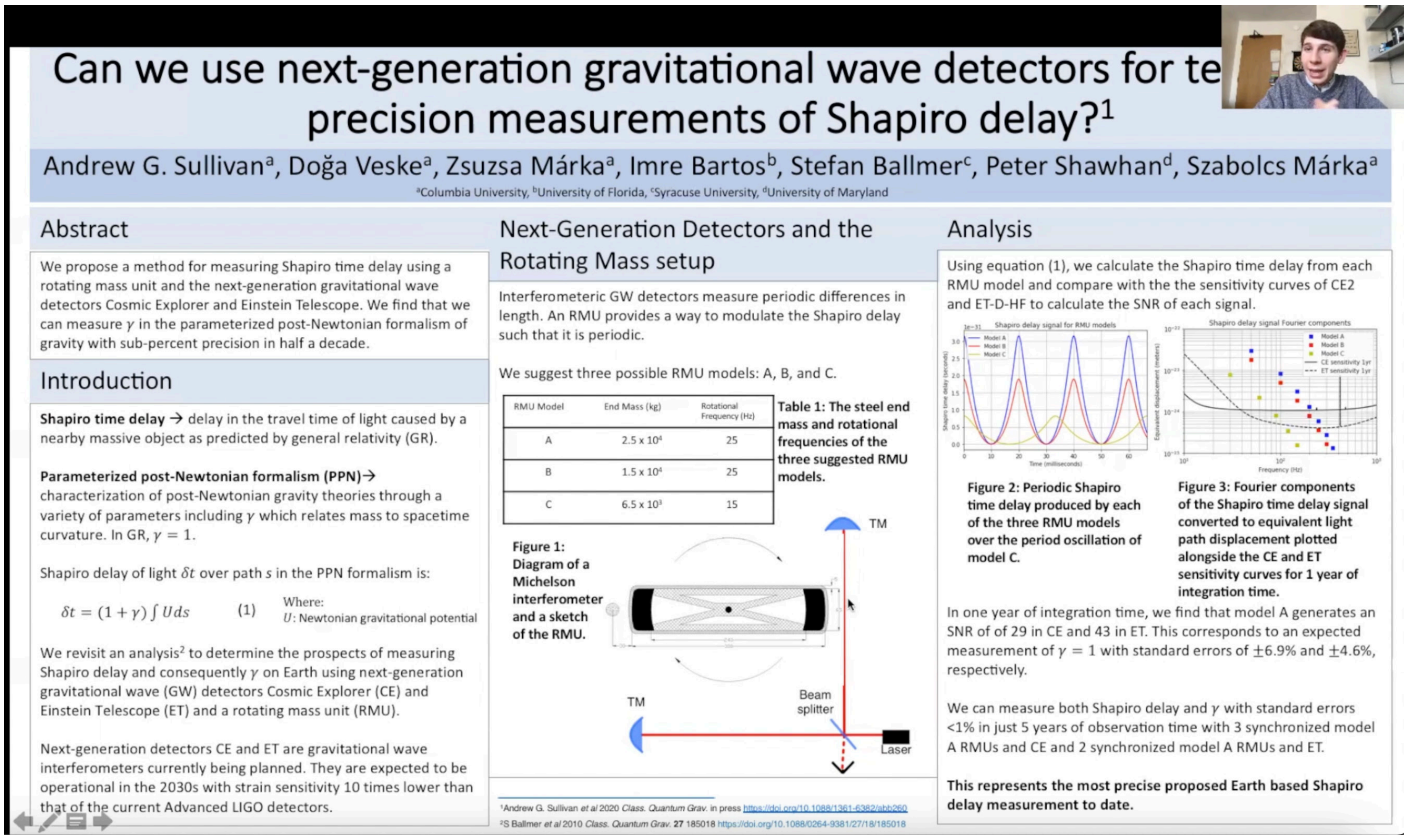

Can we use next-generation gravitational wave detectors for te precision measurements of Shapiro delay?[1]

Andrew G. Sullivan[a], Doğa Veske[a], Zsuzsa Márka[a], Imre Bartos[b], Stefan Ballmer[c], Peter Shawhan[d], Szabolcs Márka[a]

[a]Columbia University, [b]University of Florida, [c]Syracuse University, [d]University of Maryland

Abstract

We propose a method for measuring Shapiro time delay using a rotating mass unit and the next-generation gravitational wave detectors Cosmic Explorer and Einstein Telescope. We find that we can measure γ in the parameterized post-Newtonian formalism of gravity with sub-percent precision in half a decade.

Introduction

Shapiro time delay → delay in the travel time of light caused by a nearby massive object as predicted by general relativity (GR).

Parameterized post-Newtonian formalism (PPN)→ characterization of post-Newtonian gravity theories through a variety of parameters including γ which relates mass to spacetime curvature. In GR, $\gamma = 1$.

Shapiro delay of light δt over path s in the PPN formalism is:

$$\delta t = (1+\gamma)\int U ds \qquad (1)$$

Where:
U: Newtonian gravitational potential

We revisit an analysis[2] to determine the prospects of measuring Shapiro delay and consequently γ on Earth using next-generation gravitational wave (GW) detectors Cosmic Explorer (CE) and Einstein Telescope (ET) and a rotating mass unit (RMU).

Next-generation detectors CE and ET are gravitational wave interferometers currently being planned. They are expected to be operational in the 2030s with strain sensitivity 10 times lower than that of the current Advanced LIGO detectors.

Next-Generation Detectors and the Rotating Mass setup

Interferometeric GW detectors measure periodic differences in length. An RMU provides a way to modulate the Shapiro delay such that it is periodic.

We suggest three possible RMU models: A, B, and C.

RMU Model	End Mass (kg)	Rotational Frequency (Hz)
A	2.5×10^4	25
B	1.5×10^4	25
C	6.5×10^3	15

Table 1: The steel end mass and rotational frequencies of the three suggested RMU models.

Figure 1: Diagram of a Michelson interferometer and a sketch of the RMU.

[1]Andrew G. Sullivan *et al* 2020 *Class. Quantum Grav.* in press https://doi.org/10.1088/1361-6382/abb260

[2]S Ballmer *et al* 2010 *Class. Quantum Grav.* **27** 185018 https://doi.org/10.1088/0264-9381/27/18/185018

Analysis

Using equation (1), we calculate the Shapiro time delay from each RMU model and compare with the the sensitivity curves of CE2 and ET-D-HF to calculate the SNR of each signal.

Figure 2: Periodic Shapiro time delay produced by each of the three RMU models over the period oscillation of model C.

Figure 3: Fourier components of the Shapiro time delay signal converted to equivalent light path displacement plotted alongside the CE and ET sensitivity curves for 1 year of integration time.

In one year of integration time, we find that model A generates an SNR of of 29 in CE and 43 in ET. This corresponds to an expected measurement of $\gamma = 1$ with standard errors of $\pm 6.9\%$ and $\pm 4.6\%$, respectively.

We can measure both Shapiro delay and γ with standard errors <1% in just 5 years of observation time with 3 synchronized model A RMUs and CE and 2 synchronized model A RMUs and ET.

This represents the most precise proposed Earth based Shapiro delay measurement to date.

Figure: Second place poster from Victoria Ogunniyi

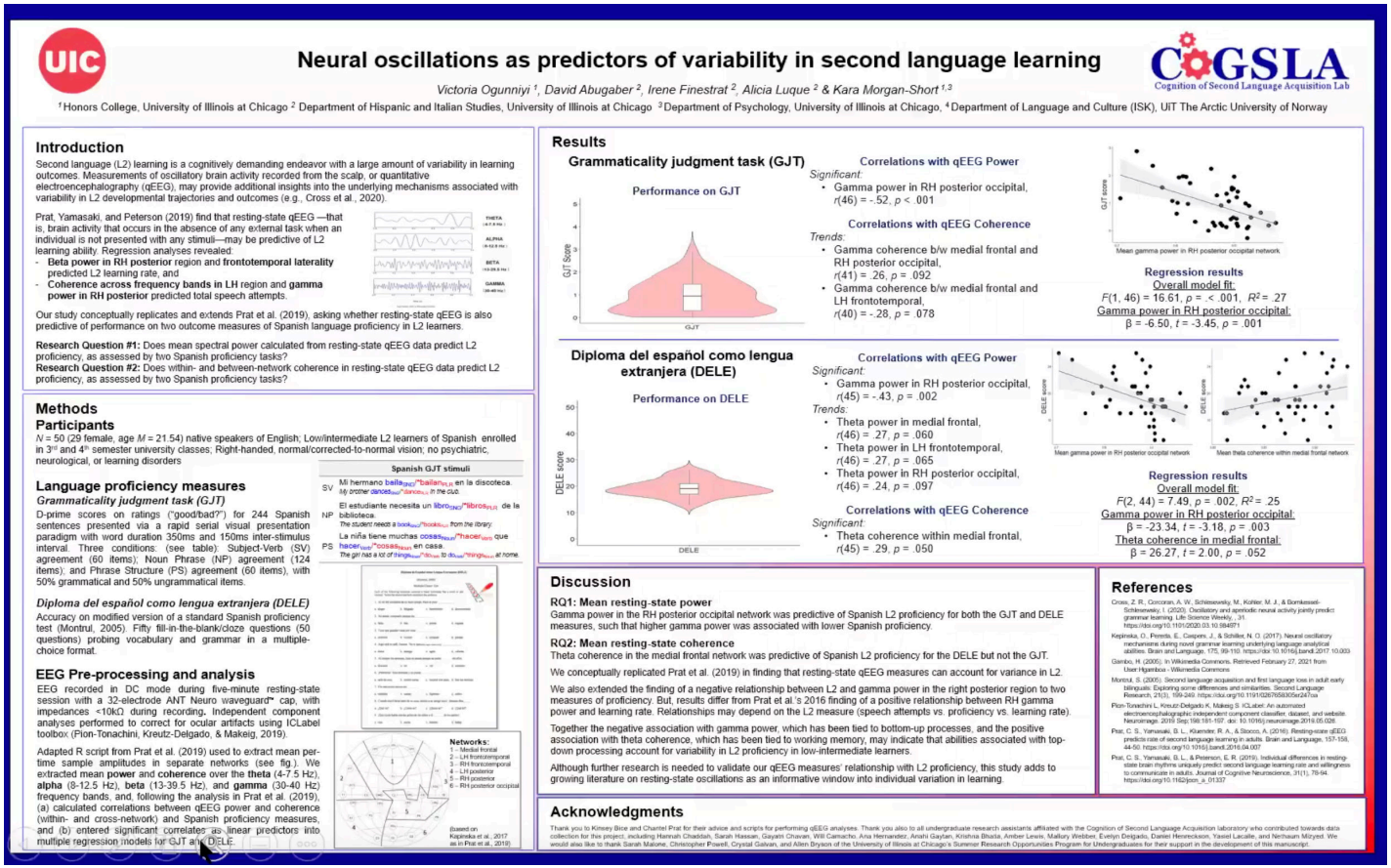

Neural oscillations as predictors of variability in second language learning

Victoria Ogunniyi [1], David Abugaber [2], Irene Finestrat [2], Alicia Luque [2] & Kara Morgan-Short [1,3]

[1] Honors College, University of Illinois at Chicago [2] Department of Hispanic and Italian Studies, University of Illinois at Chicago [3] Department of Psychology, University of Illinois at Chicago, [4] Department of Language and Culture (ISK), UiT The Arctic University of Norway

Introduction

Second language (L2) learning is a cognitively demanding endeavor with a large amount of variability in learning outcomes. Measurements of oscillatory brain activity recorded from the scalp, or quantitative electroencephalography (qEEG), may provide additional insights into the underlying mechanisms associated with variability in L2 developmental trajectories and outcomes (e.g., Cross et al., 2020).

Prat, Yamasaki, and Peterson (2019) find that resting-state qEEG —that is, brain activity that occurs in the absence of any external task when an individual is not presented with any stimuli—may be predictive of L2 learning ability. Regression analyses revealed:

- **Beta power in RH posterior** region and **frontotemporal laterality** predicted L2 learning rate, and
- **Coherence across frequency bands in LH** region and **gamma power in RH posterior** predicted total speech attempts.

Our study conceptually replicates and extends Prat et al. (2019), asking whether resting-state qEEG is also predictive of performance on two outcome measures of Spanish language proficiency in L2 learners.

Research Question #1: Does mean spectral power calculated from resting-state qEEG data predict L2 proficiency, as assessed by two Spanish proficiency tasks?
Research Question #2: Does within- and between-network coherence in resting-state qEEG data predict L2 proficiency, as assessed by two Spanish proficiency tasks?

Methods

Participants

N = 50 (29 female, age *M* = 21.54) native speakers of English; Low/intermediate L2 learners of Spanish enrolled in 3rd and 4th semester university classes; Right-handed, normal/corrected-to-normal vision; no psychiatric, neurological, or learning disorders

Language proficiency measures

Grammaticality judgment task (GJT)

D-prime scores on ratings ("good/bad?") for 244 Spanish sentences presented via a rapid serial visual presentation paradigm with word duration 350ms and 150ms inter-stimulus interval. Three conditions: (see table): Subject-Verb (SV) agreement (60 items); Noun Phrase (NP) agreement (124 items); and Phrase Structure (PS) agreement (60 items), with 50% grammatical and 50% ungrammatical items.

Diploma del español como lengua extranjera (DELE)

Accuracy on modified version of a standard Spanish proficiency test (Montrul, 2005). Fifty fill-in-the-blank/cloze questions (50 questions) probing vocabulary and grammar in a multiple-choice format.

Spanish GJT stimuli

SV	Mi hermano $baila_{3sg}$/$bailan_{3pl}$ en la discoteca. *My brother $dances_{3sg}$/$dance_{3pl}$ in the club.*
NP	El estudiante necesita un $libro_{SNG}$/$libros_{PLR}$ de la biblioteca. *The student needs a $book_{sng}$/$books_{plr}$ from the library.*
PS	La niña tiene muchas $cosas_{fem.pl}$/$hacer_{verb}$ que $hacer_{verb}$/$cosas_{fem.pl}$ en casa. *The girl has a lot of $things_{fem.pl}$/do_{verb} to do_{verb}/$things_{fem.pl}$ at home.*

EEG Pre-processing and analysis

EEG recorded in DC mode during five-minute resting-state session with a 32-electrode ANT Neuro waveguard™ cap, with impedances <10kΩ during recording. Independent component analyses performed to correct for ocular artifacts using ICLabel toolbox (Pion-Tonachini, Kreutz-Delgado, & Makeig, 2019).

Adapted R script from Prat et al. (2019) used to extract mean per-time sample amplitudes in separate networks (see fig.). We extracted mean **power** and **coherence** over the **theta** (4-7.5 Hz), **alpha** (8-12.5 Hz), **beta** (13-39.5 Hz), and **gamma** (30-40 Hz) frequency bands, and, following the analysis in Prat et al. (2019), (a) calculated correlations between qEEG power and coherence (within- and cross-network) and Spanish proficiency measures, and (b) entered significant correlates as linear predictors into multiple regression models for GJT and DELE.

Networks:
1 – Medial frontal
2 – LH frontotemporal
3 – RH frontotemporal
4 – LH posterior
5 – RH posterior
6 – RH posterior occipital

(based on Kaplanska et al., 2017 as in Prat et al., 2019)

Results

Grammaticality judgment task (GJT)

Performance on GJT

Correlations with qEEG Power

Significant:
- Gamma power in RH posterior occipital, $r(46) = -.52$, $p < .001$

Correlations with qEEG Coherence

Trends:
- Gamma coherence b/w medial frontal and RH posterior occipital, $r(41) = .26$, $p = .092$
- Gamma coherence b/w medial frontal and LH frontotemporal, $r(40) = -.28$, $p = .078$

Regression results

Overall model fit:
$F(1, 46) = 16.61$, $p = < .001$, $R^2 = .27$
Gamma power in RH posterior occipital:
$\beta = -6.50$, $t = -3.45$, $p = .001$

Diploma del español como lengua extranjera (DELE)

Performance on DELE

Correlations with qEEG Power

Significant:
- Gamma power in RH posterior occipital, $r(45) = -.43$, $p = .002$

Trends:
- Theta power in medial frontal, $r(46) = .27$, $p = .060$
- Theta power in LH frontotemporal, $r(46) = .27$, $p = .065$
- Theta power in RH posterior occipital, $r(46) = .24$, $p = .097$

Correlations with qEEG Coherence

Significant:
- Theta coherence within medial frontal, $r(45) = .29$, $p = .050$

Regression results

Overall model fit:
$F(2, 44) = 7.49$, $p = .002$, $R^2 = .25$
Gamma power in RH posterior occipital:
$\beta = -23.34$, $t = -3.18$, $p = .003$
Theta coherence in medial frontal:
$\beta = 26.27$, $t = 2.00$, $p = .052$

Discussion

RQ1: Mean resting-state power
Gamma power in the RH posterior occipital network was predictive of Spanish L2 proficiency for both the GJT and DELE measures, such that higher gamma power was associated with lower Spanish proficiency.

RQ2: Mean resting-state coherence
Theta coherence in the medial frontal network was predictive of Spanish L2 proficiency for the DELE but not the GJT.

We conceptually replicated Prat et al. (2019) in finding that resting-state qEEG measures can account for variance in L2.

We also extended the finding of a negative relationship between L2 and gamma power in the right posterior region to two measures of proficiency. But, results differ from Prat et al.'s 2016 finding of a positive relationship between RH gamma power and learning rate. Relationships may depend on the L2 measure (speech attempts vs. proficiency vs. learning rate).

Together the negative association with gamma power, which has been tied to bottom-up processes, and the positive association with theta coherence, which has been tied to working memory, may indicate that abilities associated with top-down processing account for variability in L2 proficiency in low-intermediate learners.

Although further research is needed to validate our qEEG measures' relationship with L2 proficiency, this study adds to growing literature on resting-state oscillations as an informative window into individual variation in learning.

References

Cross, Z. R., Corcoran, A. W., Schlesewsky, M., Kohler, M. J., & Bornkessel-Schlesewsky, I. (2020). Oscillatory and aperiodic neural activity jointly predict grammar learning. Life Science Weekly, , 31. https://doi.org/10.1101/2020.03.10.984971

Kepinska, O., Pereda, E., Caspers, J., & Schiller, N. O. (2017). Neural oscillatory mechanisms during novel grammar learning underlying language analytical abilities. Brain and Language, 175, 99-110. https://doi 10.1016/j.bandl.2017.10.003

Gambo, H. (2005). In Wikimedia Commons. Retrieved February 27, 2021 from User:Hgambox - Wikimedia Commons

Montrul, S. (2005). Second language acquisition and first language loss in adult early bilinguals: Exploring some differences and similarities. Second Language Research, 21(3), 199-249. https://doi.org/10.1191/0267658305sr247oa

Pion-Tonachini L, Kreutz-Delgado K, Makeig S. ICLabel: An automated electroencephalographic independent component classifier, dataset, and website. Neuroimage. 2019 Sep;198:181-197. doi: 10.1016/j.neuroimage.2019.05.026.

Prat, C. S., Yamasaki, B. L., Kluender, R. A., & Stocco, A. (2016). Resting-state qEEG predicts rate of second language learning in adults. Brain and Language, 157-158, 44-50. https://doi.org/10.1016/j.bandl.2016.04.007

Prat, C. S., Yamasaki, B. L., & Peterson, E. R. (2019). Individual differences in resting-state brain rhythms uniquely predict second language learning rate and willingness to communicate in adults. Journal of Cognitive Neuroscience, 31(1), 78-94. https://doi.org/10.1162/jocn_a_01337

Acknowledgments

Thank you to Kinsey Bice and Chantel Prat for their advice and scripts for performing qEEG analyses. Thank you also to all undergraduate research assistants affiliated with the Cognition of Second Language Acquisition laboratory who contributed towards data collection for this project, including Hannah Chaddah, Sarah Hassan, Gayatri Chavan, Will Camacho, Ana Hernandez, Anahi Gaytan, Krishna Bhatia, Amber Lewis, Mallory Webber, Evelyn Delgado, Daniel Herenkoson, Yasiel Lacalle, and Nehaum Mityet. We would also like to thank Sarah Malone, Christopher Powell, Crystal Galvan, and Allen Bryson of the University of Illinois at Chicago's Summer Research Opportunities Program for Undergraduates for their support in the development of this manuscript.

Figure: Third place poster from Amanda Beck

Probing the Statistical Relationship Between BBH Mergers and AGN Hosts

[1]Amanda Beck, [1]Yasmeen Asali, [2]Eve Cully, and [1]Dr. Zsuzsa Marka
[1]Department of Astronomy, Columbia University | [2]Department of Physics, Durham University

Why BBHs and AGN?

LIGO/Virgo → many binary black hole merger GW detections. Identifying the origins of these is key to discover more about these mergers!

Rare host galaxies, like AGN, present a favorable environment for these events due to the possible dynamical interactions in their accretion disks.

Ref. [1] → association between BBH mergers and rare host galaxies can be statistically established using LIGO/ Virgo detections.

We are developing a framework to study the relationship between the localization of known AGN from the WISE R90 catalog Ref. [2], and the 90% probability density localization of BBH events detected by LIGO/Virgo.

References

[1] I. Bartos, et al. 2017
[2] Assef R. J., et al. 2018
[3] M. Bilicki, et al. 2018
[4] Hopkins, et. al. 2006
[5] DigitizeIt
Background picture: Emanuele Petrilli

AGN & BBH

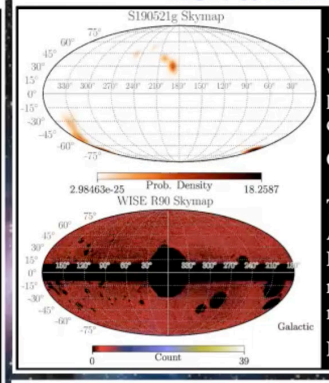

Healpy skymaps with localization probability density per pixel.

Goes out to z ~ 2

The WISE R90 AGN catalog, Ref. [2], has 90% reliability, ~4.5 million AGN.

No distances or z.

The Overlap

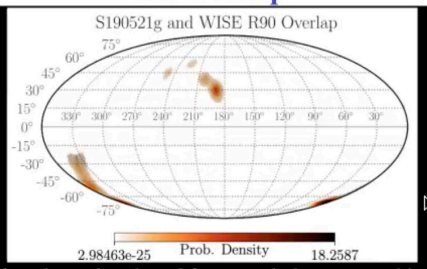

We developed a python-based framework that can get this volume overlap. It can be used to establish the fraction of BBH GW detections that come from AGN and to inform real-time EM follow-up.

Future Plans

AGN Distances for Volume Crossmatch

Ref. [3] ➡ use ML to predict Z values for galaxies.

Dr. Imre Bartos and Nihar Gupte have created an ANN algorithm to predict R90 redshifts. We are integrating its results with our computations.

Statistical Analysis (Ref. [1])

If event didn't come from AGN: AGN in GW Volume follows Poisson distribution.

If event did come from AGN: 1 guaranteed AGN in GW Volume.

Combining this with our crossmatch results, we can find the likelihood ratios for BBH coming from AGN.

Completeness

Ref. [4] ➡ Quasar Luminosity Function.

Compare to R90. Get completeness in each pixel, at each distance of the 90% area.

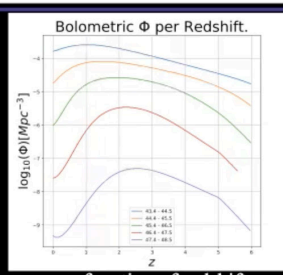

Number density of quasars as a function of redshift. Graph replicated from Ref. [4] using DigitizeIt (Ref. [5])

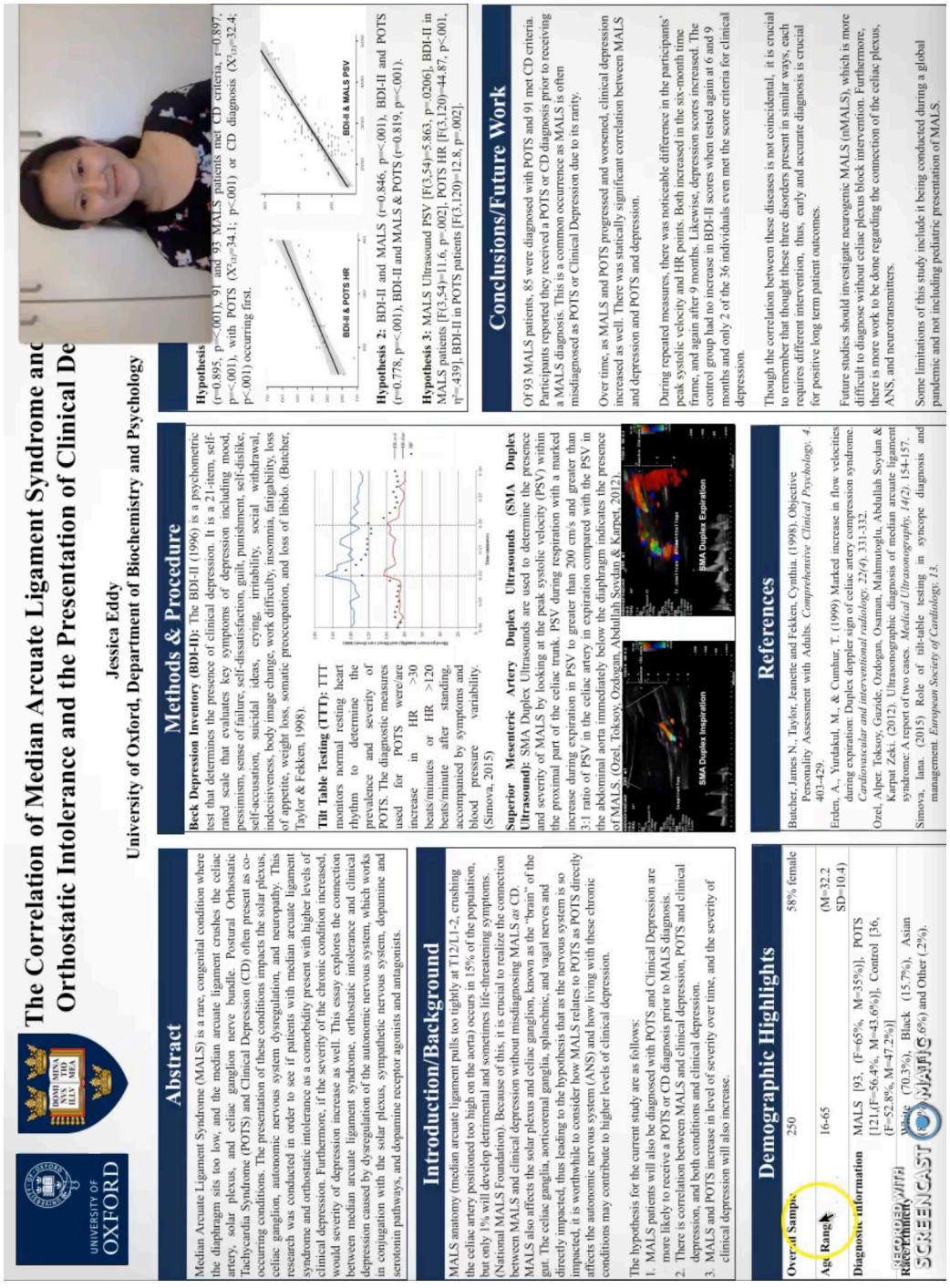

Figure: Fourth place poster from Jessica Eddy